الجـــمـهـوريـــة الجـــزائـريـة الديمـــقـراطيـة الـشـــعبيـة

People's Democratic Republic of Algeria

وزارة التـــــعـليـم العـــــالي و البـــــــحث العـــلـمـــي

Ministry of Higher Education and Scientific Research

جـــــــــــامعة أبي بكـــر بـلـقـايد – تـلمســـــــــــان–

University of Aboubakr Belkaïd –Tlemcen– Faculty of Technology

Laboratory of Computational Mechanics

THESIS

Presented for obtaining the degree of DOCTORATE 3rd Cycle

In: Mechanical Engineering

Specialty: Computational Mechanics

Presented by: **ZAOUAGUI Bilel**

Subject

Vibration analysis of cracked nano-plates

Publicly defended, 27/06/2022, in front of a board of examiners:

M. BENACHOUR Mustapha	Professor	Univ. Tlemcen	Chairman
M. BELALIA Sid Ahmed	Professor	Univ. Tlemcen	Thesis director
M. BOUKHALFA Abdelkrim	Professor	Univ. Tlemcen	Co-thesis director
M. HAMZA CHERIF Sidi Med	MCA	Univ. Tlemcen	Examiner 1
M. SERDOUN Med Nadjib	MCA	ESSA. Tlemcen	Examiner 2

Abstract

The thesis presents an h-p FEM model for analyzing linear/nonlinear free vibrations of cracked isotropic/FGM nanoplates using nonlocal elasticity theory and the first-order shear deformation theory under the assumptions of the geometrical non-linearity of Von Karman. Non-local elasticity has been used to capture the small-scale effect that has a significant influence at the nano-scale. The h-p FEM has been employed due to its advantages in modeling cracked structures where two different meshing strategies have been used; full p-refinement on few simple elements is used for linear analysis and selective p-refinement around the crack tip on an h-refinement dominated mesh is used for nonlinear analysis. The results obtained are compared with those available in the literature and show the fast convergence, accuracy, and efficiency of the h-p FEM numerical model. Original results are presented and discussed through several parametric studies whereas the influence of crack parameters (length, orientation, and position), non-local parameter, plate geometry (aspect ratio and thickness), material volume fraction exponent, and large amplitude vibrations on linear/nonlinear free vibrations of cracked nanoplates under several cases of boundary conditions.

Key words: *h-p version of finite elements method; free vibrations; non-linear; functionally graded materials; crack; non-local elasticity; nanoplate.*

ملخص

الأطروحة تقدم نموذج رقمي لـ h-p لطريقة العناصر المتناهية لتحليل الاهتزازات الحرة الخطية و اللاخطية للصفائح النانومترية المشقوقة المصنوعة من مواد متماثلة الخواص أو مواد متدرجة وظيفيا، باستعمال نظرية المرونة اللاموضعية و نظرية الدرجة الأولى للصفائح تحت فرضيات اللاخطية الهندسية لـ Von Karman.نظرية المرونة اللاموضعية استعملت بهدف التقاط تأثير السلم الصغير الذي يكون ذو تأثير واضح في السلم النانومتري.حسب هذه النظرية المعقدة، فإن حالة الضغط في نقطة معينة من المادة تحدد ليس فقط بحالة التشوه في هذه النقطة، وإنما بحالة التشوهه في كل النقط الأخرى. h-p لطريقة العناصر المتناهية استعملت نظرا للأفضلية التي توفرها في نمذجة البنيات المشقوقة، أين تم استخدام استراتيجيتان مختلفتان للربط؛ تحسين كامل من نوع p على عدد صغير من العناصر البسيطة استعمل للتحليل الخطي و تحسين جزئي من نوع p حول طرف الشق على شبكة ربط يهيمن عليها تحسين من نوع h استعملت هذه الاستراتيجية للتحليل اللاخطي. النتائج المتحصل عليها تم تقديمها و مناقشتها عن طريق عدة دراسات تبين تأثير: عوامل الشق (الطول، الزاوية و الموضع)، عامل اللاموضعية، هندسة الصفيحة (نسبة الطول/العرض و السمك)، أس النسبة الحجمية للمادة و سعة الاهتزازات، على الاهتزازات الخطية و اللاخطية للصفائح النانومترية المشقوقة تحت تأثير عدة شروط حدية.

كلمات مفتاحية: h-p لطريقة العناصر المتناهية؛ اهتزازات حرة؛ اللاخطية؛ مواد متدرجة وظيفيا؛ شق؛ المرونة اللاموضعية؛ صفيحة نانومترية

Résumé

La thèse présente un modèle h-p MEF pour l'analyse linéaire/non-linéaire des vibrations libres des nano-plaques fissurées en matériaux isotropes et en matériaux à gradient fonctionnel, en utilisant la théorie d'élasticité nonlocal et la théorie du premier ordre des plaques sous les hypothèses de la non-linéarité géométrique de Von Karman. L'élasticité nonlocal a été utilisé dans le but de capturer l'effet de petite échelle dont il a une influence significatif à l'échelle nano. h-p MEF a été utilisé pour ces avantages dans la modélisation des structures fissurées, deux stratégies différentes de maillage ont été utilisées; p-raffinement entier sur peu des éléments simples utilisés pour l'analyse linéaire et p-raffinement sélectif autour du front de fissure sur un maillage dominé par h-raffinement utilisé pour l'analyse non-linéaire. Les résultats obtenus sont présentés et discutés à travers plusieurs études paramétriques tandis que l'influence des: paramètres de fissure (longueur, orientation et position), paramètre non-local, geometry de la plaque (rapport hauteur/largeur et épaisseur), exposant de la fraction volumique du matériau et l'amplitude des vibrations, sur les vibrations libres linéaires/non-linéaires des nano-plaques fissurées avec plusieurs conditions aux limites.

Mots clés: version h-p de la méthode des éléments finis; vibration libre; non-linéaire; matériaux à gradient fonctionnel; fissure; élasticité nonlocal; nano-plaque.

Acknowledgement

This research was carried out at Tlemcen University and it involved several people that I would like to thank here for their help and support.

Completion of this doctoral dissertation was possible with the support of several people. I would like to express my sincere gratitude to all of them. First of all, I am extremely grateful to my research supervisors, Pr. S.A. Belalia, Pr. A. Boukhalfa, for their unconditional support, valuable guidance, scholarly inputs and consistent encouragement I received throughout the research work. It has been a privilege to work with you all. Hope to be able to work with you again in the near future. I am also grateful for having been supported by the work of Pr. Houmat, and the colleagues of research team. Special thanks to my colleague of research team Ahmed Aouinet, who provided me with a friendly and inspiring environment to work and have fun. Wish you all the best.

The work presented in this thesis has been critically assessed and approved by an outstanding committee to whom I am more than grateful.

Fortunately, I have also the privilege of having a lovely family and friends who had a fundamental role in getting me through the PhD process successfully: Mother, Father, thanks for your trust in my life choices and your support.

There was no way of not loving Tlemcen after the warmest welcome from my dear friends Houssem Hamdoun, Abderrahim Med Amine, Anes and Adel. thank you all for the lovely and fun time spent together during my PhD.

Nomenclature

Acronyms

CPT	Classical Plate Theory
DSG	Discrete Shear Gap method
FEM	Finite Elements Method
FGM	Functionally Graded Material
FSDT	The first order shear deformation theory
GFEM	Generalized finite element method
h-p FEM	h-p version of finite elements method
HSDT	higher-order shear deformation plate theory
IDI	Inplane deformation and inertia
IGA	Isogeometric Analysis
LUM	Linearized Update Method
MD	Molecular Dynamics
VDQ	Variational Differential Quadrature method
XFEM	Extended finite element method
XIGA	Extended Isogeometric Analysis

Greek Letters

γ	Crack position to length ratio
α	Crack angle
β	Crack length ratio
κ	Averaging kernel or the spatial non-local kernel
γ_{xy}, γ_{xz}, γ_{yz}	Shear strains
μ	The non-local parameter
ν_f	The distribution of effective Poisson's ratio
ω	Vibration frequency
ω_{nl}	non-linear frequency
$\overline{\omega}$	Non dimentional frequency parameter
$\overline{\sigma}_{ij}$	the non-local stress components
ρ	Material density
$\tau_i(t)$	Time functions
θ_x, θ_y	The rotations of transverse normal to the mid-plane about the x and y axes
ε_{xx}, ε_{yy}	Normal strains
$\varphi_i(x,y)$	Shape functions
ϖ_i	Numerical integration weight
ξ, η	Coordinates in the space of reference element
א	Non-linear term

σ_{ij}	stress tensor

Latin Letters

$-C-$	Clamped edge
$-F-$	Free edge
$-S-$	Simply supported edge
$[K]$	Stifness matrix
$[M]$	Mass matrix
$[J]$	The jacobian matrix for geometric transformation
$\{q\}$	Vector of generalized degrees of freedom
$\mathbb{P}_f(z)$	The distribution of effective material properties
a, b	Plate length and width
A_{ij}	Extensional stiffness coefficients
B_{ij}	Bending-extensional coupling stiffness
D_{ij}	Bending stiffness coefficients
e_0	non-dimensional parameter considered as a constant appropriate for the material
$E_f(z)$	The distribution of effective Young's modulus
h	Plate thickness
I_0, I_1, I_2	The mass moments of inertia
K	Kinetic energy
K_0	The modified Bessel's function of the second kind of order zero

l_e	The external characteristic length
n	Volume fraction exponent
N, M, Q	The stress resultant forces and moments
p	Degree of polynomial aproximation
T	Temperature
U	Elastic potential energy
u, v	In-plane displacement
u_0, v_0	Mid-plane In-plane displacement
V	External work
V_c	Volume fraction of ceramic
V_m	Volume fraction of metal
w	transversal displacement
w_0	Mid-plane transversal displacement
x, y, z	Cartisian coordinates

Operators

$\mathscr{L}$	linear differential operator
∇^2	Laplace operator $\sum_i \frac{\partial}{\partial x_i}$

Contents

List of Tables

List of Figures

Introduction

A perception of the mechanical properties of nano structures is absolutely necessary for an efficient and reliable designing of nanodevices. Consequently, the modeling methods to predict their mechanical behavior are challenging research problems. The mechanical behavior of nano structures can be computed by means of various theoretical and computational methods, involving quantum mechanical-based methods, atomistic modeling methods, continuum modeling methods and multi-scale and multi physics simulation methods. Evidently, the quantum mechanical approaches are the most accurate methods to determine the behavior of nano structures, as the dynamics of the electrons and the nuclei are described using solutions of the many-body Schrödinger equation [1]. In spite of that they are restricted to very small systems containing a few tens to a few hundreds of atoms, due to the fact that they are inherently computationally very expensive and time-consuming [2].

The atomistic modeling techniques are used to provide fundamental descriptions of the behavior of nano structures. These methods have been broadly used to complement experimental testing, and to obtain input data for continuum models, Besides they can be used to predict the mechanical properties of nano structures. Theses techniques are based on the use of inter-atomic potentials and empirical force fields. The atomistic methods include classical molecular dynamics (MD) with empirical inter-atomic potentials and semi-empirical (SE) methods (tight-binding (TB) method) [3]. Compared to the quantum mechanical-based methods, the atomistic-based methods can be used to study much larger systems. However, atomistic modeling methods are still limited to relatively small systems containing up to several million atoms for very short time scales, from picoseconds to

nanoseconds [4]. That being so, aiming for alternative approaches such as the continuum-based modeling methods, is highly advisable seeing that they are the most computationally efficient methods for the analysis of nano structures.

Classical continuum mechanics applicability is limited due to long-range inter-atomic attractions at small scales (or lattice spacing between individual atoms) as well as the discrete material structure that cannot be homogenized into a continuum. Hence, material properties at small scales are size-dependent. Therefore, the small scale effect must be considered for accurate prediction of the mechanical behavior of nanomaterials. For that reason, in the continuum models classical mechanical structures such as rods, beams, plates and shells are used combined with modified non local constitutive law namely the non local elasticity, in order to capture the small scale effect. The emergence of non-local continuum models sparked an inflationary development of research on modeling mechanical behavior of nanostructures.

The non-local elasticity theory has the great potential to predict the mechanical behavior of both small and relatively larger nanoscopic structures without solving a large number of highly complex equations. This theory differs from the local classical elasticity theory only in the constitutive equations describing the material medium. In non-local elasticity the state of stress at a given point in a material depends not only on the state of strain at that point, but also on the state of strain at other points. This agrees with the concept of the many-body Schrödinger equation where inter-atomic forces acting on a certain atom in a material depend not only on the local interaction between this certain atom and its adjacent neighbors, but also non-local interactions among all other atoms far of this certain atom. Therefore, deformation over all material points is required to acquire the stress state of the body at a particular point. Based on this hypothesis, the long-range inter-atomic interactions between material points are naturally taken into account and so the model is dependent on the size of the structure.

Moreover the presence of a crack in a structure is a complicating effect that makes its mechanical behavior significantly different from that of an intact structure especially for the dynamic behavior. A crack can be defined as a geometric discontinuity in a solid body which is characterized by an initiation (or nucleation) point. Hence, The use of numerical methods is the most suitable approach to solve cracked structures problems, more

precisely multi domain methods such as domain decomposition methods, finite element method (FEA) and its variants, which provides easy fitting of complex geometries and arbitrary combinations of boundary conditions (i.e., discontinuities, curves and irregular domains) by dividing the complex original geometric domain into a small number of manageable subdomains (i.e., elements). Plenty of research work has been performed on the computation of stress intensity factor (i.e., static analysis) for cracked local plates, However free vibrations studies of cracked local plate are comparatively little and absent for cracked nanoplates. Furthermore the literature on the vibrations of cracked plates using *h-p* FEM is still in its infancy.

This thesis addresses the absence of linear and nonlinear analysis of free vibrations of cracked nanoplates and the scarcity of employing the *h-p version* of finite elements method to solve vibration problems of cracked plates.

Aims and objectives

The overall aim of this thesis is to advance the understanding linear and nonlinear behavior of cracked nanoplates and develop techniques for modelling cracks using the *h-p* version of finite element method.

It has been accomplished through achieving 04 main objectives:

- Develop and verify and *h-p* FEM numerical model based on first order shear deformation theory and nonlocal elasticity.
- Investigate the linear free vibration behavior of isotropic nanoplates with different crack parameters.
- Further explore linear free vibration behavior of FGM cracked nanoplates.
- Investigate nonlinear free vibration behavior of cracked nanoplates using *h-p* FEM with an alternative refinement approach.

.

Thesis outline

Present work deals with free vibrations of cracked nanoplates Accordingly this thesis is organized into 06 chapters as follow:

- Chapter 1, a brief literature review is presented, related to nonlocal elasticity of Eringen in modeling vibrations of nanoplates and numerical models employed to solve cracked plates problems. In the first section 1.1, we discuss the significant role of scale effects on behavior of intact nanoplates and present importance of nonlocal elasticity theory through previous researchers work. After that we present gaps in current literature about linear/nonlinear free vibrations of cracked nanoplates.

  In the second section 1.2, we explore the literature of numerical models used to model cracked plates and discuss their accuracy and efficiency. Then we discuss the potential advantages of *h-p* version of finite element method to model cracked structures and the scarcity of research on this topic.

- Chapter 2, introduces a *h-p* FEM model to solve linear/nonlinear cracked nanoplates free vibration problems based on first order shear deformation theory (FSDT) and nonlocal elasticity theory of Eringen. In section 2.1 we present the mathematical description of interactions between points in a solid nano-structure based on the on nonlocal elasticity theory. Then in section 2.2, the first order shear deformation theory of plates is used in conjunction with nonlocal elasticity to derive equations of motions for nanoplates. Section 2.3 is dedicated to functionally graded materials effective properties.

  In section 2.4 the finite element method is used with the obtained equations of motion to derive a system of algebraic equation, to be constructed and solve numerically. The numerical methods used to construct the system of equations and solve it, are presented in section 2.5. Computer implementation and computational considerations employed in order to efficiently conduct calculations on machines are discussed in section 2.6.

- Chapter 3, we investigate linear free vibrations behavior of isotropic cracked nanoplates where the influence of crack parameters and the non-local parameter are

studied and discussed. In section 3.1, convergence of the linear solution is presented for intact and cracked local/nonlocal plates. Then a comparison is carried out in order to validate the accuracy of the presented model. In section 3.2, we study the influence of crack parameters such as crack position (central, side), crack length and orientation on frequency parameters for different values of nonlocal parameter and for different cases of boundary conditions.

- Chapter 4, the linear free vibrations behavior of FGM cracked nanoplates is investigated, by studying the influence of material parameters (i.e. volume fraction exponent n) along with crack parameters (position, length and orientation) and nonlocal parameter. In section 4.1 we study convergence for intact and cracked FGM plates, and present a comparison with results in literature to verify the accuracy of the model for intact FGM plates. In section 4.2, we conduct parametric studies for cracked nonlocal FGM plates, involving several cases of boundary conditions, in order to investigate the influence of volume fraction exponent, crack length and orientation and nonlocal parameter. Then we study the effect of crack position along volume fraction exponent on linear free vibrations of cracked FGM nanoplates.

- Chapter 5, the nonlinear free vibration of cracked nanoplates has been studied using *h-p* FEM with selective *p*-refinement around the crack tip. In section 5.1, we verify the convergence of full and selective *p*-refinement for the linear and nonlinear solutions of intact and cracked plates. Then a comparison is conducted to verify the accuracy of nonlinear solutions for intact isotropic/FGM plates. In section 5.2, we investigate the effect of horizontal crack length and nonlocal parameter on non-linear free vibrations of cracked nanoplates under several boundary conditions. Finally we study the effect of horizontal crack position and non-local parameter on nonlinear free vibrations of cracked nanoplates.

- Chapter 5.3, the conclusions and potential further work are discussed.

Chapter 1

Literature review

In this chapter, a brief literature review is presented, focusing on two key points, nonlocal elasticity of Eringen in modeling vibrations of nanoplates and numerical methods and approaches employed to solve cracked plates problems.

1.1 Vibration of nanoplates

In light of the development and excellent properties of nanostructures, modeling and predicting their behavior has become a pertinent issue. On one hand, the classical continuum model usually overestimates the frequencies of nanoplates because it does not take into account the scale effect, on the other hand, accurate results can be obtained by means of atomistic and hybrid atomistic-continuum simulation but that would be computationally expensive for large scale systems. The emergence of non-local elasticity theory of Eringen and Wegner [5] enabled researchers to account for scale effect and make use of continuum models simplicity. According to this theory, the stress state at a point depends on the strain at all points of the structure. Several researchers have extensively studied the role of non-local elasticity theory in modeling nanostructures and identified its importance. Liew et al. [3] introduce a literature review on the applications of non local elasticity theory in modeling nanoplates. Ansari et al. [6], Pradhan and Kumar [7] used a generalized differential quadrature model based on Eringen's non-local elasticity and the classical plate theory to

conduct vibration analysis of graphene sheets. Malekzadeh et al. [8] employed the differential quadrature method to investigate the free vibration of orthotropic arbitrary straight-sided quadrilateral nanoplates based on the non-local theory and the first order shear deformation theory (FSDT). Wang et al. [9] studied the non-local effect on the vibration of mono-layer graphene and boron-nitride sheets. Huang et al. [10] calibrated the small scale effect parameter of simply supported graphene sheets under bending by matching results obtained from non-local elasticity theory and molecular dynamics (MD) simulations. Chen et al. [11] used the non-local theory and the classical plate theory to analytically determine the thermo-electro-mechanical free vibration of piezoelectric nanoplates. Malekzadeh and Shojaee [12] applied a two-variable refined plate theory and non-local elasticity of Eringen to determine the effect of the non-local parameter on the vibration of nanoplates. Hosseini et al. [13] used an analytical model based on non-local constitutive relations and third-order shear deformation plate theory to investigate the buckling and free vibration of rectangular nanoplates.

Pradhan and Phadikar [14] reformulated classical plate theory (CPT) and first-order shear deformation theory (FSDT) using the non-local elasticity constitutive relations of Eringen, and employed Navier's approach to solve the resulting equations of motion for simply supported boundary conditions. Moreover the authors investigated the effect of the non-local parameter on natural frequencies of the nanoplates. Furthermore the analysis of double layered nanoplates has been carried out to study the effect of non-local parameter, length, height, elastic modulus and stiffness of Winkler foundation of the plate on natural frequencies. Liu et al. [15] Solved analytically the thermo-electro-mechanical free vibration of piezoelectric nanoplates using Kirchhoff plate theory in conjunction with non-local elasticity theory. Analooei et al.,[16] studied the buckling and vibrations of isotropic and orthotropic nano-plates using finite strip method and Eringen's non-local elasticity. The authors determined the effects of plate size, non-local parameter, aspect ratio and boundary conditions on natural frequencies and buckling load. Aksencer and Aydogdu [17] reported the forced vibration of nano-plates based on non-local elasticity using the Navier type solution method. Their work considered different values of non-local parameter, length of plates and several loading cases. Aghababaei and Reddy [18] introduced the third-order shear deformation plate theory of Reddy [19] in conjunction with non-local

elasticity constitutive relations. Their study presented analytical solutions of bending and free vibration of simply supported rectangular nanoplates. Wang and Wang [20] proposed consideration of surface energy to study vibration of simply supported nanoplates based on non-local elasticity, Kirchhoff's and Mindlin's plate theories. solution are obtained in a closed form using Navier's approach. The authors have concluded that surface energy increases natural frequencies of the nanoplates (i.e., stiffening effect). Chakraverty and Behera [21] employed the Rayleigh-Ritz method with algebraic polynomial displacement function, based on non-local elasticity and classical plate theory to determine the vibration of isotropic rectangular nanoplates subjected to different boundary conditions. Necira et al.[22] used a curved hierarchical quadrilateral element to study free vibration of arbitrary shaped Mindlin's nanoplates. Zhang et al. [23] performed free vibration analysis of a graphene sheet by combining non-local elasticity and classical plate theory in the framework of the kp-Ritz method. The authors obtained the values of non-local parameter by matching results with Molecular dynamics models, their results showed that non-local parameter depends on boundary conditions. Kiani [24] investigated the dynamic response of thin nanoplates subjected to moving nanoparticle taking into account the presence of Coulomb friction, the study has been accomplished by employing the eigen function technique and the Laplace transform method to solve the non-local equations of motion. Wang et al. [25] explored the nonlinear vibrations of double-layered nano-plates subjected to several boundary conditions based on non-local elasticity. Jomehzedeh and Saidi [26] studied the nonlinear free and forced vibration of simply supported and clamped nanoplates using the von Karman geometrical model and non-local elasticity theory.

Functionally graded nanoplates have been also studied extensively by other researchers. Natarajan et al. [27] studied the linear vibration behavior of functionally graded nanoplates using the iso-geometric analysis in conjunction with non-local elasticity constitutive relations and the Mori–Tanaka homogenization scheme. The author investigated the effect of material gradient index, the non-local parameter, the plate thickness, the plate aspect ratio and the boundary conditions on the natural frequencies of the nano-plate. Nami et al. [28] investigated the effects of gradient parameter, aspect ratio and non-local parameter on natural frequencies of FGM nanoplates using the non-local Kirchhoff plate. Belkorissat et al. [29] presented a hyperbolic refined plate model in conjunction with non-local elasticity

to study free vibration properties of FGM nano-plates, the study considered investigating the effects of non-local parameter, the plate thickness, the plate aspect ratio, and various material compositions on natural frequencies of FGM nano-plate. Ansari et al. [30] used variational differential quadrature (VDQ) method to solve the three dimensional flexural vibrations problem of FGM nano-plates based on non-local elasticity theory.

The considerable amount of research on vibrational behavior of nanoplates and other simple structures (nanotubes...) is a consequence to its importance in different applications in fields as electronics, optics, sensor devices, and nano-electromechanical devices. The experience gained from studying these simple nanostructures enabled researchers to study the mechanical behavior of more complex nanoscopic structures (Resonant Sensors and nanoturbines). Resonant sensors belong to a class of novel devices in nanometrology, these sensors are mechanically triggered and used to detect the presence of nanoparticles and biomolecules or to survey temperature or pressure at the nanoscale. Their detection criteria is obtained by the measurement of the resonant frequency shift of the sensor which is sensitive to the position, size and shape of the detected particle. Shen et al. [31] investigated vibration of graphene-based nanomechanical sensor based on the non-local Kirchhoff plate theory, the sensor is considered as a simply supported rectangular nanoplate carrying a nanoparticle considered as a concentrated mass, the authors explored the effects of the mass and position of the nanoparticle on the frequency shift which would be helpful to the design of nanomechanical mass sensor with mass sensitivity that can reach $10^{-21}g$. Similar findings has been reported by other researchers [32, 33]. Fazelzadeh and Ghavanloo [34] investigated the application of single layered graphene sheet as nanomechanical mass sensors in thermal environments, the results indicated that the sensitivity of the mass sensor increases with increasing temperature difference. Shen et al. [35] explored the possibility of development of a new generation of resonant mass sensors using double-layered graphene sheets. Murmu and Adhikari [36] compared the results obtained by non-local elasticity and molecular dynamics when modeling a nanomechanical sensor and reasonable agreement has been observed. Consequently it was concluded that the non-local theory can be used to model nanomechanical mass sensors. Jalali et al. [37] investigated the application of single layered graphene sheets as resonant sensors in detection of ultra-fine nanoparticles via MD

and non-local elasticity approaches. To take into consideration the effect of geometric non-linearity, non-locality and atomic interactions between graphene sheets and nanoparticles, a nonlinear non-local plate model carrying an attached mass-spring system is introduced. MD simulations, are employed in order to calibrate the non-local small-scale parameter by matching frequency shifts obtained by non-local and MD simulation approaches. The field of research on nanoturbines is in the primary stages, a conceptual design proposed by Li et al. [38], composed of an single-wall carbon nanotube and graphene sheets. They studied the rotational motion of the proposed nanoturbine quantitatively by using MD simulations. This work attracted the attention of other researchers Shafiei et al. [39] who attempted to apply the non-local elasticity theory to perform vibration analysis of nanoturbine blade subjected to rotation effects of the nanoturbine. The previously mentioned works employed the non-local elasticity theory to model and design nanodevices which would offer support for the plausibility of this theory.

1.2 Vibration of cracked plates

The presence of a crack in a plate is a complicating effect that renders its mechanical behavior significantly different from that of an intact plate especially for the dynamic behavior. A crack can be defined as a geometric discontinuity in a solid body which is characterized by an initiation (or nucleation) point. Hence, The use of numerical methods is the most suitable approach to solve cracked structures problems, more precisely multi domain methods such as domain decomposition methods, finite element method (FEM) and its variants, which provides easy fitting of complex geometries and arbitrary combinations of boundary conditions (i.e., discontinuities, curves and irregular domains) by dividing the complex original geometric domain into a small number of manageable subdomains (i.e., elements). Plenty of research work has been performed on the computation of stress intensity factor (i.e., static analysis) for cracked local plates, However studies of cracked local plate free vibrations are comparatively little and absent for cracked nanoplates.

Most of the investigations in literature considered the classical plate theory (CPT) for thin plates to determine vibrational behavior of rectangular plates having cracks parallel to one of the edges, with simply supported conditions at all edges or two opposite edges. Stahl

and Keer [40] determined the natural frequencies of rectangular plates with mixed boundary conditions arising from a crack parallel and symmetric to two opposite edges using Fourier series, the resulted dual series equations are converted to homogeneous Fredholm integral equation to determine natural frequencies and mode shapes. Solecki [41] solved vibration problems of a rectangular, simply supported, isotropic plate by means of finite Fourier transformation of discontinuous functions, with a crack located parallel to one edge, symmetrically with respect to one symmetry axis which allowed the use of mixed boundary conditions to model the crack. While Hirano and Okazaki [42] studied the vibration problems of cracked rectangular plates with two opposite edges perpendicular to the line of the crack assumed to be simply supported, the Levy-Nadia's form of solution is employed and the weighted residual methods was used to establish the mixed boundary conditions on the line of the crack. The use of mixed boundary conditions to model a crack in the aforementioned works is limited to parallel and symmetrically positioned cracks with respect to one symmetry axis. Having that said, Liew et al. and Lee and Lim [43, 44] employed the Ritz method in conjunction with domain decomposition method to determine the vibration frequencies of cracked plates. Which enable the subdivision of cracked plate domain into a number of subdomains according to the crack location. These subdomains are assembled to form the complete domain through a continuity matrix. Although the studied cracks in this two papers are parallel to one edge, the model can be further extended to plates with cracks in any orientation as shown by Huang and Leissa [45, 46]. However a considerable amount of tedious procedure would be encountered to implement geometric transformation due to the inherit lack of automation of the method.

Several interesting studies used finite elements method variants to investigate the vibration and buckling of cracked plates using Kirchhoff (ie,. CPT) and Reissner-Mindlin plate theory. Qian et al. [47] generalized an FEM approach developed for beams in a previous paper [48] to two-dimensional structure. The stiffness matrix of the plate element with crack is obtained by a flexibility coefficient that is expressed by the stress intensity factor which is related to the additional strain energy caused by the presence of the crack. Krawczuk [49] employed a similar to the method described by Qian et al. [47] but contrary to their approach, the stiffness matrix of the element with a crack is presented in the closed form. Despite the fact that the two previously mentioned works [47, 49] are quite common

in literature and considered as the simplest model since it is based on reducing the elastic coefficients of the element at the crack location. The downside of this approaches is that the reduced elastic coefficients are not related to the geometry of the crack and the stress concentration around the crack tip is neglected.

The most promising and realistic approach is based on separating the nodes of the elements on both sides of the crack [50, 51]. In this approach the mesh has to be established so that element edges coincide with the crack lines and nodes must be placed on each side of the crack to allow material separation along the crack. This would provide realistic description of the geometric discontinuity of the crack and the singular nature of stresses and strains fields near the crack tip, the results obtained by this approach are highly accurate. However, a dense mesh around the crack tip is necessary (i.e., significant h-refinement) which increases the computational cost drastically and tedious amount of post processing tasks is required even with the use of highly developed software. Natarajan et al. [52] studied linear free vibrations of FGM plates with a through center crack using the finite element method based on FSDT and eight-nodes quadrilateral element (h-refinement and nodes separation). Alternatively the previously mentioned approach can be further optimized by employing special elements with singular shape functions [53, 54, 55, 56] that produces strain singularities with minimal mesh condensation when careful treatment is carried out.

Another thriving variants of FEM in modeling cracked structures is the generalized / extended finite element method (XFEM and GFEM) which are basically identical methods. In this method the mesh is completely independent of the crack surfaces and tip, contrary to h-FEM (standard FEM) where the element edges must fit to the crack geometry and duplicate nodes must be placed there. And since the singular aspects of stresses and strains fields are known for cracks, based on these fields, additional basis functions that approximate the near tip behavior are introduced to elements containing the crack. The advantage here is a convenient simulation of crack evolution because as a crack grows there is no need for re-meshing. Bachene et al. [57] adopted the extended finite element method (XFEM) to analyze vibrations of cracked plates, based on Mindlin's plate theory and taking into account rotatory inertia, where enriched elements by discontinuous functions proposed by Moës et

al. [58] are implemented. followed by another free vibration study [59] where isotropic homogeneous plates having a through crack located at various positions are studied. Natarajan et al. [60] performed the vibration analysis of cracked FGM (functionally graded material) plates using 4-noded quadrilateral plate element using XFEM based on first order shear deformation theory. their work studied rigorously the effect of crack length, crack location, crack orientation and gradient index of the material on the free flexural vibrations of the plates under various cases of boundary conditions. Although the first order shear deformation theory (FSDT) suffers from shear locking when implemented with FEM, this can be addressed by reduced integration on linear elements, or by using higher order elements (Reddy). However Bletzinger et al. [61] introduced the discrete shear gap method (DSG) as an efficient approach to prevent shear locking, Which has been integrated with XFEM by Yu et al. [62] to investigate vibration of cracked Mindlin plates.

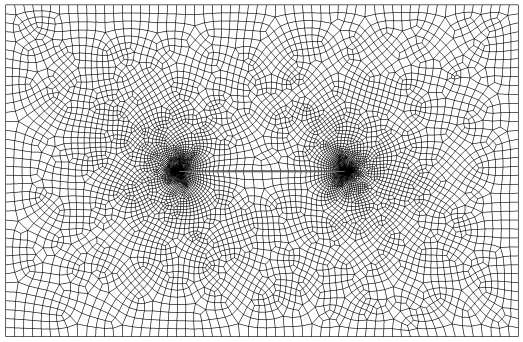

(a) h-version of finite element method (node separation)

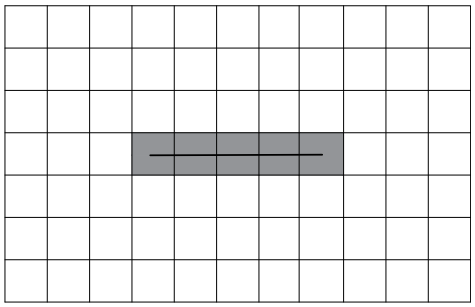

(b) extended finite element method, gray elements are enriched elements

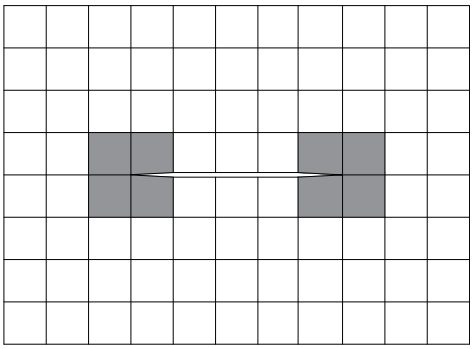

(c) h-p version of finite element method (node separation), gray elements are selectively p-refined elements

Figure 1.1: Discretization of a cracked plate with different variants of FEM

Other works exploited the advantage of higher-order inter-element continuity of isogeometric analysis (IGA) to studied the vibration of cracked plates. Tran et al. [63] employed extended isogemetric analysis (XIGA) to study the free vibration of cracked FGM plates based on HSDT. Yin et al. [64] studied the free vibration and buckling analysis of imperfect (i.e. crack and cutout) Reissner-Mindlin plate using XIGA. Further, Yu et al. [65] investigated the thermal buckling of functionally graded plates with internal defects (i.e., crack or cutout) by FSDT based XIGA. Tan et al. [66] employed XIGA in conjunction with two-variable refined plate theory to perform the dynamic analysis of cracked FGM

plate. Singh et al.[67] solved several isotropic cracked plates problems using XIGA based on HSDT.

The *h-p* version of finite element method (*h-p* FEM) is a combination of the conventional *h*-version and *p*-version, where convergence can be achieved by refining the mesh or/and increasing the degree of polynomial interpolation of the elements. Hence it inherits the merits of the flexibility of finite element method when modeling specific structural geometries, and enables the user to select an optimal choice of *h*-refinement and *p*-refinement. Based on numerical experience in linear elastic fracture mechanics Szabo et al. [68] found that the rate of convergence of *p*-refinement is substantially greater than that of *h*-refinement and requires substantially fewer degrees of freedom to achieve similar levels of precision. Consequently mesh density would be only dependent on the complexity of geometry (i.e. the minimum number of elements needed to fit crack edges) and not dependent on requirements of solution precision. Moreover *p*-refinement can be selectively applied only to elements around crack tip to capture the singular nature of stress and strain fields. However there is a paucity of literature on the vibrations of cracked plates using *h-p* FEM. Only two papers in the published literature applied *h-p* FEM on the vibrations of cracked plates. Bardell et al. [69] studied the natural frequencies and modes of laminated cantilever plate subjected to a through-the-thickness cracks along the center-line. And extended the geometric complication by studying free vibration of C shaped laminated plates having through-the-thickness corner cracks. Hadjoui et al. [70] investigated the free vibrations of triangular cracked orthotropic plates based on Mindlin's plate theory in the framework of *h-p* FEM, their study considered different crack lengths, locations and different angles of fiber orientation.

1.3 Summary

In this chapter, the literature about vibration of nanoplates using nonlocal elasticity and numerical methods used to model cracked plates was explored and discussed.

In section 1.1, the literature about the vibration of nanoplates and the different trends in models used were discussed. Among these models, the non-local elasticity theory seems to be of prime importance as it results in less computationally expensive simulations. The

overwhelming amount of research that is using non-local elasticity to model and design nanodevices, offers support for the plausibility of this theory. However, the calibration of the non-local parameter may be problematic.

Based on the observations in section 1.1, the following points are concluded:

- Scale effects plays a significant role in predicting behavior of nanostructures, thus the effect of non-local parameter will be investigated in this thesis.
- All previous work on vibration of nanoplates, considered only intact nanoplates, hence this thesis will further explore the vibration of cracked nanoplates.
- The nonlinear free vibration of nanoplates studies in literature are scarce, and consider only uncracked plates, thus in this work nonlinear vibration will be examined, to better understand non-linearity in cracked local/nonlocal plates.

As a mathematical model is the basis of studying mechanical systems, in section 1.2, the literature about a number of powerful methods for studying cracked plates were reviewed, and the limitations of these methods were discussed. For example, some of them are simple and based on reduction of the elastic coefficients at the crack location. However the geometry of the crack is not considered and the stress concentration at the crack tip is neglected. Other methods, suffer from the lack of automation and the need for extensive preprocessing. Based on the discussion in section 1.2, the following points are concluded:

- An accurate prediction of behavior of cracked structures requires a nodes separation approach. However, a dense mesh around the crack tip is required, hence a significant amount of preprocessing is used, thus in this work *h-p* FEM is employed to exploit its potential advantages in solving cracked plates problems.
- The *h-p* FEM is a promising method to model cracked structures due to its advantages inherited from *h*-version and *p*-version. However a lack of research on vibration cracked plates using *h-p* FEM is observed.

In the following chapter, an *h-p* FEM model is developed to model cracked nanoplates based on first order shear deformation theory and nonlocal elasticity theory.

Chapter 2

Preliminaries

In the previous chapter, a literature review has been conducted in order to convey what theories, numerical methods and approaches have been employed on the topic of vibration of nanoplates and vibration of cracked plates, and what their advantages and gaps. The aim of this chapter is to develop an *h-p* FEM model to solve linear/nonlinear cracked nanoplates problems based on first order shear deformation theory (FSDT) and nonlocal elasticity theory of Eringen.

In this chapter we:

- Introduce the concept of nonlocal elasticity and its mathematical description of interactions between points in a solid nano-structure.
- Employ nonlocal elasticity in conjunction with first order shear deformation plate theory (FSDT) to derive equations of motion of nonlocal plate.
- Present Functionally graded material effective properties.
- Use *h-p* FEM to discretize the obtained equations of motion, present numerical methods employed to construct and solve the discretized system and introduce computer implementation approaches used to efficiently conduct calculations.

2.1 Non-local elasticity theory

According to the non-local elasticity theory, the state of stress at a point $\mathbf{x}(x,y,z)$ in a material is given not only by the state of strain at that point, but also by the state of strain at all other points $\mathbf{x}'(x',y',z')$. This concept is consistent with the quantum physics description of interactions between atoms in material which considers that an certain atom is interacting locally with adjacent atoms and non-locally with remote atoms (see Figure 2.1).

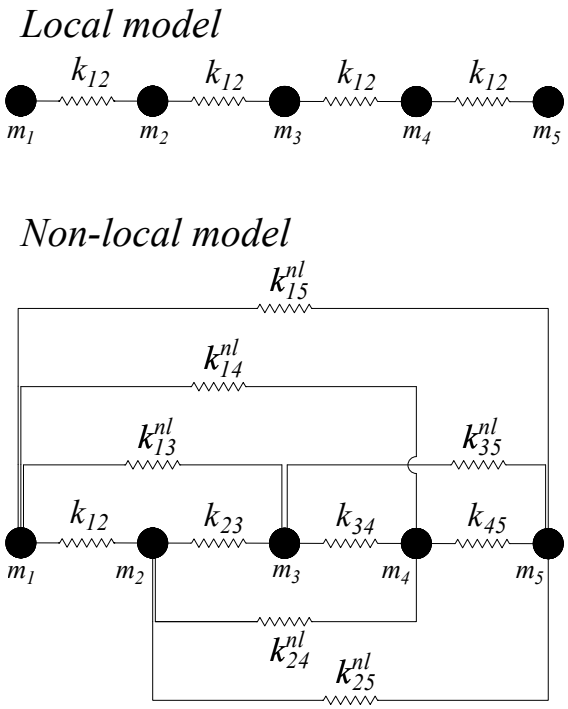

Figure 2.1: Mass spring discrete models illustrating difference between local and non-local concepts

Thus the non-locality or the non-local average of a local physical quantity field (e.g., stress) $\sigma_{ij}(x,y,z,t)$ in a domain Ω and time t is described by a weighted average formula [5]:

$$\overline{\sigma}_{ij}(x,y,z,t) = \int_{\Omega} \kappa\left(\left\|\mathbf{x}'-\mathbf{x}\right\|,\mu\right)\sigma_{ij}\left(x',y',z',t\right)dx'dy'dz' \quad / \quad \mu = \frac{e_0 l_i}{l_e} \tag{2.1}$$

Where $\overline{\sigma}_{ij}$ is the non-local stress component. κ is a continuous function called averaging kernel or the spatial non-local kernel, and μ is the non-local parameter which represent the rate of spatial decay of the averaging kernel κ, $e_0$is a non-dimensional parameter considered as a constant appropriate for the material, l_e is the external characteristic length that may refer to the size of the structure, l_i is the internal characteristic length that may refer to the spacing between atoms. For nano-structures, the external characteristic length is of the same order of magnitude as the internal one (i.e., $\frac{l_i}{l_e} \sim 1$). The non-local constitutive equation of elasticity can be written as [4]:

$$\overline{\sigma}_{ij}(x,y,z,t) = \int_{\Omega} \kappa\left(\left\|\mathbf{x}'-\mathbf{x}\right\|,\mu\right)E_{ijkl}\varepsilon_{kl}\left(x',y',z',t\right)dx'dy'dz' \tag{2.2}$$

The non-local kernels substantially affect the spatial distribution of the considered physical quantity (i.e., the spatial decay of the long range interactions). Therefore, a non-local kernel has the following essential properties [71]:

- It describes correctly the long-range inter-atomic interactions between material points by acquiring its maximum at $\mathbf{x}' = \mathbf{x}$ and decreasing rapidly to zero at large distances. Hence that non-local interactions are only effective in a finite vicinity of the point.

- When $\mu \to 0$ must revert to the Dirac delta function and the non-local elasticity reduces to the classical elasticity.

$$\lim_{\mu\to 0} \kappa\left(\left\|\mathbf{x}'-\mathbf{x}\right\|,\mu\right) = \hat{\delta}\left(\left\|\mathbf{x}'-\mathbf{x}\right\|\right) \tag{2.3}$$

- The non-local kernel is symmetric with respect to $\mathbf{x}$, i.e., $\kappa(\|\mathbf{x}'-\mathbf{x}\|,\mu) = \kappa(\|\mathbf{x}-\mathbf{x}'\|,\mu)$.

- Non-local kernel must be normalized so that their integrals over the domain of integration (line, surface, volume) give unity.

$$\int_{\Omega} \kappa\left(\left\|\mathbf{x}'-\mathbf{x}\right\|,\mu\right) dx\,dy\,dz = 1 \tag{2.4}$$

The above considerations further suggest that Eq.((2.1)) may be considered as the probabilistic average of σ_{ij}, if κ is considered to be a probability density function. Such a consideration resembles the method of analysis of quantum mechanics with the probability density function [2].

Based on the aforementioned proprieties of a non-local kernel, a handful of non-local kernels have been proposed in the literature like the cone-shaped function [5], the bell-shaped function [72], the Gaussian function [5], the exponential function [73], the atomistically-based kernel [74].

However mathematical difficulties emerges when solving non-local elasticity problems by directly using these kernels, since it involves integropartial differential equations. In order to overcome these difficulty, Eringen [75] proposed to replace the spatial integrals by differential operators, by assuming that the kernel κ is a Green's function Eq.(2.5) of a linear differential operator $\mathscr{L}$ [76].

$$\kappa\left(\left\|\mathbf{x}'-\mathbf{x}\right\|,\mu\right) = \frac{1}{2\pi\left(\mu l_e\right)^2} K_0\left(-\frac{\left\|\mathbf{x}'-\mathbf{x}\right\|}{\mu l_e}\right) \tag{2.5}$$

where K_0 is the modified Bessel's function of the second kind of order zero. The differential operator $\mathscr{L}$ has the following propriety Eq.((2.6))

$$\mathscr{L}\kappa\left(\left\|\mathbf{x}'-\mathbf{x}\right\|,\mu\right) = \hat{\delta}\left(\mathbf{x}'-\mathbf{x}\right) \tag{2.6}$$

Where $\hat{\delta}$ is the Dirac unit impulse. Applying operator $\mathscr{L}$ to Eq.((2.1)) leads to the following differential equation Eq.(2.7):

$$\mathscr{L}\overline{\sigma}_{ij}\left(x,y,z,t\right) = \sigma_{ij}\left(x',y',z',t\right) \tag{2.7}$$

Further more if $\mathscr{L}$ is a differential operator with constant coefficients, we have the following propriety [2]:

$$\frac{\partial}{\partial x_j}\left(\mathscr{L}\overline{\sigma}_{ij}\right) = \mathscr{L}\left(\frac{\partial \overline{\sigma}_{ij}}{\partial x_j}\right) \tag{2.8}$$

Applying operator $\mathscr{L}$ to the equation of motion of elastic solid body Eq.(2.9) and taking into account the previously mentioned proprieties, the equation of motion is reduced to the partial differential equation Eq.(2.10):

$$\frac{\partial \overline{\sigma}_{ij}}{\partial x_j} + f_i - \rho \frac{\partial^2 u_i}{\partial t^2} = 0 \tag{2.9}$$

$$\frac{\partial \sigma_{ij}}{\partial x_j} + \mathscr{L}\left(f_i - \rho \frac{\partial^2 u_i}{\partial t^2}\right) = 0 \tag{2.10}$$

The statement in Eq.(2.10) is by analogy equivalent to the following expression of Hamilton's principle (i.e., weak form)

$$\int_0^T \delta U + \delta V - \delta K = \int_0^T \int_\Omega \sigma_{ij}\delta\varepsilon_{ij} + \mathscr{L}\left(f_i\right)\delta u_i - \mathscr{L}\left(\rho \frac{\partial u_i}{\partial t}\right)\delta\left(\frac{\partial u_i}{\partial t}\right) dv dt = 0 \tag{2.11}$$

The obtained partial differential equation can be easily solved using well known analytical or numerical methods. That being said, the differential operator associated with the Green's function kernel proposed by Eringen is the Helmholtz operator, which is a second-order linear operator with constant coefficients expressed as [2]:

$$\mathscr{L} = 1 - \mu l_e^2 \nabla^2 \quad / \quad \nabla^2 = \sum_i \frac{\partial}{\partial x_i} \tag{2.12}$$

2.2 Non-local first order shear deformation theory

According to the first order shear deformation theory the displacement field u, v and w at a point (x, y, z) are defined as

$$\begin{cases} u(x,y,z,t) = & u_0 - z\theta_x(x,y,t) \\ v(x,y,z,t) = & v_0 - z\theta_y(x,y,t) \\ w(x,y,z,t) = & w_0(x,y,t) \end{cases} \tag{2.13}$$

where θ_x and θ_y are the rotation of transverse normal to the mid-plane about the x and y axes. The strain field is defined as

$$\begin{Bmatrix} \varepsilon_{xx} \\ \varepsilon_{yy} \\ \gamma_{yz} \\ \gamma_{xz} \\ \gamma_{xy} \end{Bmatrix} = \begin{Bmatrix} \varepsilon_{xx}^{(0)} \\ \varepsilon_{yy}^{(0)} \\ \gamma_{yz}^{(0)} \\ \gamma_{xz}^{(0)} \\ \gamma_{xy}^{(0)} \end{Bmatrix} + z \begin{Bmatrix} \varepsilon_{xx}^{(1)} \\ \varepsilon_{yy}^{(1)} \\ 0 \\ 0 \\ \gamma_{xy}^{(1)} \end{Bmatrix} = \begin{Bmatrix} \frac{\partial u_0}{\partial x} + \frac{1}{2}\left(\frac{\partial w_0}{\partial x}\right)^2 \\ \frac{\partial v_0}{\partial y} + \frac{1}{2}\left(\frac{\partial w_0}{\partial y}\right)^2 \\ \theta_y + \frac{\partial w_0}{\partial y} \\ \theta_x + \frac{\partial w_0}{\partial x} \\ \frac{\partial u_0}{\partial y} + \frac{\partial v_0}{\partial x} + \frac{\partial w_0}{\partial x}\frac{\partial w_0}{\partial y} \end{Bmatrix} + z \begin{Bmatrix} \frac{\partial \theta_x}{\partial x} \\ \frac{\partial \theta_y}{\partial y} \\ 0 \\ 0 \\ \frac{\partial \theta_x}{\partial y} + \frac{\partial \theta_y}{\partial x} \end{Bmatrix} \tag{2.14}$$

Using variational calculus we obtain virtual strains

$$\begin{Bmatrix} \delta\varepsilon_{xx}^{(0)} \\ \delta\varepsilon_{yy}^{(0)} \\ \delta\gamma_{yz}^{(0)} \\ \delta\gamma_{xz}^{(0)} \\ \delta\gamma_{xy}^{(0)} \end{Bmatrix} = \begin{Bmatrix} \delta\left(\frac{\partial u_0}{\partial x}\right) + \delta\left(\frac{\partial w_0}{\partial x}\right)\frac{\partial w_0}{\partial x} \\ \delta\left(\frac{\partial v_0}{\partial y}\right) + \delta\left(\frac{\partial w_0}{\partial y}\right)\frac{\partial w_0}{\partial y} \\ \delta\theta_y + \delta\left(\frac{\partial w_0}{\partial y}\right) \\ \delta\theta_x + \delta\left(\frac{\partial w_0}{\partial x}\right) \\ \delta\left(\frac{\partial u_0}{\partial y}\right) + \delta\left(\frac{\partial v_0}{\partial x}\right) + \delta\left(\frac{\partial w_0}{\partial x}\right)\frac{\partial w_0}{\partial y} + \frac{\partial w_0}{\partial x}\delta\left(\frac{\partial w_0}{\partial y}\right) \end{Bmatrix} \tag{2.15}$$

$$\begin{Bmatrix} \delta\varepsilon_{xx}^{(1)} \\ \delta\varepsilon_{yy}^{(1)} \\ 0 \\ 0 \\ \delta\gamma_{xy}^{(1)} \end{Bmatrix} = \begin{Bmatrix} \delta\left(\frac{\partial \theta_x}{\partial x}\right) \\ \delta\left(\frac{\partial \theta_y}{\partial y}\right) \\ 0 \\ 0 \\ \delta\left(\frac{\partial \theta_x}{\partial y}\right) + \delta\left(\frac{\partial \theta_y}{\partial x}\right) \end{Bmatrix} \tag{2.16}$$

where $\left(\varepsilon_{xx}^{(0)}, \varepsilon_{yy}^{(0)}, \gamma_{yz}^{(0)}, \gamma_{xz}^{(0)}, \gamma_{xy}^{(0)}\right)$ are the middle surface strain also known as membrane strains, and $\left(\varepsilon_{xx}^{(1)}, \varepsilon_{yy}^{(1)}, \gamma_{yz}^{(1)}, \gamma_{xz}^{(1)}, \gamma_{xy}^{(1)}\right)$ are the flexural strains.

$$\left\{\begin{array}{c}\sigma_{xx}\\ \sigma_{yy}\\ \sigma_{xy}\\ \sigma_{xz}\\ \sigma_{yz}\end{array}\right\} = \left(1-\mu\nabla^2\right)\left\{\begin{array}{c}\bar{\sigma}_{xx}\\ \bar{\sigma}_{yy}\\ \bar{\sigma}_{xy}\\ \bar{\sigma}_{xz}\\ \bar{\sigma}_{yz}\end{array}\right\} = \left[\begin{array}{ccccc} C_{11} & C_{12} & 0 & 0 & 0\\ C_{21} & C_{22} & 0 & 0 & 0\\ 0 & 0 & C_{66} & 0 & 0\\ 0 & 0 & 0 & \kappa_s C_{55} & 0\\ 0 & 0 & 0 & 0 & \kappa_s C_{44}\end{array}\right]\left\{\begin{array}{c}\varepsilon_{xx}\\ \varepsilon_{yy}\\ \gamma_{xy}\\ \gamma_{xz}\\ \gamma_{yz}\end{array}\right\} \tag{2.17}$$

where $\mu = (e_0 l_i)^2$ denotes the nonlocal parameter in terms of a material constant e_0 and the internal characteristic length l_i, C_{ij} are coefficients of the elastic matrix $[C]$ given by

$$\left\{\begin{array}{l} C_{11}(z) = C_{22}(z) = \dfrac{E_f(z)}{1-v_f^2(z)}\\ C_{12}(z) = v_f(z) C_{11}\\ C_{44}(z) = C_{55}(z) = C_{66}(z) = \dfrac{E_f(z)}{2\left(1+v_f(z)\right)}\end{array}\right. \tag{2.18}$$

where $E_f(z)$ and $v_f(z)$ are Young's modulus and Poisson's ratio respectively. κ_s is the shear correction factor taken as $5/6$ [77].

The governing equation for the first-order plate theory can be obtained using Hamilton's principle

$$\int_0^T \delta U - \delta K = 0 \tag{2.19}$$

Where δU and δK are the virtual strain and kinetic energy, the virtual strain energy δU is expressed as:

$$\delta U = \int_\Omega \left\{ \int_{-\frac{h}{2}}^{\frac{h}{2}} \left[\sigma_{xx}\delta\varepsilon_{xx} + \sigma_{yy}\delta\varepsilon_{yy} + \sigma_{xy}\delta\gamma_{xy} + \sigma_{xz}\delta\gamma_{xz} + \sigma_{yz}\delta\gamma_{yz}\right] dz \right\} dxdy \tag{2.20}$$

Substituting Eqs.(2.14-2.17) into Eq.(2.20) we obtain the expression for the virtual strain energy.

$$\begin{aligned}\delta U = \int_{\Omega} \Bigg\{ & N_{xx}\left(\delta\left(\frac{\partial u_0}{\partial x}\right)+\delta\left(\frac{\partial w_0}{\partial x}\right)\frac{\partial w_0}{\partial x}\right)+N_{yy}\left(\delta\left(\frac{\partial v_0}{\partial y}\right)+\delta\left(\frac{\partial w_0}{\partial y}\right)\frac{\partial w_0}{\partial y}\right) \\ & +N_{xy}\left(\delta\left(\frac{\partial u_0}{\partial y}\right)+\delta\left(\frac{\partial v_0}{\partial x}\right)+\delta\left(\frac{\partial w_0}{\partial x}\right)\frac{\partial w_0}{\partial y}+\frac{\partial w_0}{\partial x}\delta\left(\frac{\partial w_0}{\partial y}\right)\right) \\ & +M_{xx}\delta\left(\frac{\partial \theta_x}{\partial x}\right)+M_{yy}\delta\left(\frac{\partial \theta_y}{\partial y}\right)+M_{xy}\left(\delta\left(\frac{\partial \theta_x}{\partial y}\right)+\delta\left(\frac{\partial \theta_y}{\partial x}\right)\right) \\ & +Q_x\left(\delta\theta_x+\delta\left(\frac{\partial w_0}{\partial x}\right)\right)+Q_y\left(\delta\theta_y+\delta\left(\frac{\partial w_0}{\partial y}\right)\right)\Bigg\}dxdy \end{aligned} \tag{2.21}$$

N, M, Q are the stress resultant forces and moments expressed as follows

$$\begin{Bmatrix} N_{xx} \\ N_{yy} \\ N_{xy} \end{Bmatrix} = \begin{bmatrix} A_{11} & A_{12} & 0 \\ A_{12} & A_{22} & 0 \\ 0 & 0 & A_{66} \end{bmatrix} \begin{Bmatrix} \varepsilon_{xx}^{(0)} \\ \varepsilon_{yy}^{(0)} \\ \varepsilon_{xy}^{(0)} \end{Bmatrix} + \begin{bmatrix} B_{11} & B_{12} & 0 \\ B_{12} & B_{22} & 0 \\ 0 & 0 & B_{66} \end{bmatrix} \begin{Bmatrix} \varepsilon_{xx}^{(1)} \\ \varepsilon_{yy}^{(1)} \\ \varepsilon_{xy}^{(1)} \end{Bmatrix} \tag{2.22}$$

$$\begin{Bmatrix} M_{xx} \\ M_{yy} \\ M_{xy} \end{Bmatrix} = \begin{bmatrix} B_{11} & B_{12} & 0 \\ B_{12} & B_{22} & 0 \\ 0 & 0 & B_{66} \end{bmatrix} \begin{Bmatrix} \varepsilon_{xx}^{(0)} \\ \varepsilon_{yy}^{(0)} \\ \varepsilon_{xy}^{(0)} \end{Bmatrix} + \begin{bmatrix} D_{11} & D_{12} & 0 \\ D_{12} & D_{22} & 0 \\ 0 & 0 & D_{66} \end{bmatrix} \begin{Bmatrix} \varepsilon_{xx}^{(1)} \\ \varepsilon_{yy}^{(1)} \\ \varepsilon_{xy}^{(1)} \end{Bmatrix} \tag{2.23}$$

$$\begin{Bmatrix} Q_y^l \\ Q_x^l \end{Bmatrix} = \kappa_s \begin{bmatrix} A_{44} & 0 \\ 0 & A_{55} \end{bmatrix} \begin{Bmatrix} \gamma_{yz}^{(0)} \\ \gamma_{xz}^{(0)} \end{Bmatrix} \tag{2.24}$$

where A_{ij} are extensional stiffness coefficients, D_{ij} are bending stiffness coefficients and B_{ij} are bending-extensional coupling stiffness, which are defined as

$$A_{ij} = \int_{-\frac{h}{2}}^{\frac{h}{2}} C_{ij}(z)\, dz \tag{2.25}$$

$$B_{ij} = \int_{-\frac{h}{2}}^{\frac{h}{2}} z C_{ij}(z)\, dz \tag{2.26}$$

$$D_{ij} = \int_{-\frac{h}{2}}^{\frac{h}{2}} z^2 C_{ij}(z)\, dz \tag{2.27}$$

For an isotropic material Young's modulus E and Poisson's ratio ν are *constants* through the plate thickness, hence stiffness coefficients yields

$$A_{ij} = hC_{ij}, \tag{2.28}$$

$$B_{ij} = 0, \tag{2.29}$$

$$D_{ij} = \frac{h^3}{12} C_{ij} \tag{2.30}$$

The virtual kinetic energy δK is expressed as:

$$\delta K = \int_{\Omega} \left(1 - \mu\nabla^2\right) \int_{-\frac{h}{2}}^{\frac{h}{2}} \rho(z) \left(\delta\dot{u}\dot{u} + \delta\dot{v}\dot{v} + \delta\dot{w}\dot{w}\right) dz dx dy \tag{2.31}$$

Substituting displacement field relation Eq.(2.1) into Eq.(2.31) we obtain the expression for the virtual kinetic energy.

$$\begin{aligned}\delta K = & \int_{\Omega} \left(1 - \mu\nabla^2\right) I_0 \left(\delta\dot{u}_0\dot{u}_0 + \delta\dot{v}_0\dot{v}_0 + \delta\dot{w}_0\dot{w}_0\right) \\ & + I_1 \left(\delta\dot{u}_0\dot{\theta}_x + \delta\dot{v}_0\dot{\theta}_y + \delta\dot{\theta}_x\dot{u}_0 + \delta\dot{\theta}_y\dot{v}_0\right) \\ & + I_2 \left(\delta\dot{\theta}_x\dot{\theta}_x + \delta\dot{\theta}_y\dot{\theta}_y\right) dx dy\end{aligned} \tag{2.32}$$

I_0, I_1 and I_2 are the mass moments of inertia expressed as

$$I_0 = \int_{-\frac{h}{2}}^{\frac{h}{2}} \rho\,(z)\,dz \tag{2.33}$$

$$I_1 = \int_{-\frac{h}{2}}^{\frac{h}{2}} \rho\,(z)\,z\,dz \tag{2.34}$$

$$I_2 = \int_{-\frac{h}{2}}^{\frac{h}{2}} \rho\,(z)\,z^2\,dz \tag{2.35}$$

Using Eqs.(2.22-2.24) and Eq.(2.19) the weak form of the governing equation of motion is obtained Eq.(2.36) after performing both spatial and time integration-by-parts.

$$\begin{aligned}
0=&\int_0^T \int_\Omega \frac{\partial \delta u_0}{\partial x}\left(A_{11}\frac{\partial u_0}{\partial x}+A_{12}\frac{\partial v_0}{\partial y}+B_{11}\frac{\partial \theta_x}{\partial x}+B_{12}\frac{\partial \theta_y}{\partial y}\right)\\
&+\frac{\partial \delta v_0}{\partial y}\left(A_{12}\frac{\partial u_0}{\partial x}+A_{22}\frac{\partial v_0}{\partial y}+B_{12}\frac{\partial \theta_x}{\partial x}+B_{22}\frac{\partial \theta_y}{\partial y}\right)\\
&+\left(\frac{\partial \delta u_0}{\partial y}+\frac{\partial \delta v_0}{\partial x}\right)\left(A_{66}\left(\frac{\partial u_0}{\partial y}+\frac{\partial v_0}{\partial x}\right)+B_{66}\left(\frac{\partial \theta_x}{\partial y}+\frac{\partial \theta_y}{\partial x}\right)\right)\\
&+\left(\frac{\partial \delta w_0}{\partial x}+\delta\theta_x\right)A_{55}\left(\theta_x+\frac{\partial w_0}{\partial x}\right)+\left(\frac{\partial \delta w_0}{\partial y}+\delta\theta_y\right)A_{44}\left(\theta_y+\frac{\partial w_0}{\partial y}\right)\\
&+\frac{\partial \delta \theta_x}{\partial x}\left(B_{11}\frac{\partial u_0}{\partial x}+B_{12}\frac{\partial v_0}{\partial y}+D_{11}\frac{\partial \theta_x}{\partial x}+D_{12}\frac{\partial \theta_y}{\partial y}\right)\\
&+\frac{\partial \delta \theta_y}{\partial y}\left(B_{12}\frac{\partial u_0}{\partial x}+B_{22}\frac{\partial v_0}{\partial y}+D_{12}\frac{\partial \theta_x}{\partial x}+D_{22}\frac{\partial \theta_y}{\partial y}\right)\\
&+\left(\frac{\partial \delta \theta_x}{\partial y}+\frac{\partial \delta \theta_y}{\partial x}\right)\left(B_{66}\left(\frac{\partial u_0}{\partial y}+\frac{\partial v_0}{\partial x}\right)+D_{66}\left(\frac{\partial \theta_x}{\partial y}+\frac{\partial \theta_y}{\partial x}\right)\right)\\
&+\aleph\,(u_0,v_0,w_0,\theta_x,\theta_y)\,dxdydt-\int_0^T\int_\Omega I_0\,(\delta u_0\ddot{u}_0+\delta v_0\ddot{v}_0+\delta w_0\ddot{w}_0)
\end{aligned}$$

$$
\begin{aligned}
&+I_1\left(\delta u_0\ddot{\theta}_x+\delta v_0\ddot{\theta}_y+\delta\theta_x\ddot{u}_0+\delta\theta_y\ddot{v}_0\right)+I_2\left(\delta\theta_x\ddot{\theta}_x+\delta\theta_y\ddot{\theta}_y\right)\\
&+4\mu\left[I_0\left(\frac{\partial\delta u_0}{\partial x}\frac{\partial\ddot{u}_0}{\partial x}+\frac{\partial\delta u_0}{\partial y}\frac{\partial\ddot{u}_0}{\partial y}+\frac{\partial\delta v_0}{\partial x}\frac{\partial\ddot{v}_0}{\partial x}\right.\right.\\
&\left.+\frac{\partial\delta v_0}{\partial y}\frac{\partial\ddot{v}_0}{\partial y}+\frac{\partial\delta w_0}{\partial x}\frac{\partial\ddot{w}_0}{\partial x}+\frac{\partial\delta w_0}{\partial y}\frac{\partial\ddot{w}_0}{\partial y}\right)\\
&+I_1\left(\frac{\partial\delta u_0}{\partial x}\frac{\partial\ddot{\theta}_x}{\partial x}+\frac{\partial\delta u_0}{\partial y}\frac{\partial\ddot{\theta}_x}{\partial y}+\frac{\partial\delta v_0}{\partial x}\frac{\partial\ddot{\theta}_y}{\partial x}+\frac{\partial\delta v_0}{\partial y}\frac{\partial\ddot{\theta}_y}{\partial y}\right.\\
&\left.\left.+\frac{\partial\delta\theta_x}{\partial x}\frac{\partial\ddot{u}_0}{\partial x}+\frac{\partial\delta\theta_x}{\partial y}\frac{\partial\ddot{u}_0}{\partial y}+\frac{\partial\delta\theta_y}{\partial x}\frac{\partial\ddot{v}_0}{\partial x}+\frac{\partial\delta\theta_y}{\partial y}\frac{\partial\ddot{v}_0}{\partial y}\right)\right]\\
&+I_2\left(\frac{\partial\delta\theta_x}{\partial x}\frac{\partial\ddot{\theta}_x}{\partial x}+\frac{\partial\delta\theta_x}{\partial y}\frac{\partial\ddot{\theta}_x}{\partial y}+\frac{\partial\delta\theta_y}{\partial x}\frac{\partial\ddot{\theta}_y}{\partial x}+\frac{\partial\delta\theta_y}{\partial y}\frac{\partial\ddot{\theta}_y}{\partial y}\right)dxdydt
\end{aligned}
\tag{2.36}
$$

Where $\aleph\left(u_0,v_0,w_0,\theta_x,\theta_y\right)$ is the nonlinear part expressed as:

$$
\begin{aligned}
&\aleph\left(u_0,v_0,w_0,\theta_x,\theta_y\right)=\frac{1}{2}\left[\frac{\partial\delta u_0}{\partial x}\left(A_{11}\left(\frac{\partial w_0}{\partial x}\right)^2+A_{12}\left(\frac{\partial w_0}{\partial y}\right)^2\right)\right.\\
&+\frac{\partial\delta v_0}{\partial y}\left(A_{12}\left(\frac{\partial w_0}{\partial x}\right)^2+A_{22}\left(\frac{\partial w_0}{\partial y}\right)^2\right)+\frac{\partial\delta\theta_x}{\partial x}\left(B_{11}\left(\frac{\partial w_0}{\partial x}\right)^2\right.\\
&\left.+B_{12}\left(\frac{\partial w_0}{\partial y}\right)^2\right)+\frac{\partial\delta\theta_y}{\partial y}\left(B_{12}\left(\frac{\partial w_0}{\partial x}\right)^2+B_{22}\left(\frac{\partial w_0}{\partial y}\right)^2\right)\Bigg]\\
&+\left(A_{66}\left(\frac{\partial\delta u_0}{\partial y}+\frac{\partial\delta v_0}{\partial x}\right)+B_{66}\left(\frac{\partial\delta\theta_x}{\partial y}+\frac{\partial\delta\theta_y}{\partial x}\right)\right)\frac{\partial w_0}{\partial x}\frac{\partial w_0}{\partial y}\\
&+\frac{\partial\delta w_0}{\partial x}\frac{\partial w_0}{\partial x}\left(A_{11}\left(\frac{\partial u_0}{\partial x}+\frac{1}{2}\left(\frac{\partial w_0}{\partial x}\right)^2\right)+A_{12}\left(\frac{\partial v_0}{\partial y}+\frac{1}{2}\left(\frac{\partial w_0}{\partial y}\right)^2\right)\right.\\
&\left.+B_{11}\frac{\partial\theta_x}{\partial x}+B_{12}\frac{\partial\theta_y}{\partial y}\right)+\frac{\partial\delta w_0}{\partial y}\frac{\partial w_0}{\partial y}\left(A_{12}\left(\frac{\partial u_0}{\partial x}+\frac{1}{2}\left(\frac{\partial w_0}{\partial x}\right)^2\right)\right.\\
&+A_{22}\left(\frac{\partial v_0}{\partial y}+\frac{1}{2}\left(\frac{\partial w_0}{\partial y}\right)^2\right)+B_{12}\frac{\partial\theta_x}{\partial x}+B_{22}\frac{\partial\theta_y}{\partial y}\Bigg)+\left(\frac{\partial\delta w_0}{\partial x}\frac{\partial w_0}{\partial y}\right.\\
&\left.\left.+\frac{\partial\delta w_0}{\partial y}\frac{\partial w_0}{\partial x}\right)\left(A_{66}\left(\frac{\partial u_0}{\partial y}+\frac{\partial v_0}{\partial x}+\frac{\partial w_0}{\partial x}\frac{\partial w_0}{\partial y}\right)+B_{66}\left(\frac{\partial\theta_x}{\partial y}+\frac{\partial\theta_y}{\partial x}\right)\right)\right.
\end{aligned}
\tag{2.37}
$$

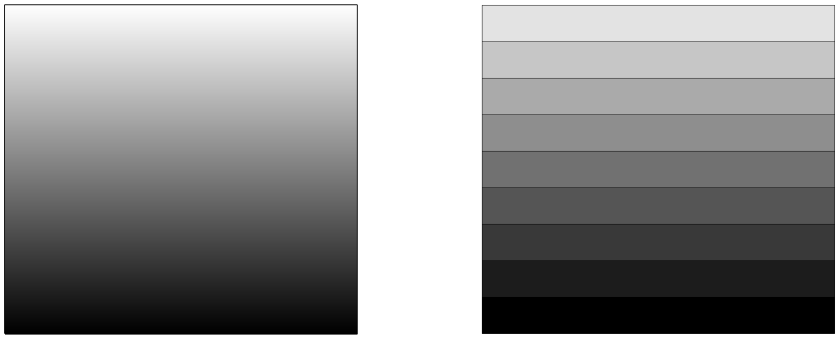

(a) continuous variation (b) discrete variation

Figure 2.2: Volume fraction variation models

2.3 Functionally graded materials effective properties

Various FGMs are composed of two phases of different materials usually ceramic and metal. Where the volume fraction of each phase gradually varies in a given direction (e.g., thickness direction), consequently the effective properties of FGMs change along this direction.

Volume fraction variation is modeled with one of two approaches: discrete variation and continuous variation. When the discrete variation of the volume fraction of ceramic or metal is assumed, the FGM is considered to be layered with constant volume fraction for each region also called quasi-homogeneous ceramic–metal layers (Figure 2.2b).

For the continuous variation of the volume fraction of ceramic or metal (Figure 2.2a), the metal and ceramic volume fractions expressed by the following function of the thickness coordinate z.

$$V_m = \left(\frac{2z+h}{2h}\right)^n \tag{2.38}$$

$$V_c = 1 - V_m \tag{2.39}$$

$$-\frac{h}{2} \leq z \leq \frac{h}{2} \;\; 0 \leq n < +\infty$$

where h is the thickness of the structure, and n is a volume fraction exponent that represent the material variation profile through the thickness2.3.

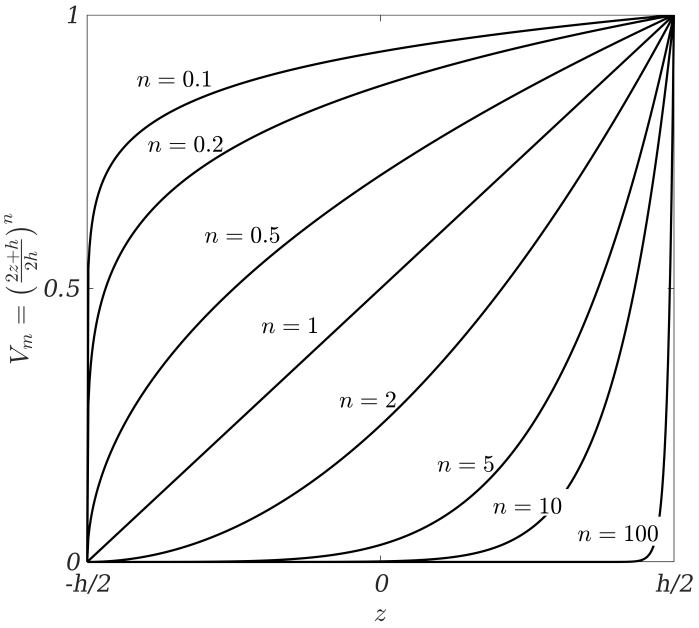

Figure 2.3: Metal volume fraction variation profile through the thickness

The distribution of effective material properties $\mathbb{P}_f(z)$ of the isotropic FGM layer, like Young's modulus $E_f(z)$, and Poisson's ratio ν_f can then be expressed as

$$\mathbb{P}_f(z) = \mathbb{P}_m V_m(z) + \mathbb{P}_c V_c(z) \tag{2.40}$$

However it is necessary to consider temperature-dependency for accurate prediction of the mechanical response, since FGMs are often employed in high-temperature environments that introduce notable changes in properties of constituent materials [78]. Thus, a constituent material property is temperature dependent and can be expressed as [79]:

$$\mathbb{P}_j(T) = P_0\left(P_{-1}T^{-1} + 1 + P_1T + P_2T^2 + P_3T^3\right) \tag{2.41}$$

where P_{-1}, P_0, P_1, P_2, and P_3 are the coefficients of temperature $T(K)$ and are unique to a constituent material j. From Eqs.(2.38-2.41) we have [80]:

$$E_f(z,T) = (E_m(T) - E_c(T))\left(\frac{2z+h}{2h}\right)^n + E_c(T) \tag{2.42}$$

$$\nu_f(z,T) = (\nu_m(T) - \nu_c(T))\left(\frac{2z+h}{2h}\right)^n + \nu_c(T) \tag{2.43}$$

Table 2.1 (from [78]) contains values of coefficients for Young's modulus and Poisson's ratio of some ceramics and metals.

2.4 Finite element model of non-local FSDT

The finite elements method consists of employing an interpolation by subdomains (i.e., elements) on unknown field variables (e.g., displacement, temperature, velocity ... etc) in order to transform integral equations (i.e., weak formulation) derived from partial differential equations (i.e., strong formulation) into a system of algebraic equations. Relating at least three branches of knowledge, engineering science to derive partial differential equations or integral equations of studied physical system, numerical methods to construct and solve algebraic equations and programming and software development to efficiently conduct calculations on a machine [81]. In this section finite element model for FSDT non-local plates is developed.

Table 2.1: Coefficients for Young's Modulus E_f and Poisson's ratio ν_f of ceramics and metals

Materials	P_0	P_{-1}	P_1	P_2	P_3
			Young's Modulus		
Zirconia	244.27e+9	0.0	-1.371e-3	1.214e-6	-3.681e-10
Aluminum oxide	349.55e+9	0.0	-3.853e-4	4.027e-7	-1.673e-10
Silicon nitride	348.48e+9	0.0	-3.070e-4	2.160e-7	-8.946e-11
Ti-6Al-4V	122.56e+9	0.0	-4.586e-4	0.0	0.0
Stainless steel	201.04e+9	0.0	3.079e-4	-6.534e-7	0.0
Nickel	223.95e+9	0.0	-2.794e-4	-3.998e-9	0.0
			Poisson's ratio		
Zirconia	0.2882	0.0	1.133e-4	0.0	0.0
Aluminum oxide	0.2600	0.0	0.0	0.0	0.0
Silicon nitride	0.2400	0.0	0.0	0.0	0.0
Ti-6Al-4V	0.2884	0.0	1.121e-4	0.0	0.0
Stainless steel	0.3262	0.0	-2.002e-4	3.797e-7	0.0
Nickel	0.3100	0.0	0.0	0.0	0.0

Source: Reddy and Chin [77]

Supposing that the dependent field variables $(u_0, v_0, w_0, \theta_x, \theta_y)$ are approximated over a finite element Ω^e by:

$$u_0(x,y,t) = \tau_1(t) \sum_{i=1}^{n} \varphi_i(x,y)\, q_{5i-4} v_0(x,y,t) = \tau_2(t) \sum_{i=1}^{n} \varphi_i(x,y)\, q_{5i-3} \tag{2.44}$$

$$w_0(x,y,t) = \tau_3(t) \sum_{i=1}^{n} \varphi_i(x,y)\, q_{5i-2} \tag{2.45}$$

$$\theta_x(x,y,t) = \tau_4(t) \sum_{i=1}^{n} \varphi_i(x,y)\, q_{5i-1} \theta_y(x,y,t) = \tau_5(t) \sum_{i=1}^{n} \varphi_i(x,y)\, q_{5i} \tag{2.46}$$

Assuming that the plate response is periodic, where τ_i $(i = 1,2,...,5)$ are the time functions taken as [82, 83].

$$\tau_1 = \tau_2 = \tau_3^2 = \tau_4^2 = \tau_5^2 = cos^2 \omega t \tag{2.47}$$

Substituting approximations Eqs.(2.44-2.46) for $(u_0, v_0, w_0, \theta_x, \theta_y)$ and their derivatives into Eq.(2.36), we obtain a system of algebraic equations of the form:

$$[M]\{\ddot{\tau} q\} + [K(\tau, q)]\{q\} = 0 \tag{2.48}$$

Using time functions Eq.(2.47), since Eq.(2.48) is a third order function of $\{q\}$ and $cos^3 \omega t = \frac{3}{4} cos \omega t + \frac{1}{4} cos 3\omega t$, applying the harmonic balance method and neglecting higher harmonic component, The resulting equation is a standard eigenvalue equation

$$-\omega^2 [M]\{q\} + [K_L + K_{NL}(q)]\{q\} = 0 \tag{2.49}$$

where $[M]$ is the element mass matrix,$[K_L]$ is linear stiffness matrix and $[K_{NL}]$ is non-linear stiffness matrix. This matrices can be arranged as follow

$$[M] = \begin{bmatrix} \left[\mathbb{M}^{11}\right] & [0] & [0] & \left[\mathbb{M}^{14}\right] & [0] \\ [0] & \left[\mathbb{M}^{22}\right] & [0] & [0] & \left[\mathbb{M}^{25}\right] \\ [0] & [0] & \left[\mathbb{M}^{33}\right] & [0] & [0] \\ \left[\mathbb{M}^{41}\right] & [0] & [0] & \left[\mathbb{M}^{44}\right] & [0] \\ [0] & \left[\mathbb{M}^{52}\right] & [0] & [0] & \left[\mathbb{M}^{55}\right] \end{bmatrix}^e \tag{2.50}$$

$$[K_L] = \begin{bmatrix} \left[\mathbb{K}^{11}\right] & \left[\mathbb{K}^{12}\right] & [0] & \left[\mathbb{K}^{14}\right] & \left[\mathbb{K}^{15}\right] \\ \left[\mathbb{K}^{12}\right]^T & \left[\mathbb{K}^{22}\right] & [0] & \left[\mathbb{K}^{24}\right] & \left[\mathbb{K}^{25}\right] \\ [0] & [0] & \left[\mathbb{K}^{33}\right] & \left[\mathbb{K}^{34}\right] & \left[\mathbb{K}^{35}\right] \\ \left[\mathbb{K}^{14}\right]^T & \left[\mathbb{K}^{24}\right]^T & \left[\mathbb{K}^{43}\right] & \left[\mathbb{K}^{44}\right] & \left[\mathbb{K}^{45}\right] \\ \left[\mathbb{K}^{15}\right]^T & \left[\mathbb{K}^{25}\right]^T & \left[\mathbb{K}^{53}\right] & \left[\mathbb{K}^{54}\right] & \left[\mathbb{K}^{55}\right] \end{bmatrix}^e \tag{2.51}$$

$$[K_{NL}] = \frac{3}{4} \begin{bmatrix} [0] & [0] & \left[\widetilde{\mathbb{K}}^{13}\right] & [0] & [0] \\ [0] & [0] & \left[\widetilde{\mathbb{K}}^{23}\right] & [0] & [0] \\ 2\left[\widetilde{\mathbb{K}}^{13}\right]^T & 2\left[\widetilde{\mathbb{K}}^{23}\right]^T & \left[\widetilde{\mathbb{K}}^{33}\right] & [0] & [0] \\ [0] & [0] & [0] & [0] & [0] \\ [0] & [0] & [0] & [0] & [0] \end{bmatrix}^e \tag{2.52}$$

$$\left[\mathbb{M}^{11}_{i,j}\right] = \left[\mathbb{M}^{22}_{i,j}\right] = \left[\mathbb{M}^{33}_{i,j}\right] = I_0 S_{ij} \tag{2.53}$$

$$\left[\mathbb{M}^{44}_{i,j}\right] = \left[\mathbb{M}^{55}_{i,j}\right] = I_2 S_{ij} \tag{2.54}$$

$$\left[\mathbb{M}^{14}_{i,j}\right] = \left[\mathbb{M}^{25}_{i,j}\right] = \left[\mathbb{M}^{25}_{i,j}\right]^T = \left[\mathbb{M}^{25}_{i,j}\right]^T = I_1 S_{ij} \tag{2.55}$$

$$S_{ij} = \int_{\Omega} \varphi_i \varphi_j + 4\mu \left(\frac{\partial \varphi_i}{\partial x} \frac{\partial \varphi_j}{\partial x} + \frac{\partial \varphi_i}{\partial y} \frac{\partial \varphi_j}{\partial y} \right) dxdy \tag{2.56}$$

$$\left[\mathbb{K}_{i,j}^{11}\right] = \int_{\Omega} A_{11}\frac{\partial \varphi_i}{\partial x}\frac{\partial \varphi_j}{\partial x} + A_{66}\frac{\partial \varphi_i}{\partial y}\frac{\partial \varphi_j}{\partial y}dxdy \tag{2.57}$$

$$\left[\mathbb{K}_{i,j}^{12}\right] = \int_{\Omega} A_{12}\frac{\partial \varphi_i}{\partial x}\frac{\partial \varphi_j}{\partial y} + A_{66}\frac{\partial \varphi_i}{\partial y}\frac{\partial \varphi_j}{\partial x}dxdy = \left[\mathbb{K}_{i,j}^{21}\right]^T \tag{2.58}$$

$$\left[\mathbb{K}_{i,j}^{14}\right] = \int_{\Omega} B_{11}\frac{\partial \varphi_i}{\partial x}\frac{\partial \varphi_j}{\partial x} + B_{66}\frac{\partial \varphi_i}{\partial y}\frac{\partial \varphi_j}{\partial y}dxdy = \left[\mathbb{K}_{i,j}^{41}\right]^T \tag{2.59}$$

$$\left[\mathbb{K}_{i,j}^{15}\right] = \int_{\Omega} B_{12}\frac{\partial \varphi_i}{\partial x}\frac{\partial \varphi_j}{\partial y} + B_{66}\frac{\partial \varphi_i}{\partial y}\frac{\partial \varphi_j}{\partial x}dxdy = \left[\mathbb{K}_{i,j}^{51}\right]^T \tag{2.60}$$

$$\left[\mathbb{K}_{i,j}^{22}\right] = \int_{\Omega} A_{22}\frac{\partial \varphi_i}{\partial y}\frac{\partial \varphi_j}{\partial y} + A_{66}\frac{\partial \varphi_i}{\partial x}\frac{\partial \varphi_j}{\partial x}dxdy \tag{2.61}$$

$$\left[\mathbb{K}_{i,j}^{24}\right] = \int_{\Omega} B_{12}\frac{\partial \varphi_i}{\partial y}\frac{\partial \varphi_j}{\partial x} + B_{66}\frac{\partial \varphi_i}{\partial x}\frac{\partial \varphi_j}{\partial y}dxdy = \left[\mathbb{K}_{i,j}^{42}\right]^T \tag{2.62}$$

$$\left[\mathbb{K}_{i,j}^{25}\right] = \int_{\Omega} B_{22}\frac{\partial \varphi_i}{\partial y}\frac{\partial \varphi_j}{\partial y} + B_{66}\frac{\partial \varphi_i}{\partial x}\frac{\partial \varphi_j}{\partial x}dxdy = \left[\mathbb{K}_{i,j}^{52}\right]^T \tag{2.63}$$

$$\left[\mathbb{K}_{i,j}^{33}\right] = \int_{\Omega} \kappa_s A_{55}\frac{\partial \varphi_i}{\partial x}\frac{\partial \varphi_j}{\partial x} + \kappa_s A_{44}\frac{\partial \varphi_i}{\partial y}\frac{\partial \varphi_j}{\partial y}dxdy \tag{2.64}$$

$$\left[\mathbb{K}_{i,j}^{34}\right] = \int_{\Omega} \kappa_s A_{55}\frac{\partial \varphi_i}{\partial x}\varphi_j dxdy = \left[\mathbb{K}_{i,j}^{43}\right]^T \tag{2.65}$$

$$\left[\mathbb{K}_{i,j}^{35}\right] = \int_{\Omega} \kappa_s A_{44}\frac{\partial \varphi_i}{\partial y}\varphi_j dxdy = \left[\mathbb{K}_{i,j}^{53}\right]^T \tag{2.66}$$

$$\left[\mathbb{K}_{i,j}^{44}\right] = \int_{\Omega} \kappa_s A_{55}\varphi_i\varphi_j + D_{11}\frac{\partial \varphi_i}{\partial x}\frac{\partial \varphi_j}{\partial x} + D_{66}\frac{\partial \varphi_i}{\partial y}\frac{\partial \varphi_j}{\partial y}dxdy \tag{2.67}$$

$$\left[\mathbb{K}_{i,j}^{45}\right] = \int_{\Omega} D_{12}\frac{\partial \varphi_i}{\partial x}\frac{\partial \varphi_j}{\partial y} + D_{66}\frac{\partial \varphi_i}{\partial y}\frac{\partial \varphi_j}{\partial x}dxdy = \left[\mathbb{K}_{i,j}^{54}\right]^T \tag{2.68}$$

$$\left[\mathbb{K}_{i,j}^{55}\right] = \int_{\Omega} \kappa_s A_{44}\varphi_i\varphi_j + D_{22}\frac{\partial \varphi_i}{\partial y}\frac{\partial \varphi_j}{\partial y} + D_{66}\frac{\partial \varphi_i}{\partial x}\frac{\partial \varphi_j}{\partial x}dxdy \tag{2.69}$$

$$\left[\widetilde{\mathbb{K}}_{i,j}^{13}\right] = \frac{1}{2}\int_{\Omega}\left(\frac{\partial\varphi_i}{\partial x}\left(A_{11}\frac{\partial w_0}{\partial x}\frac{\partial\varphi_j}{\partial x}+A_{12}\frac{\partial w_0}{\partial y}\frac{\partial\varphi_j}{\partial y}\right)\right.$$
$$\left.+A_{66}\frac{\partial\varphi_i}{\partial y}\left(\frac{\partial w_0}{\partial x}\frac{\partial\varphi_j}{\partial y}+\frac{\partial w_0}{\partial y}\frac{\partial\varphi_j}{\partial x}\right)\right)dxdy = \frac{1}{2}\left[\widetilde{\mathbb{K}}_{i,j}^{31}\right]^T \tag{2.70}$$

$$\left[\widetilde{\mathbb{K}}_{i,j}^{23}\right] = \frac{1}{2}\int_{\Omega}\left[\frac{\partial\varphi_i}{\partial y}\left(A_{12}\frac{\partial w_0}{\partial x}\frac{\partial\varphi_j}{\partial x}+A_{22}\frac{\partial w_0}{\partial y}\frac{\partial\varphi_j}{\partial y}\right)\right.$$
$$\left.+A_{66}\frac{\partial\varphi_i}{\partial x}\left(\frac{\partial w_0}{\partial x}\frac{\partial\varphi_j}{\partial y}+\frac{\partial w_0}{\partial y}\frac{\partial\varphi_j}{\partial x}\right)\right]dxdy = \frac{1}{2}\left[\widetilde{\mathbb{K}}_{i,j}^{32}\right]^T \tag{2.71}$$

$$\left[\widetilde{\mathbb{K}}_{i,j}^{33}\right] = \frac{1}{2}\int_{\Omega}\left\{\frac{\partial\varphi_i}{\partial x}\frac{\partial\varphi_j}{\partial x}\left[A_{11}\left(\frac{\partial w_0}{\partial x}\right)^2+A_{12}\left(\frac{\partial w_0}{\partial y}\right)^2\right]\right.$$
$$+\frac{\partial\varphi_i}{\partial y}\frac{\partial\varphi_j}{\partial y}\left[A_{22}\left(\frac{\partial w_0}{\partial y}\right)^2+A_{12}\left(\frac{\partial w_0}{\partial x}\right)^2\right]$$
$$\left.+2A_{66}\frac{\partial w_0}{\partial x}\frac{\partial w_0}{\partial y}\left(\frac{\partial\varphi_i}{\partial x}\frac{\partial\varphi_j}{\partial y}+\frac{\partial\varphi_i}{\partial y}\frac{\partial\varphi_j}{\partial x}\right)\right\}dxdy \tag{2.72}$$

2.4.1 Polynomial spaces

In this work standard quadrilateral elements are defined as shown in Figure 2.4 are used,

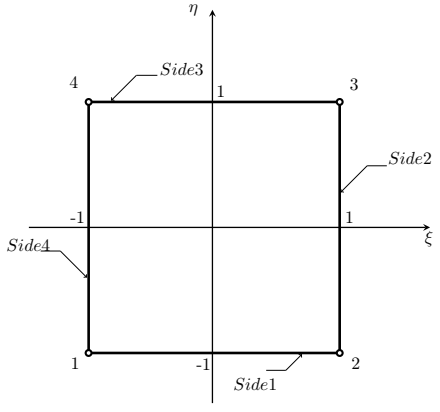

Figure 2.4: Square reference element

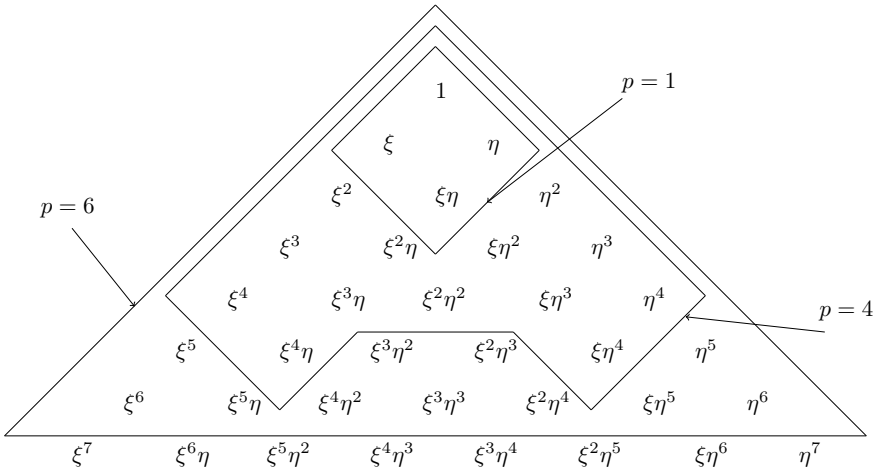

Figure 2.5: Monomials in the trunk space polynomials

Trunk spaces

Trunk spaces, also known as "Serendipity" spaces, are polynomials containing the monomials $\xi^i \eta^j$, $i, j = 0, 1, 2, ..., p$ where $i + j = 0, 1, 2, ..., p$. Regarding quadrilateral elements monomials $\xi\eta$ for $p = 1$ and by $\xi^p\eta, \xi\eta^p$ for $p \geq 2$ are also added. Hence the dimension of the polynomial space yields (see Figure 2.5) [84]:

$$n(p) = \begin{cases} 4p & \text{for } p < 4 \\ 4p + \dfrac{(p-2)(p-3)}{2} & \text{for } p \geq 4 \end{cases} \tag{2.73}$$

Product spaces

Product space polynomials contain the monomials $1, \xi, \xi^2, ..., \xi^p$ and $1, \eta, \eta^2, ..., \eta^q$ in addition to their products (see Figure 2.6) [84]. Hence a product spaces dimension is $n(p,q) = (p+1)(q+1)$.

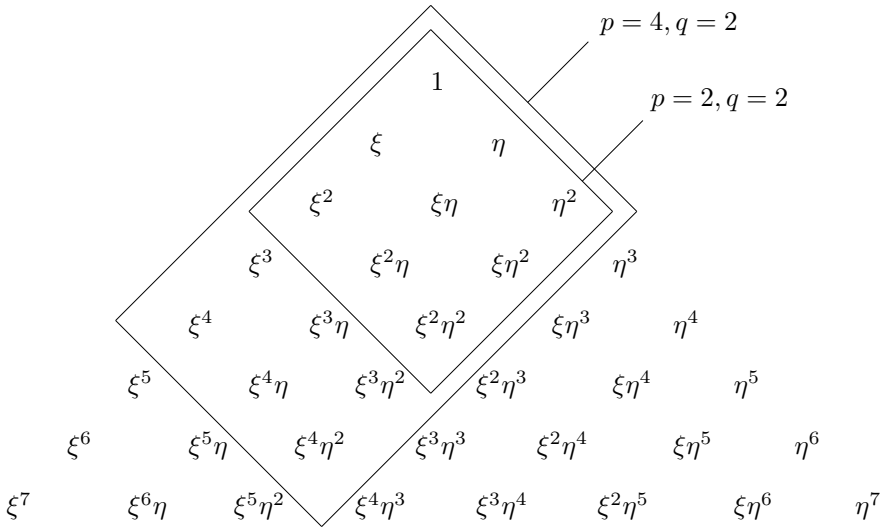

Figure 2.6: Monomials in the product space polynomials

2.4.2 Hierarchic shape functions for quadrilaterals

The shape functions of the four nodes are defined as [85]

$$\begin{cases} \varphi_1(\xi,\eta) = \dfrac{1}{4}(1-\xi)(1-\eta) \\ \varphi_2(\xi,\eta) = \dfrac{1}{4}(1+\xi)(1-\eta) \\ \varphi_3(\xi,\eta) = \dfrac{1}{4}(1+\xi)(1+\eta) \\ \varphi_4(\xi,\eta) = \dfrac{1}{4}(1-\xi)(1+\eta) \end{cases} \tag{2.74}$$

The shape functions of the four sides are defined for $p \geq 2$ and $k = 2,3,...,p$ as [84]

$$\begin{cases} \varphi_1^k(\xi,\eta) = \dfrac{1}{2}(1-\eta)\,\psi_{k+1}(\xi) \\ \varphi_2^k(\xi,\eta) = \dfrac{1}{2}(1+\xi)\,\psi_{k+1}(\eta) \\ \varphi_3^k(\xi,\eta) = \dfrac{1}{2}(1+\eta)\,\psi_{k+1}(-\xi) \\ \varphi_4^k(\xi,\eta) = \dfrac{1}{2}(1-\xi)\,\psi_{k+1}(-\eta) \end{cases} \tag{2.75}$$

Thus we obtain $4(p-1)$ side functions. The internal shape functions for the *serendipity space* are defined for $p \geq 4$ as

$$\varphi^{(k,l)}(\xi,\eta) = \psi_{k+1}(\xi)\,\psi_{l+1}(\eta),\ k,l = 2,3,...,p,\ k+l = 4,5,...,p \tag{2.76}$$

Resulting in $(p-2)(p-3)/2$ internal shape functions. For the *product space* the internal shape functions are defined for $p \geq 2$ and $q \geq 2$ as

$$\varphi^{(k,l)}(\xi,\eta) = \psi_{k+1}(\xi)\,\psi_{l+1}(\eta),\ k = 2,3,...,p,\ l = 2,3,...,q,\ k+l \leq p+q \tag{2.77}$$

where $\psi_s(\xi)$ are blending function defined by using Rodrigues' form of Legendre polynomials as [86]

$$\psi_s(\xi) = \sum_{i=0}^{[s/2]} \frac{(-1)^i (2s-2i-5)!!}{2^i i!\,(s-2i-1)!}\xi^{s-2i-1},\ s > 2 \tag{2.78}$$

$[s/2]$ denotes the integer part of $s/2$ and $n!!$ is defined by the following recursive relation:

$$n!! = \begin{cases} 1 & \text{if } n = 0 \text{ or } n = -1 \\ n \times (n-2)!! & \text{if } n \geq 1 \end{cases} \tag{2.79}$$

The hierarchic feature is achieved by assigning unique sequential numbers to the shape functions according to their polynomial degree as shown for example in Figure A.1

2.4.3 Mapping

Fitting irregular domains with a small number of elements can not be achieved with simple rectangles. This can be achieved by distorting simple forms into others of more arbitrary shaped through a geometric transformation , where standard elements (i.e., reference elements, local elements or parent elements) will be 'mapped' into distorted forms (i.e., real element). In Figure 2.7 it is shown that the local coordinates ξ,η are transformed to the

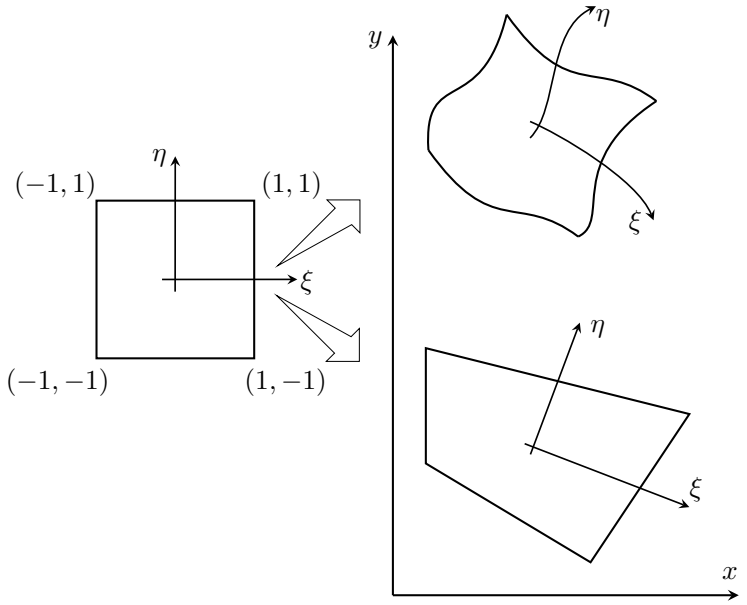

Figure 2.7: Geometric transformation of reference element from the local coordinates ξ,η space to the global cartesian x,y space

global Cartesian x,y space. Thus shape functions and their derivatives can be specified in local coordinates and by suitable transformations the element properties established in the global coordinate system [81].

The problems treated in the present work does not involve any curved geometries, hence requires only mapping using bi-linear Lagrange functions identical to those used for displacement approximation with $p = 1$.

$$\begin{cases} x(\xi,\eta) = \sum_{i=1}^{4} \bar{\varphi}_i(\xi,\eta) X_i \\ y(\xi,\eta) = \sum_{i=1}^{4} \bar{\varphi}_i(\xi,\eta) Y_i \end{cases} \tag{2.80}$$

Where X_i, Y_i are the coordinates of element nodes in the global coordinate system. From Eq.(2.80) one can see that this transformation defines the x,y coordinates of each point in the real element using ξ,η coordinates of the corresponding point in the standard element.

Also this transformation depends on the form and position of the real element because it involves X_i, Y_i the coordinates of element nodes, consequently the transformation is different for each element.

The most important property of mapping to ensure is *uniqueness* (i.e., one-to-one mapping), in other words the transformation must be *bijective* where each point on the parent element corresponds to one and only one point in real element and inversely. This leads to the definition of a quantity called the jacobian determinant where the uniqueness of mapping is ensured if the sign of the jacobian determinant remains unchanged at all points of the element. It can be shown that the transformation based on Lagrange bi-linear shape functions is *unique* only and only if no internal angle is equal or greater than 180° (see Figure 2.8) [81].

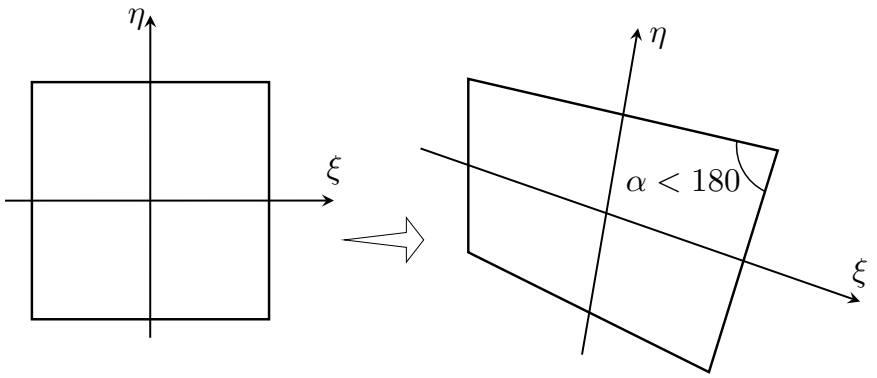

Figure 2.8: Mapping uniqueness condition for quadrilateral elements

In order to evaluate mass and stiffness matrices two transformations are needed. First, expressing the global derivatives $\left(\frac{\partial \varphi}{\partial x}, \frac{\partial \varphi}{\partial y}\right)$ in terms of local derivatives $\left(\frac{\partial \varphi}{\partial \xi}, \frac{\partial \varphi}{\partial \eta}\right)$ and $\left(\frac{\partial x}{\partial \xi}, \frac{\partial x}{\partial \eta}, \frac{\partial y}{\partial \xi}, \frac{\partial y}{\partial \eta}\right)$. Secondly the element of surface over which the integration is carried out must be expressed in terms of the local coordinates.

Global derivatives

Using the usual rules of partial differentiation Eqs.(2.81, 2.82) we have the derivatives with respect to ξ and η in matrix form is expressed by Eq.(2.83)

$$\frac{\partial}{\partial \xi} = \frac{\partial x}{\partial \xi}\frac{\partial}{\partial x} + \frac{\partial y}{\partial \xi}\frac{\partial}{\partial y} \tag{2.81}$$

$$\frac{\partial}{\partial \eta} = \frac{\partial x}{\partial \eta}\frac{\partial}{\partial x} + \frac{\partial y}{\partial \eta}\frac{\partial}{\partial y} \tag{2.82}$$

$$\left\{ \begin{array}{c} \frac{\partial}{\partial \xi} \\ \\ \frac{\partial}{\partial \xi} \end{array} \right\} = \left[\begin{array}{cc} \frac{\partial x}{\partial \xi} & \frac{\partial y}{\partial \xi} \\ \\ \frac{\partial x}{\partial \eta} & \frac{\partial y}{\partial \eta} \end{array} \right] \left\{ \begin{array}{c} \frac{\partial}{\partial x} \\ \\ \frac{\partial}{\partial y} \end{array} \right\} = [J] \left\{ \begin{array}{c} \frac{\partial}{\partial x} \\ \\ \frac{\partial}{\partial y} \end{array} \right\} \tag{2.83}$$

Where the matrix $[J]$ is known as the *jacobian matrix* for the transformation. if the *jacobian matrix* is not singular (i.e., $|J| \neq 0$ hence the transformation is unique), the derivatives with respect to x and y are defined in terms of local coordinates as

$$\left\{ \begin{array}{c} \frac{\partial}{\partial x} \\ \\ \frac{\partial}{\partial y} \end{array} \right\} = [J]^{-1} \left\{ \begin{array}{c} \frac{\partial}{\partial \xi} \\ \\ \frac{\partial}{\partial \eta} \end{array} \right\} \tag{2.84}$$

where

$$[J]^{-1} = \frac{1}{|J|} \left[\begin{array}{cc} J_{22} & -J_{12} \\ -J_{21} & J_{11} \end{array} \right] \tag{2.85}$$

Substituting the transformation 2.80 in the expression of the jacobian matrix we obtain in terms shape functions and nodes coordinates the following

$$[J] = \left[\begin{array}{cccc} \frac{\partial \overline{\varphi}_1}{\partial \xi} & \frac{\partial \overline{\varphi}_2}{\partial \xi} & \frac{\partial \overline{\varphi}_3}{\partial \xi} & \frac{\partial \overline{\varphi}_4}{\partial \xi} \\ \\ \frac{\partial \overline{\varphi}_1}{\partial \eta} & \frac{\partial \overline{\varphi}_2}{\partial \eta} & \frac{\partial \overline{\varphi}_3}{\partial \eta} & \frac{\partial \overline{\varphi}_4}{\partial \eta} \end{array} \right] \left[\begin{array}{cc} X_1 & Y_1 \\ X_2 & Y_2 \\ X_3 & Y_3 \\ X_4 & Y_4 \end{array} \right] \tag{2.86}$$

Integrals

To transform the variables and the domain from global domain to the local domain on which the integration is made we have

$$dxdy = |J|(\xi,\eta)\,d\xi d\eta, \quad |J| \neq 0 \tag{2.87}$$

Hence

$$\int_{\Omega} F(x,y)\,dxdy = \int_{-1}^{1}\int_{-1}^{1} \overline{F}(\xi,\eta)\,|J|(\xi,\eta)\,d\xi d\eta \tag{2.88}$$

Where $\overline{F}(\xi,\eta) = F(x(\xi,\eta), y(\xi,\eta))$.

2.5 Numerical Methods

2.5.1 Numerical integration

Explicit calculation of the above integrals is generally impossible. Therefore, the integrals are evaluated numerically using the Gauss–Legendre quadrature.

$$\int_{-1}^{1} f(\xi)\,d\xi = \sum_{i=1}^{n} f(\xi_i)\,\varpi_i \tag{2.89}$$

Where ξ_i is the i-th root of Legendre polynomial P_n . The weights ϖ_i are defined as

$$\varpi_i = \frac{2}{\left(1-\xi_i^2\right)\left[P_n'(\xi_i)\right]^2} \tag{2.90}$$

The error term is given by Eq.(2.91), where $f^{(2n)}$ is 2^{nd} derivative of f. The error term indicates that if $f(\xi)$ is a polynomial of degree p and then the integral will be exact if $n \geq (p+1)/2$.

$$E_n = \frac{2^{2n+1}(n!)^4}{(2n+1)\left[(2n)!\right]^3} f^{(2n)}(\xi) \tag{2.91}$$

The integration procedure can be extended directly to the local quadrilateral element

$$\int_{-1}^{1}\int_{-1}^{1} f(\xi,\eta)\,d\xi\,d\eta = \sum_{i=1}^{n_\xi}\sum_{j=1}^{n_\eta} f\left(\xi_i,\eta_j\right)\varpi_i\varpi_j \tag{2.92}$$

where n_ξ and n_η is the number quadrature points in the ξ axis and η axis respectively.

2.5.2 Solving generalized eigenvalue problems

Solving a generalized eigenvalue problem $[K]\{q\} = \omega^2[M]\{q\}$, yields n eigenvalues $\omega_1^2, \omega_2^2, ... \omega_n^2$, and corresponding eigenvectors $\{q\}_1, \{q\}_2, ... \{q\}_n$, Each eigenpair $\left(\omega_i^2, \{q\}_i\right)$ satisfies:

$$[K]\{q\}_i = \omega_i^2[M]\{q\}_i;\ i = 1,2,..,n$$

Several eigensystem solutions methods have been developed. However, In finite element analysis the involved matrices has specific properties such as being sparse, banded, positive definite, and so on. Therefor the solution algorithm should take advantage of these properties so that it delivers a solution accurately and efficiently. The solution methods can be subdivided into several groups, corresponding to which basic property is used as the basis of the solution algorithm [], The vector iteration methods, The transformation methods, subspace iteration methods

2.5.3 Nonlinear solution process

Several iterative methods are applied to solve the nonlinear equations of motion in the frequency domain 2.49. Among these methods we have, the linearized update mode (LUM) method, Newton method that has better rates of convergence than LUM method and the continuation method which is based on the Newton method and a constrain equation. In this work the LUM method is employed due to its simplicity. The LUM method consists of the following steps: refs

Step 1: Solve the linear eigenvalue problem

$$\left(-\omega^2 [M] + [K_L]\right) \{q\} = 0 \tag{2.93}$$

Step 2: Normalize the specified Mode shape $\{q\}_i$

Find the maximum transverse displacement w_0 according to the mode $\{q\}_i$ using the expression:

$$w_0 = \sum_{j=1}^{n} \varphi_j (x,y)\, q_{j(i)} \tag{2.94}$$

Normalize $\{q\}_i$ using:

$$\{q\}_i \leftarrow \frac{w_m}{w_0} \{q\}_i \tag{2.95}$$

Step 3: Construct the complete stiffness matrix using the normalized mode shape $\{q\}_i$

$$[K]_i = [K_L + K_{NL}(\{q\}_i)] \tag{2.96}$$

Step 4: Solve the linearized eigenvalue/eigenvector problem for the specified mode

$$\left(-\omega_{i+1}^2 [M] + [K]_i\right) \{q\}_{i+1} = 0 \tag{2.97}$$

The improved solution ω_{i+1}^2 and $\{q\}_{i+1}$ is obtained.

Step 5: Check convergence

$$Err_{i+1} = \left| \frac{\omega_{i+1}^2 - \omega_i^2}{\omega_{i+1}^2} \right| \tag{2.98}$$

If $Err_{i+1} > Tol$ then go to Step 2. Tol is generally taken between $10^{-3} \sim 10^{-6}$.

Step 6: Output results and terminate

When studying cracked plates with crack length ratio $\beta \geq 0.3$, it is observed that the previously presented LUM method is not successful at obtaining result for amplitudes $w/h > 0.8$

and convergence is not attained because successive iterations jump between two values. According to Reibero [87] the difficulty to attain convergence is due to the big difference between the two eigenvectors of the previous successive iterations. In order to address this difficulty, Reibero [87] used the average of the two or three eingenvectors of the preceding iterations to construct the non-linear terms of the stiffness matrix, hence Step 2 become as follow:

Step 2:

1. Normalize the specified Mode shape $\{q\}_i$

$$w_0 = \sum_{j=1}^{n} \varphi_j(x,y)\, q_{j(i)} \tag{2.99}$$

Normalize $\{q\}_i$ using:

$$\{q\}_i \leftarrow \frac{w_m}{w_0} \{q\}_i \tag{2.100}$$

2. Calculate the average of eigenvectors from the last three solutions

$$\{q\}_i \leftarrow \frac{1}{3} \left(\{q\}_i + \{q\}_{i-1} + \{q\}_{i-2} \right) \tag{2.101}$$

2.6 Computer implementation

In this section, we present two important programming techniques employed in this work in order to improve the efficiency and minimize the calculation time on one hand, and to reduce the storage requirements on the other hand.

2.6.1 Constructing stiffness/mass matrices

One difficulty associated with the p-refinement is that of accurately calculating all the integrals required to establish the stiffness and mass matrices of high order elements especially nonlinear terms. Through numerical experimentation it is found that a bottleneck arises at

the integration step, since the number of terms to integrate and the number of integration points increase simultaneously as the degree p is increased see Figures 2.9 & 2.10. One attempt to solve this problem is the use symbolic computing [86], however this technique is would be difficult to apply on distorted and curved elements since the integrals to be evaluated are no longer polynomials. In this work, this problem is solved using parallel computing where all entries in element mass/stiffness matrix are integrated simultaneously on a multi-core processor or even better a graphics processing unit (GPU) with hundreds of cores allowing much better parallelism. In this work, the graphics processing unit used is an Nvidea Quadro K2100M card.

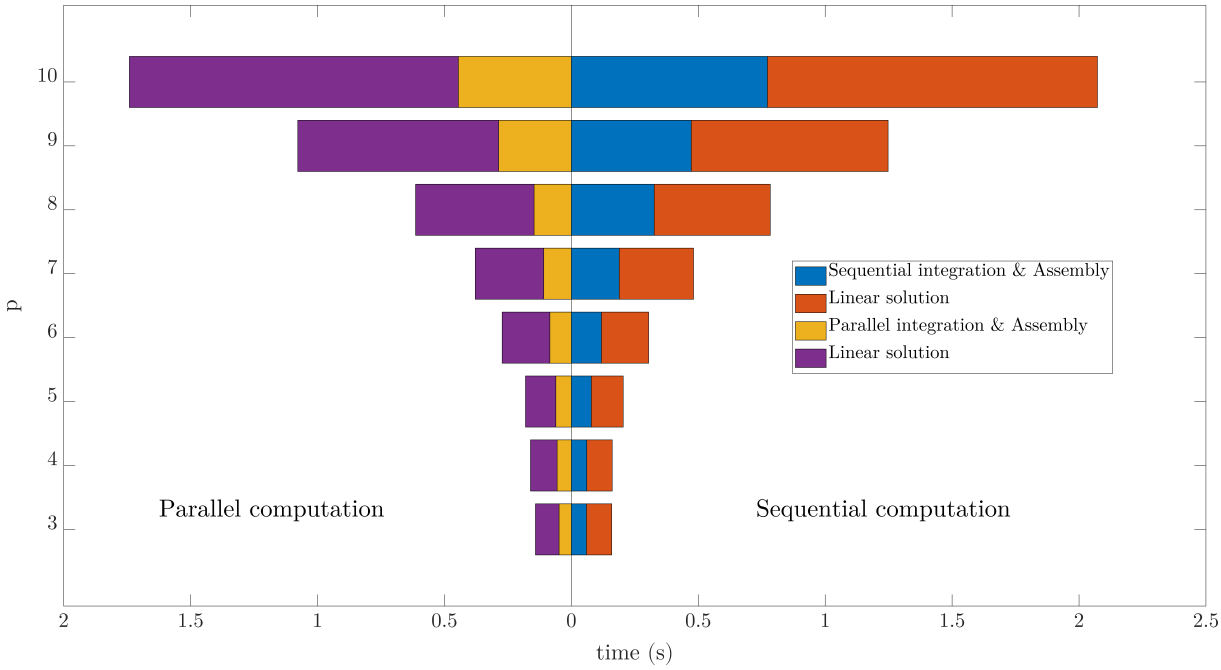

Figure 2.9: Bar diagram comparing computation time using parallel computation and sequential computation for linear vibration of a simply supported square plate at different p-refinement values.

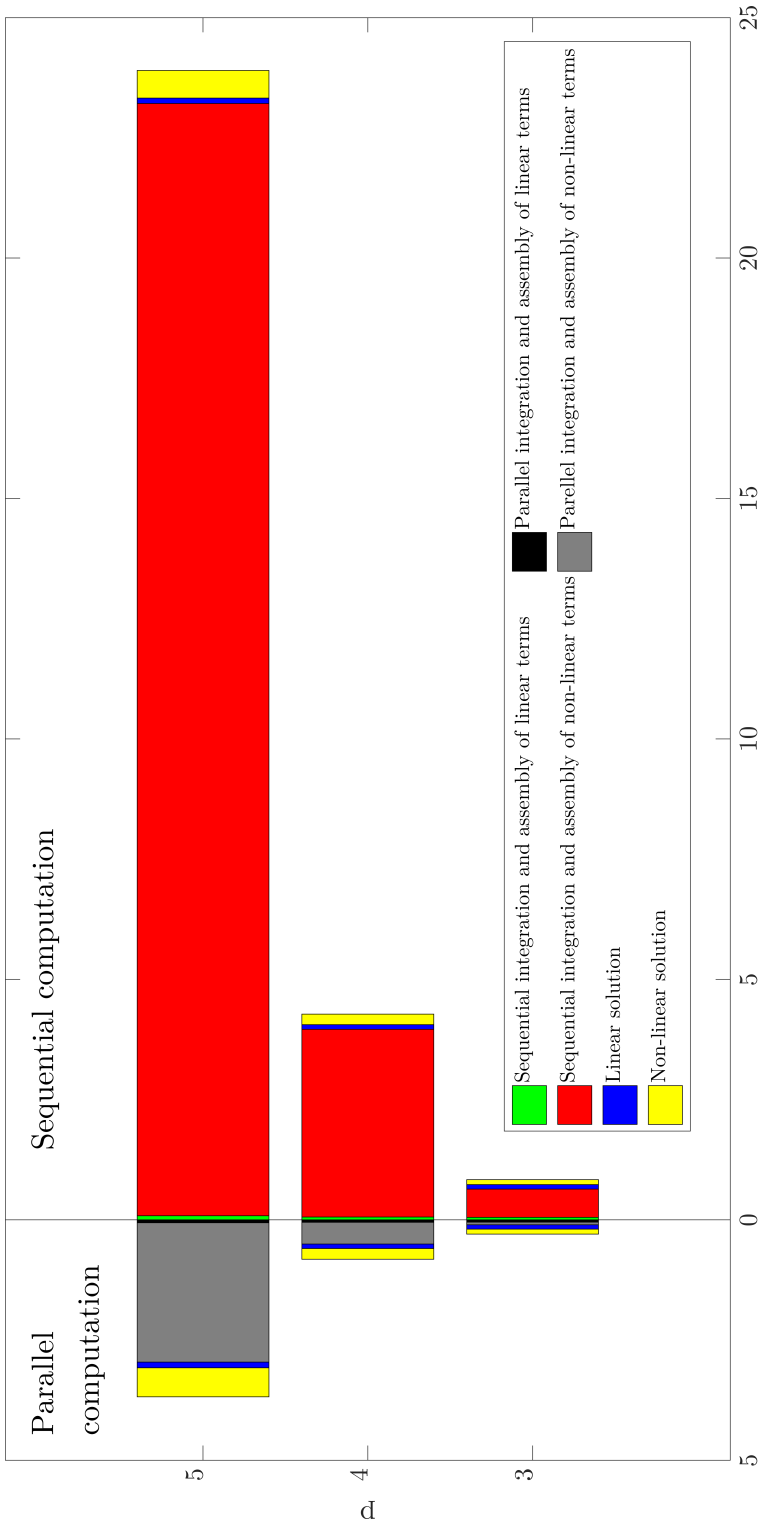

Figure 2.10: Bar diagram comparing computation time using parallel computation and sequential computation for non-linear vibration of a simply supported square plate at different p-refinement values.

2.6.2 Storage Scheme

The assembly of global mass and stiffness matrices results in sparse matrices with large number of zero elements (see Figure 2.11), hence special schemes are used to store these matrices. Obviously, the purpose is to avoid storage and computational redundancy, by storing only the nonzero elements, sparse matrix data structures require *less computer memory*. And by avoiding arithmetic operations on zero elements when performing common matrix operations by employing sparse matrix adapted algorithms that require *less computing time* [88].

The main parameter of a sparse square matrix $S(n \times n)$ is nz, the number of nonzero elements. Computer storage requirements are proportional to nz. The computational complexity of simple array operations should also be proportional to nz, and perhaps also depend linearly on n, but be independent n^2. A sparse matrix is stored using the *Compressed Sparse Column* (CSC) scheme (see Figure2.12). This format is commonly used to store general sparse matrices. It consists of three arrays that are structured as follow: [89]

- A real array $\overline{S}$ consists of the nonzero real values S_{ij} stored column by column, from column 1 to n, the length of $\overline{S}$ is nz.
- An integer array IS contains the row indices i of the nonzero elements S_{ij} , the length of IS is nz.
- An integer array JS contains the pointers to the beginning of each column in the arrays $\overline{S}_p$ and IS. Thus, the content of $JS(j)$ is the position in arrays $\overline{S}_p$ and IS where the *j-th* column starts.

The storage requirement for an $n \times n$ real sparse matrix with nz nonzero entries is nz reals and $nz+n$ integers. On typical *32–bit* architecture machines with *8-byte* reals and *4-byte* integers, this is $12nz+4n\,bytes$ [90]. Table 2.2 gives an example of the memory requirements for storing mass/stiffness matrices as sparse matrices and as a traditional full matrices, as well as the execution time for solving their associated generalized eigenvalues problem.

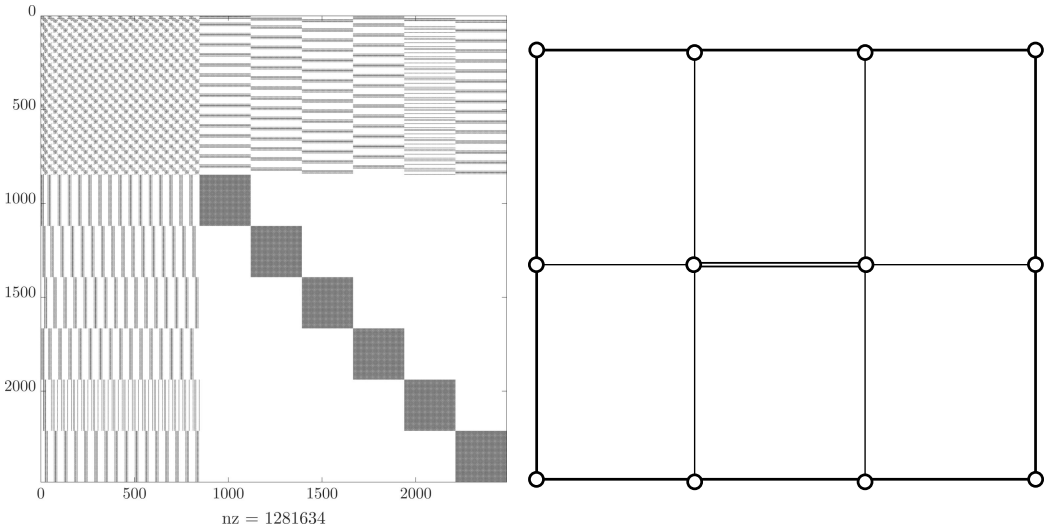

(a) Sparsity pattern associated with p-refinement dominated mesh, All elements are p-refined $p = 16$

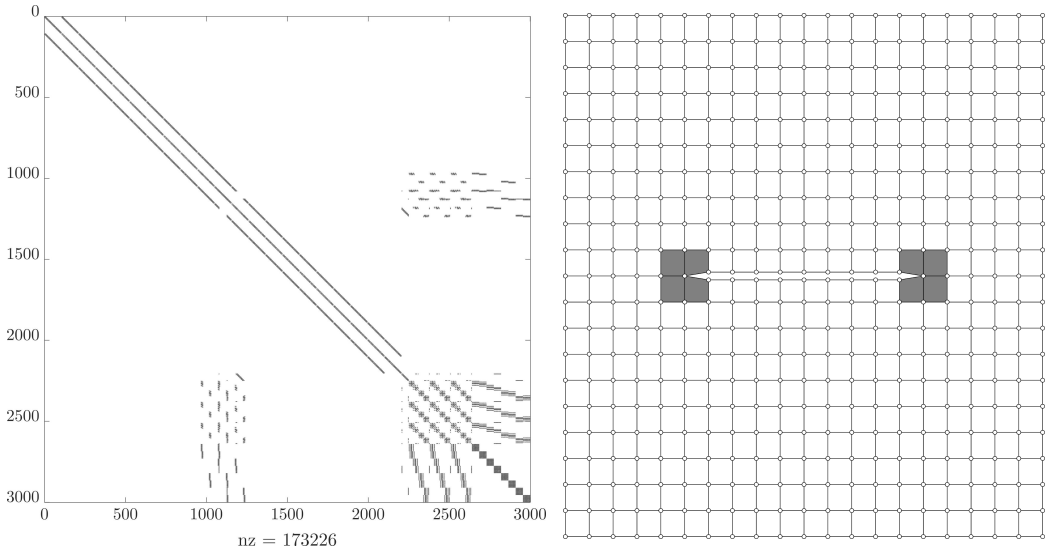

(b) Sparsity pattern associated with h-refinement dominated mesh, only gray elements are p-refined $p = 4$

Figure 2.11: Plots of the sparsity pattern in stiffness matrices encountered in h-p FEM, for a centrally cracked plate

Table 2.2: Exemple of storage requirements & computationale cost for sparse matrices

	Sparse	Full
h-refinement dominated mesh Figure 2.11b $p = 6$, matrices size 3900×3900 mass matrix $nz = 202626$, stiffness matrix $nz = 467678$		
Memory of stiffness matrix $(Mbytes)$	8.23	121.68
Memory of mass matrix $(Mbytes)$	3.27	121.68
Solving time $(seconds)$	2.28†	9.99‡
p-refinement dominated mesh Figure 2.11a $p = 11$, matrices size 3960×3960 mass matrix $nz = 1111698$, stiffness matrix $nz = 2590044$		
Memory of stiffness matrix $(Mbytes)$	45.43	125.45
Memory of mass matrix $(Mbytes)$	17.82	125.45
Solving time $(seconds)$	2.88†	797.05‡

†Solved using

‡Solved using

$$S = \begin{pmatrix} 1.2 & 0.0 & 0.0 & 2.3 & 0.0 \\ 3.4 & 4.5 & 0.0 & 5.6 & 0.0 \\ 6.7 & 0.0 & 7.8 & 8.9 & 9.1 \\ 0.0 & 0.0 & 10.0 & 11.0 & 0.0 \\ 0.0 & 0.0 & 0.0 & 0.0 & 12.0 \end{pmatrix}$$

$\overline{S}$	1.2	3.4	6.7	4.5	7.8	10.0	2.3	5.6	8.9	11.0	9.1	12.0
IS	1	1	1	2	3	3	4	4	4	4	5	5
JS	1	4	5	7	11							

Figure 2.12: Exemple of how the *Compressed Sparse Column* (CSC) scheme is used to store a sparse matrix

2.7 Summary

In this chapter, we developed a *h-p* FEM model to handle problems of linear/nonlinear free vibrations of cracked nanoplates, the model is based on first order shear deformation theory (FSDT) and nonlocal elasticity theory of Eringen. First we introduced the concept of nonlocal elasticity and its description of interactions in a solid nano-structure. The importance of employing the differential form of nonlocal elasticity has been also highlighted. Then, the *first order shear deformation theory* of plates with *nonlocal elasticity* are employed to derive equations of motions for nanoplates. The obtained equations of motion are reduced to a system of algebraic equations using finite element approximations. Then we have presented the numerical methods to be used in order to construct and solve the system of equations. Finally, we have presented and discussed computer implementation techniques such as parallel computing and sparse matrices storage scheme employed in order to efficiently conduct calculations on machines.

Chapter 3

Linear Vibration of isotropic cracked nanoplates

In this chapter, firstly, the rate of convergence is investigated for intact and cracked plates in both local and non-local cases. Secondly, the accuracy of the present model is verified for intact local and non-local plates, then the accuracy is investigated again for cracked local plates with respect to analytical, numerical and experimental results in literature. Thus original results for cracked non-local plates, subjected to several cases of boundary conditions, can be presented and discussed in a series of parametric studies involving plate aspect ratio a/b, crack length ratio β, crack angle α, and non-local parameter μ.

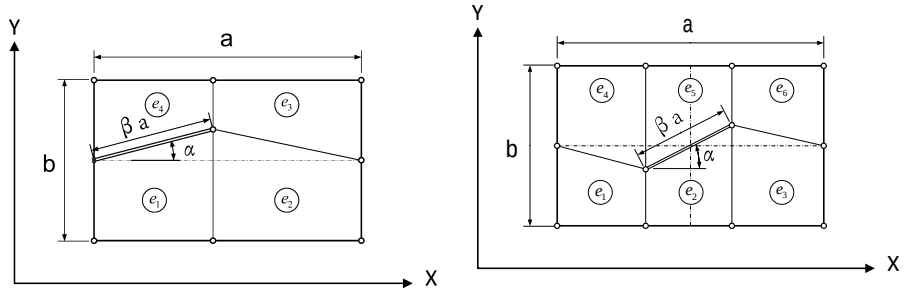

(a) plate with side crack (b) plate with central crack

Figure 3.1: Geometric parameters and mesh configuration for cracked plates

3.1 Convergence and Comparison

In order to establish the number elements and the correspondent order of interpolation p needed to reach convergence, a test is carried out. The variation of frequency parameters as a function of mesh size and order of interpolation is investigated. Table 3.1 shows the rate of convergence for a simply supported square plate. It is observed that for a 1×1 mesh with $p = 12$ and a 4×4 mesh with $p = 8$, the frequency parameters are increasingly refined and approach a fixed value in both local and non-local cases.

Table 3.1: Convergence of frequency parameters $\overline{\omega} = \omega \frac{a^2}{\pi^2} \sqrt{\frac{\rho h}{D_{22}}}$ for a simply supported isotropic square plate w/o non-local effect

mode	mesh	1×1				4×4			
	p	4	8	12	16	4	8	12	16
Isotropic local Plate ($\nu = 0.25$, $\mu = 0$)									
1		2.125	2.000	2.000	2.000	2.015	2.000	2.000	2.000
2		3398	5.017	5.000	5.000	5.186	5.000	5.000	5.000
3		3398	5.017	5.000	5.000	5.186	5.000	5.000	5.000
4		3398	8.045	8.000	8.000	8.348	7.999	8.000	8.000
Isotropic non-local Plate $\nu = 0.25$, $\mu = 0.5$									
1		17.73	1.694	1.694	1.694	1.710	1.694	1.694	1.694
2		3398	3.558	3.547	3.547	3.712	3.547	3.547	3.547
3		3398	3.558	3.547	3.547	3.712	3.547	3.547	3.547
4		3398	5.006	4.981	4.981	5.263	4.981	4.981	4.981

On the other hand, the rate of convergence for a simply supported square plate in the presence of a side crack and a central crack is studied in Table 3.2 using a 2×2 and 3×2 mesh (Figure 3.1). It is observed that for $p \geq 16$, the frequency parameters for local and non-local plate reach a reasonable convergence in both cases of crack length ratios $\beta = 0.3$ and $\beta = 0.7$.

Table 3.2: Convergence of frequency parameters $\overline{\omega} = \omega \frac{a^2}{\pi^2}\sqrt{\frac{\rho h}{D_{22}}}$ for a simply supported isotropic cracked ($\beta = [0.3, 0.7]$) square plates w/ and w/o non-local effect

mode n°		$\beta = 0.3$					$\beta = 0.7$				
	p	8	12	16	18	20	8	12	16	18	20
Side crack	Isotropic local Plate $\nu = 0.25$, $\mu = 0$										
	1	1.990	1.986	1.985	1.984	1.984	1.817	1.792	1.783	1.781	1.779
	2	4.971	4.962	4.958	4.957	4.957	3.169	3.124	3.109	3.105	3.102
	3	4.980	4.977	4.976	4.976	4.976	4.882	4.878	4.876	4.876	4.875
	4	7.853	7.837	7.832	7.830	7.829	6.315	6.312	6.311	6.311	6.310
	Isotropic non-local Plate $\nu = 0.25$, $\mu = 0.1$										
	1	1.916	1.912	1.911	1.910	1.910	1.747	1.722	1.714	1.711	1.710
	2	4.543	4.533	4.530	4.529	4.528	3.007	2.965	2.952	2.948	2.946
	3	4.555	4.553	4.553	4.553	4.552	4.452	4.449	4.448	4.448	4.447
	4	6.880	6.869	6.866	6.865	6.864	5.555	5.554	5.553	5.553	5.553
Central crack	Isotropic local Plate $\nu = 0.25$, $\mu = 0$										
	1	1.956	1.935	1.928	1.925	1.924	1.777	1.744	1.735	1.733	1.731
	2	4.933	4.923	4.920	4.920	4.918	3.499	3.408	3.380	3.373	3.368
	3	4.999	4.995	4.993	4.992	4.992	4.922	4.887	4.876	4.873	4.871
	4	7.996	7.994	7.994	7.994	7.993	7.408	7.328	7.302	7.295	7.290
	Isotropic non-local Plate $\nu = 0.25$, $\mu = 0.1$										
	1	1.948	1.928	1.920	1.918	1.916	1.770	1.737	1.728	1.725	1.724
	2	4.887	4.878	4.874	4.873	4.873	3.481	3.391	3.364	3.357	3.352
	3	4.950	4.946	4.944	4.944	4.944	4.874	4.839	4.828	4.826	4.824
	4	7.873	7.871	7.870	7.870	7.870	7.310	7.233	7.208	7.202	7.197

To validate the present model predictions accuracy, the obtained results are compared with the analytical, numerical and experimental results reported by other researchers [21, 40, 43, 91].

In Table 3.3 the first four frequency parameters for square *nanoplates* ($a = 5nm$) with several boundary conditions *(S-S-S-S, F-C-F-C and F-S-F-S)* and non-local parameters ranging between $\left(0nm^2\text{–}4nm^2\right)$, are compared with numerical results presented by Chakraverty and Behera [21] based on the *classical plate theory* using *Rayleigh-Ritz method* . The obtained results are in good agreement and relative differences are less than

0.4% due to the different assumptions adopted in plate theories and the solution method in the two studies.

Table 3.3: Comparison of first four frequency parameters $\overline{\omega} = \omega a^2 \sqrt{\frac{\rho h}{D_{22}}}$ for a square nanoplate $(a = 5nm)$ subjected to several boundary conditions

	$\mu = 0$		$\mu = 1$		$\mu = 2$		$\mu = 4$	
mode n°	present	ref[21]	present	ref[21]	present	ref[21]	present	ref[21]
	S-S-S-S							
1	19.739	19.700	14.755	14.755	12.291	12.291	9.680	9.680
2	49.347	49.300	28.615	28.615	22.185	22.185	16.545	16.545
3	49.347	49.300	28.615	28.615	22.185	22.185	16.545	16.545
4	78.956	79	38.719	38.719	29.189	29.190	21.383	21.384
	C-C-C-C							
1	35.994	36	25.627	25.618	20.937	20.929	16.214	16.207
2	73.430	73.400	40.327	40.281	30.904	30.865	22.867	22.836
3	73.430	73.400	40.327	40.281	30.904	30.865	22.867	22.836
4	108.235	108.200	50.334	50.272	37.654	37.598	27.453	27.408
	S-C-S-C							
1	28.950	29	21.109	21.109	17.409	17.409	13.591	13.591
2	54.748	54.700	31.363	31.361	24.251	24.249	18.053	18.052
3	69.326	69.300	38.478	38.478	29.553	29.553	21.901	21.901
4	94.591	94.600	45.115	45.113	33.871	33.869	24.749	24.748
	F-C-F-C							
1	22.196	22.200	18.067	18.058	15.296	15.293	11.793	11.790
2	26.454	26.500	18.790	18.787	15.544	15.536	12.437	12.429
3	43.624	43.600	23.511	23.507	18.017	18.013	13.526	13.524
4	61.224	61.200	33.317	33.313	24.845	24.843	18.166	18.165
	F-S-F-S							
1	9.628	9.600	8.1344	8	7.1707	7.173	5.962	5.964
2	16.134	16.100	11.7854	11	9.7192	9.719	7.585	7.585
3	36.622	36.700	19.9499	20	15.269	15.324	11.297	11.339
4	38.929	38.900	24.1200	24	18.958	18.974	14.267	14.281

Table 3.4 shows a comparison of the first six frequency parameters obtained the present model, analytical results of Stahl and Keer [40] and numerical results of Liew et al.[43], for simply supported rectangular *local* plate $a/b = 2.0$ with a side crack, for several crack length ratios $(0-0.8)$. It is observed that the results of the present study are in good agreement with those in references.

Table 3.4: Comparison of the first six frequency parameters $\overline{\omega} = \omega a^2\sqrt{\frac{\rho h}{D_{22}}}$, for simply supported isotropic $\nu = 0.31$ rectangular $a/b = 2.0$ local plate with a side crack

Crack ratio	Source	Mode n°					
β		1	2	3	4	5	6
0.0	ref[40]	49.35	78.96	128.3	167.8	197.4	-
	ref[43]	49.35	78.96	128.3	167.8	197.4	197.4
	present	49.35	78.96	128.3	167.8	197.4	197.4
0.2	ref[40]	48.95	77.87	126.6	167.1	194.0	-
	ref[43]	49.05	78.08	126.9	167.2	194.7	195.6
	present	49.03	78.08	126.9	167.2	194.3	195.7
0.4	ref[40]	44.51	73.28	100.1	124.5	173.8	-
	Liew[43]	45.40	73.82	104.7	124.5	173.7	193.9
	present	45.12	73.95	102.5	125.0	173.8	194.5
0.5	ref[40]	40.37	72.79	73.63	123.4	168.6	-
	ref[43]	41.62	72.89	76.55	123.8	170.5	192.5
	present	41.26	73.34	75.58	124.3	169.7	193.1
0.6	ref[40]	36.17	57.49	72.59	121.3	141.4	190.1
	ref[43]	37.44	59.31	72.62	121.0	145.8	190.3
	present	37.22	59.12	73.22	122.6	144.0	190.3
0.8	ref[40]	29.90	39.53	68.20	94.50	120.2	166.4
	ref[43]	30.50	40.02	68.82	95.79	120.3	168.0
	present	30.87	40.77	69.51	96.67	121.5	168.9

Table 3.5 lists experimental and numerical results reported by Fujimoto [91] and numerical results of Liew et al. [43] compared to results obtained by the present study. Numerical results of Fujimoto [91] are obtained by the *h-version of the finite element method* using the triangular elements with very fine meshes along the crack tip, the experimental data reported in the same article, are obtained from the *laser holography* technique. Numerical

results of Liew et al. [43] are based on the *classical plate theory* and solved using *domain decomposition method*. The considered plate is centrally cracked, subjected to *C-F-C-F* boundary conditions, and have the following properties: $E = 6.9GPa$, $v = 0.31$, the aspect ratio $a/b = 0.5$ and crack length ratio $\beta = 0.4$. It is again noticed that the present model can accurately predict solutions for *cracked local plates*.

Table 3.5: Comparison of the first five frequency parameters $\overline{\omega} = \omega a^2\sqrt{\frac{\rho h}{D_{22}}}$, for an *C-F-C-F* rectangular local plate with central crack ($E = 6.9GPa$, $v = 0.31$, $\beta = 0.4$, $a/b = 0.5$)

mode n°	finite element [91]	Domain decomposition [43]	Experimental with laser holography[91]	Present
1	5.33	5.26	5.3	5.317
2	8.93	8.98	9.0	8.936
3	15.32	15.11	15.6	15.13
4	20.63	20.50	20.6	20.51
5	26.37	26.56	26.3	26.73

Figure 3.2 represents the first four modes shapes of a simply supported square plate with a central crack ($\beta = 0.5$,$\alpha = 0°$)

3.2 Parametric study of cracked nano-plates

The influence of different values of plate aspect ratios a/b and crack length ratio β is presented in Table 3.6 for a side and central horizontal crack $\alpha = 0$ in simply supported nanoplate. It is observed in both cases of side and central crack that, the frequency parameters in all four modes decrease with the growth of crack length, whereas for plates with a certain crack length, the frequency parameters increase with the increase of plate aspect ratio a/b.

The effect of different values of side to thickness ratios a/h, plate aspect ratios a/b and crack length ratio β is presented in Table 3.7 for a side and central horizontal cracks $\alpha = 0$ in simply supported nanoplate. It is observed in both cases of side and central crack that,

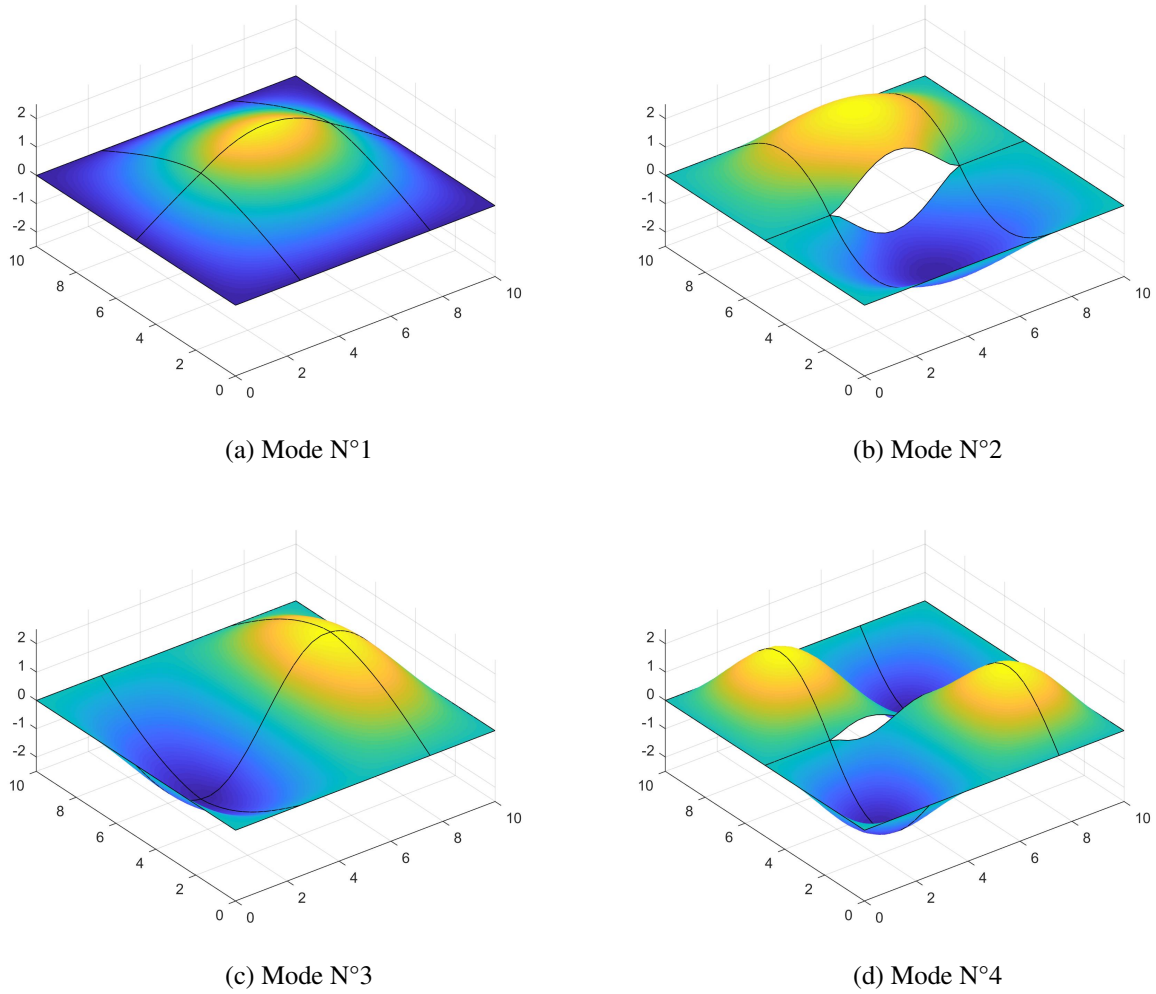

(a) Mode N°1

(b) Mode N°2

(c) Mode N°3

(d) Mode N°4

Figure 3.2: The first four mode shapes of a simply supported square plate with a central crack ($\beta = 0.5, \alpha = 0°$)

the fundamental frequency parameter decreases with the growth of crack length, whereas for plates with a certain crack length, the fundamental frequency parameter increases with the increase of plate aspect ratio a/b and the increase of side to thickness ratios a/h.

Table 3.6: Effect of plate aspect ratios a/b and crack length ratio β on the first four frequency parameters $\overline{\omega} = \omega a^2 \sqrt{\frac{\rho h}{D_{22}}}$, for an *S-S-S-S* rectangular nanoplates with side and central crack $(\nu = 0.3\,,\ \alpha = 0\,,\ \mu = 0.1nm^2\,,\ a = 10nm\,,\ a/h = 10^3)$

mode n°	a/b	0.5			1			2		
	β	0.25	0.5	0.75	0.25	0.5	0.75	0.25	0.5	0.75
		Side crack								
1		12.03	11.89	11.57	18.92	17.99	16.28	44.31	36.72	28.14
2		19.00	18.74	16.76	44.80	40.60	26.14	66.88	63.18	38.19
3		30.10	28.99	26.97	45.04	43.65	43.42	101.74	63.83	60.31
4		38.74	38.46	30.70	68.46	57.11	54.46	128.39	99.89	86.33
		Central crack								
1		11.96	11.74	11.49	18.43	17.09	15.89	40.43	32.17	26.59
2		18.98	18.64	17.18	44.83	40.49	28.98	68.52	65.04	42.93
3		29.58	28.00	26.54	45.06	44.53	43.28	101.30	72.86	58.58
4		38.80	38.68	34.05	68.82	68.10	61.97	125.89	100.2	92.49

Table 3.7: Effect of side to thickness ratios a/h, plate aspect ratios a/b and crack length ratio β on the fundamental frequency parameter $\overline{\omega} = \omega a^2 \sqrt{\frac{\rho h}{D_{22}}}$, for an *S-S-S-S* rectangular nanoplates with side and central crack $(\nu = 0.3\,,\ \alpha = 0\,,\ \mu = 0.1nm^2\,,\ a = 10nm)$

	a/b	0.5			1			2		
a/h	β	0.25	0.5	0.75	0.25	0.5	0.75	0.25	0.5	0.75
		Side crack								
10		11.81	11.63	11.28	18.35	17.20	15.49	41.10	33.08	25.49
50		12.02	11.86	11.53	18.87	17.83	16.11	44.00	35.88	27.52
100		12.03	11.87	11.55	18.90	17.89	16.18	44.16	36.20	27.78
1000		12.03	11.89	11.57	18.92	17.99	16.28	44.31	36.72	28.14
		Central crack								
10		11.70	11.43	11.19	17.62	16.17	15.13	36.24	28.59	24.09
50		11.93	11.68	11.44	18.27	16.86	15.73	39.46	31.19	26.00
100		11.94	11.70	11.46	18.33	16.95	15.80	39.83	31.56	26.26
1000		11.96	11.74	11.49	18.43	17.09	15.89	40.44	32.17	26.59

3.2.1 Side crack

Here, we consider a plate with aspect ratio $a/b = 1$, as shown in Figure 3.1a, a 2×2 mesh is used for plates with side crack, the interpolation order is $p = 16$ for each element. The effect of crack length ratio β and crack angle α on frequency parameters $\overline{\omega} = \omega a^2 \sqrt{\frac{\rho h}{D_{22}}}$, is studied for different values of non-local parameter $\mu \in \{0nm^2, 0.06nm^2, 0.1nm^2\}$ and several cases of boundary conditions *(S-S-S-S, C-F-C-F and S-F-S-F)*.

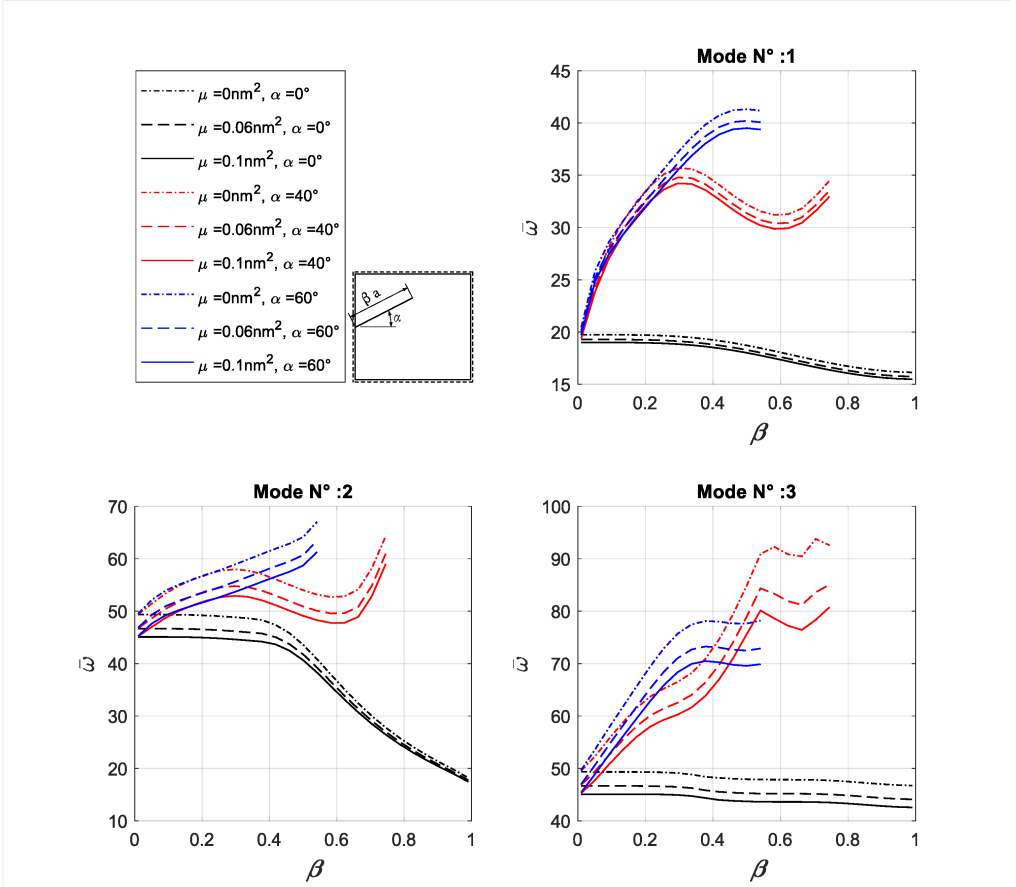

Figure 3.3: Plots of the first three frequency parameters $\overline{\omega}$ versus crack length ratio β for an *S-S-S-S* nanoplate with a *side crack* and different values of crack angle α and non-local parameter μ.

Figures (3.3, 3.4 and 3.5) depicts the effects of the crack length ratio β on the three first frequency parameters for a square nanoplate with a side crack, subjected to *(S-S-S-S, C-F-C-F and S-F-S-F)* boundary conditions respectively. Again it is seen that the frequency parameters decrease with the increasing values of non-local parameter μ for nanoplates with side crack for all cases of boundary conditions and for all values of crack length ratio β and crack angle α.

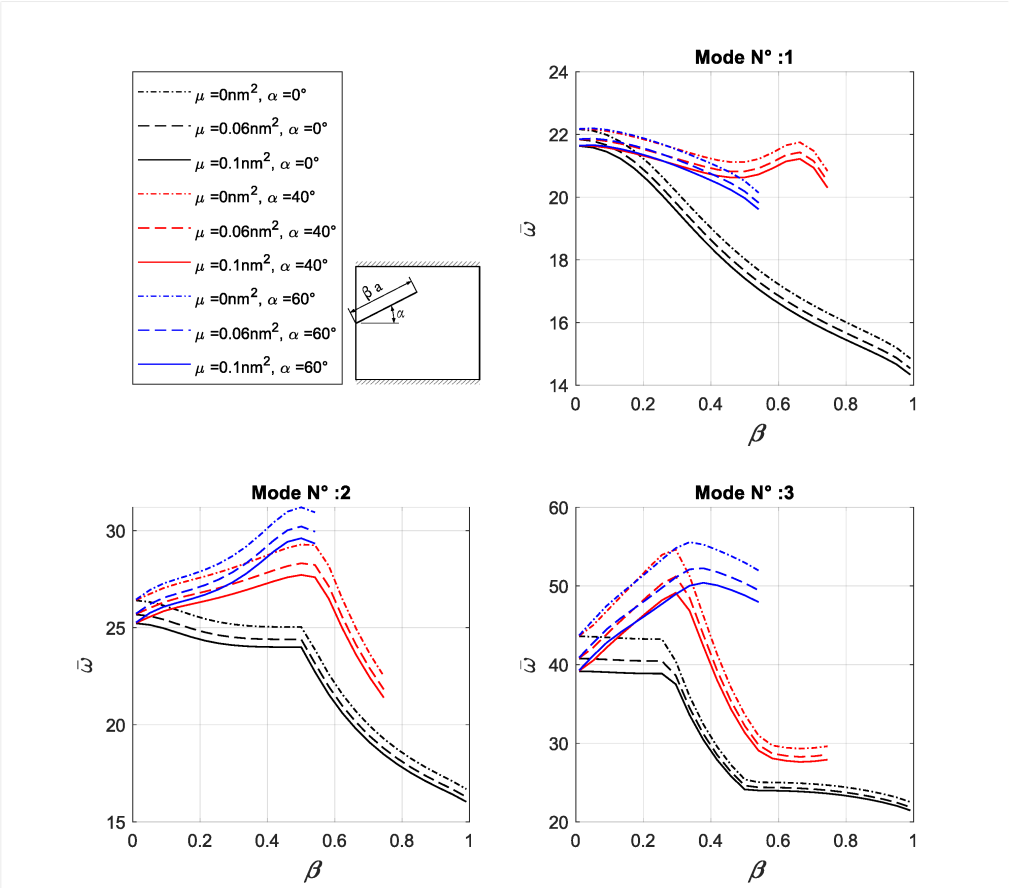

Figure 3.4: plots of the first three frequency parameters $\overline{\omega}$ versus crack length ratio β for an *C-F-C-F* nanoplate with a *side crack* and different values of crack angle α and non-local parameter μ.

For crack angle $\alpha = 0$, it is observed that with respect to crack length ratio β all the frequency parameters are decreasing. For inclined side crack $(\alpha = 30^{\circ})$ non-monotonic

behavior is observed for all frequency parameters in all cases of boundary conditions. For inclined side crack $(\alpha = 60°)$ and *(S-S-S-S)* boundary condition, it is observed that frequency parameters exhibit an increasing behavior with respect to crack length ratio β.

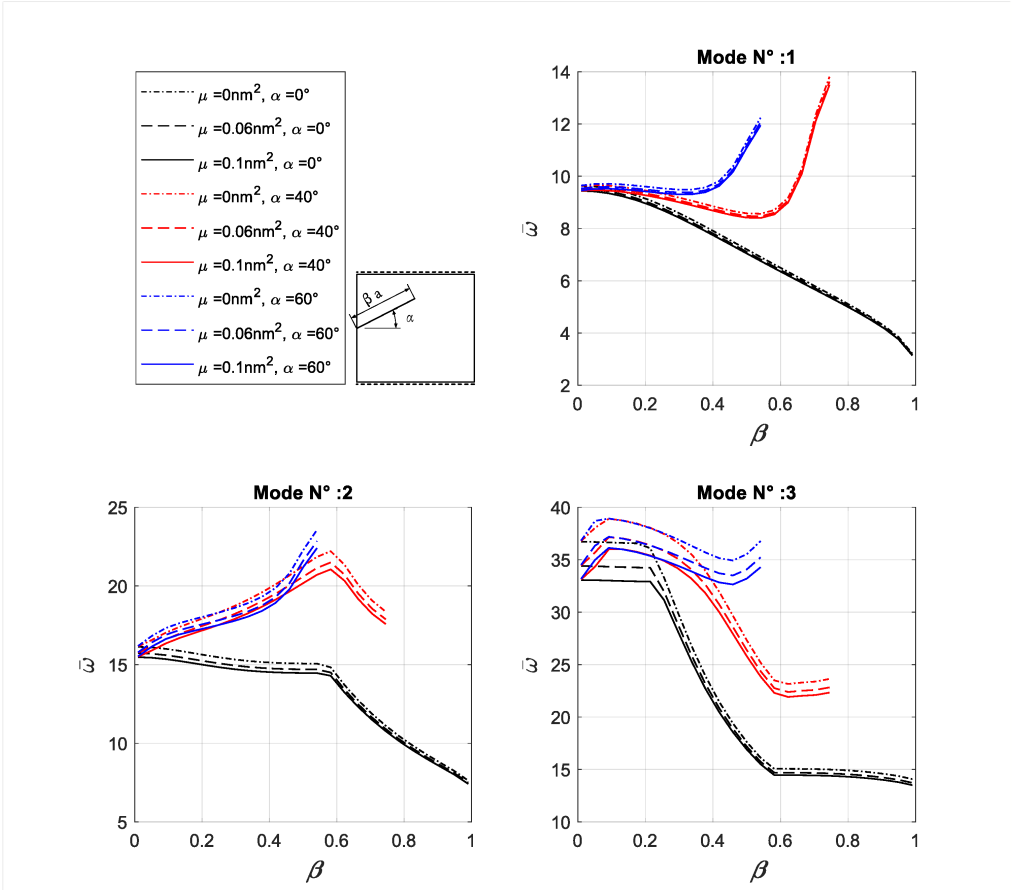

Figure 3.5: plots of the first three frequency parameters $\overline{\omega}$ versus crack length ratio β for an *S-F-S-F* nanoplate with a *side crack* and different values of crack angle α and non-local parameter μ.

However, in the case of *(C-F-C-F and S-F-S-F)* configurations, the first frequency parameter is decreasing for *(C-F-C-F)* case and decreasing with a low rate then increases with a high rate at $\beta \geq 0.3$ for *(S-F-S-F)* configuration, whereas the third frequency parameter increases then decreases at $\beta \geq 0.35$ for *(C-F-C-F)* case and exhibits non-monotonic behavior for *(S-F-S-F)* configuration.

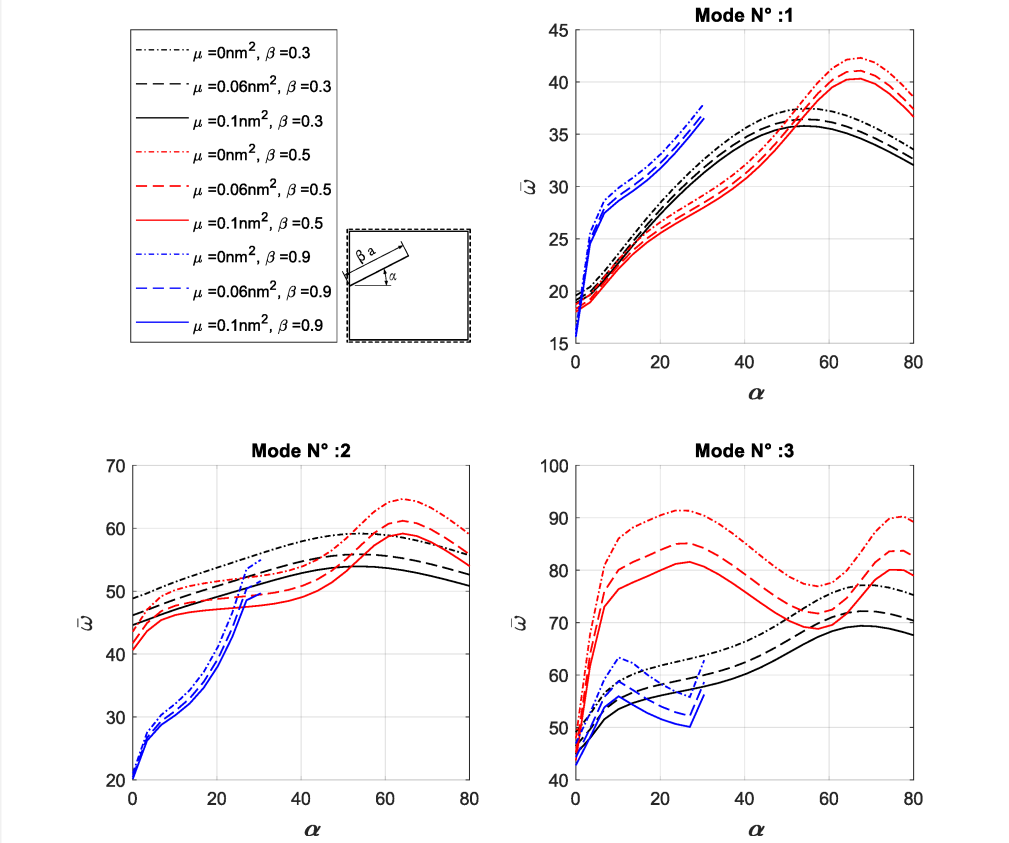

Figure 3.6: plots of the first three frequency parameters $\overline{\omega}$ versus crack angle α for an *S-S-S-S* nanoplate with a *side crack* and different values of crack length ratio β and non-local parameter μ.

Figures (3.6, 3.7 and 3.8) shows the impact of the crack angle α on the three first frequency parameters for a square nanoplate with a side crack, subjected to *(S-S-S-S, C-F-C-F and S-F-S-F)* boundary conditions respectively.

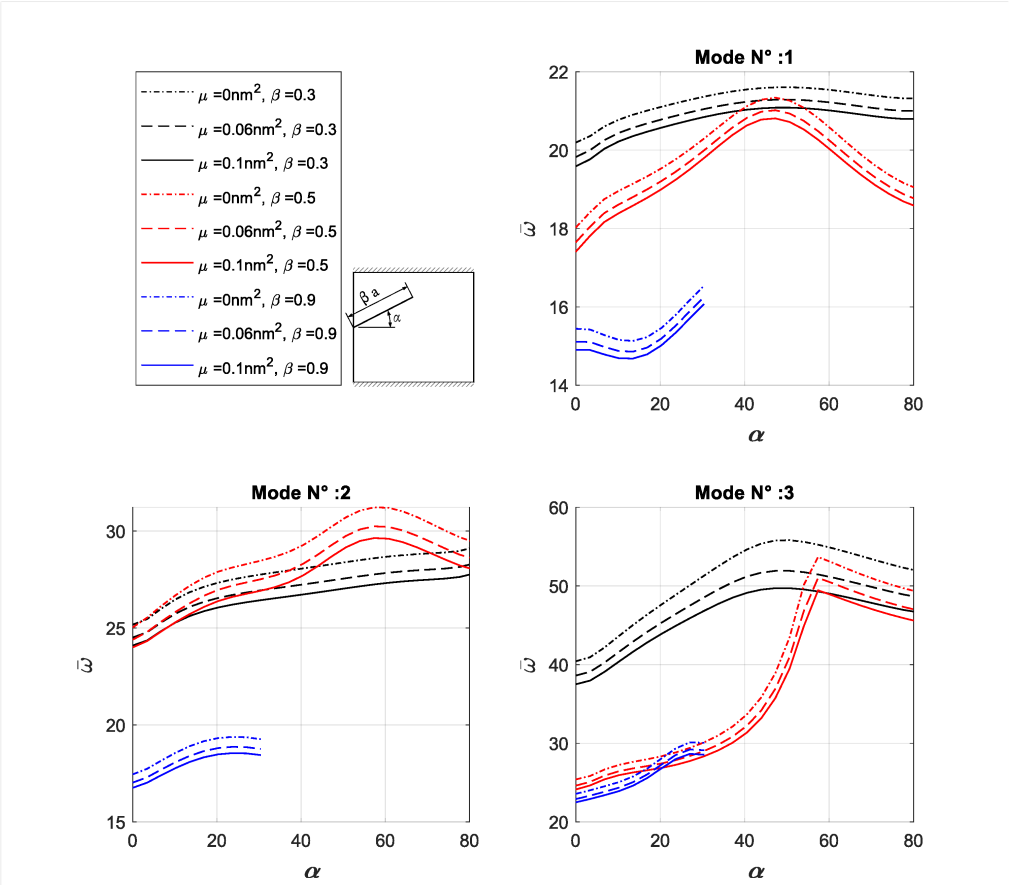

Figure 3.7: plots of the first three frequency parameters $\overline{\omega}$ versus crack angle α for an *C-F-C-F* nanoplate with a *side crack* and different values of crack length ratio β and non-local parameter μ.

Once again an examination of the results shows that the non-local parameter μ is causing frequency parameters to drop for all cases of boundary conditions and for all values of crack length ratio β and crack angle α. It is also observed that for all boundary conditions configurations, frequency parameters are often increased as a function of crack angle α, except for the cases where crack length ratio $\beta = 0.5$ frequency parameters start to decrease after a certain value of crack angle α.

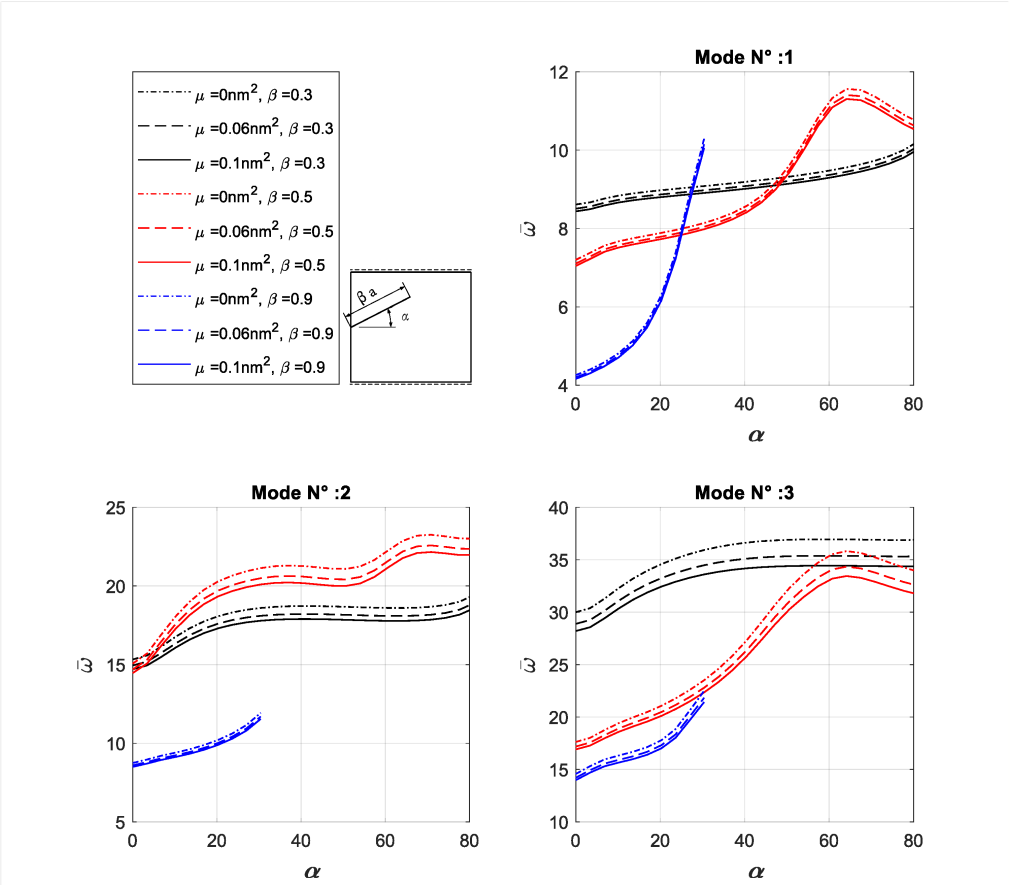

Figure 3.8: plots of the first three frequency parameters $\overline{\omega}$ versus crack angle α for an *S-F-S-F* nanoplate with a *side crack* and different values of crack length ratio β and non-local parameter μ.

In order gain a more comprehensive view of effect of crack length ratio β and crack angle α on the three first frequency parameters for square nanoplates $\mu = 0.1nm^2$ with side crack, contour plots for *(S-S-S-S, C-F-C-F and S-F-S-F)* boundary conditions are presented in Figures (3.9, 3.10 and 3.11) respectively. Again it is noticed that increasing crack angle α often causes frequency parameters to increase. On the other hand, increasing crack length ratio causes frequencies to drop for crack angle $\alpha = 0$, but for crack angle $\alpha \neq 0$, it is noticed that increasing crack length ratio β often amplifies the effect of crack angle α on the frequency parameters.

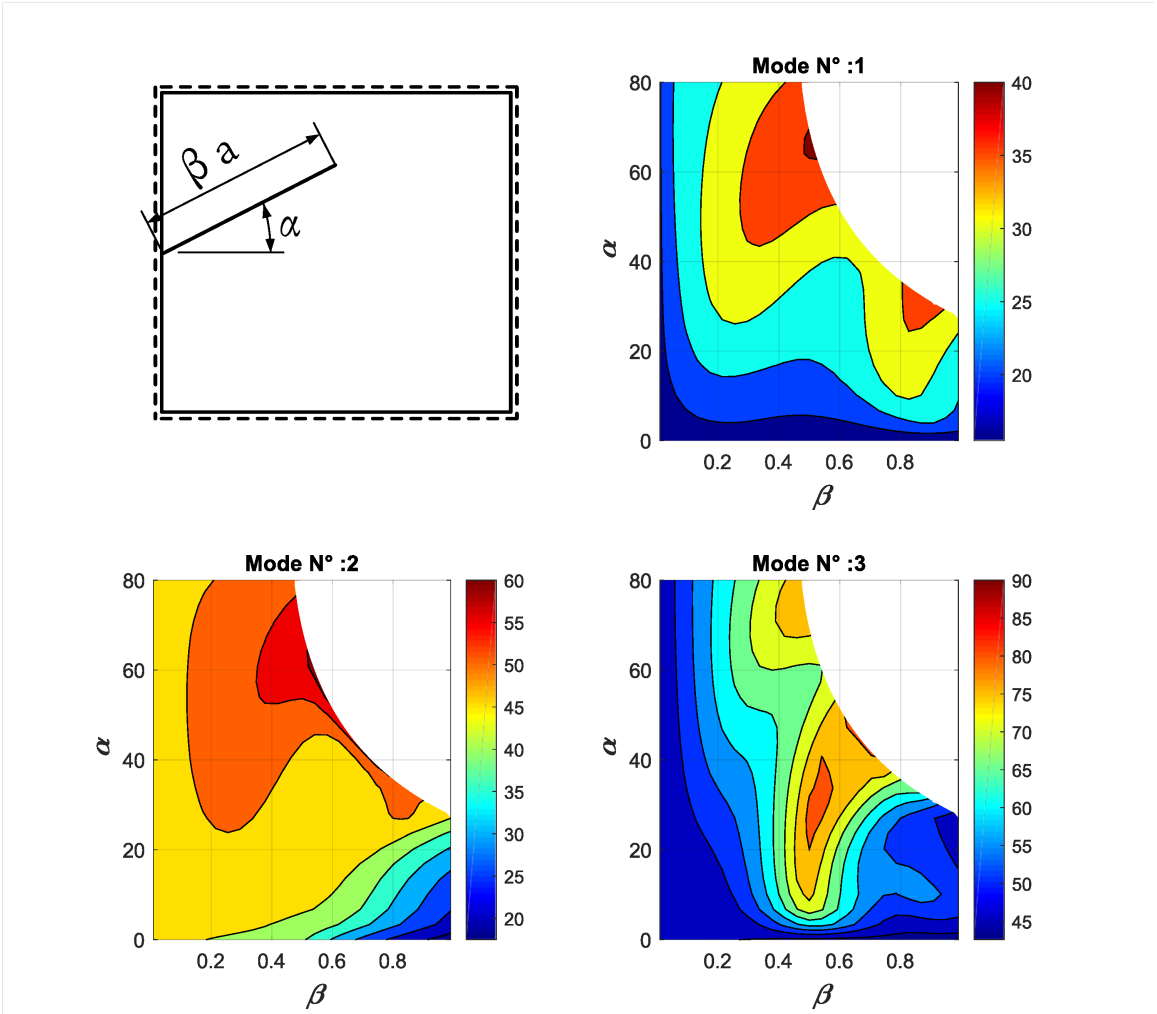

Figure 3.9: contour plots of the first three frequency parameters $\overline{\omega}$ versus crack angle α and crack length ratio β for an *S-S-S-S* nanoplate $\mu = 0.1nm^2$ with a *side crack*.

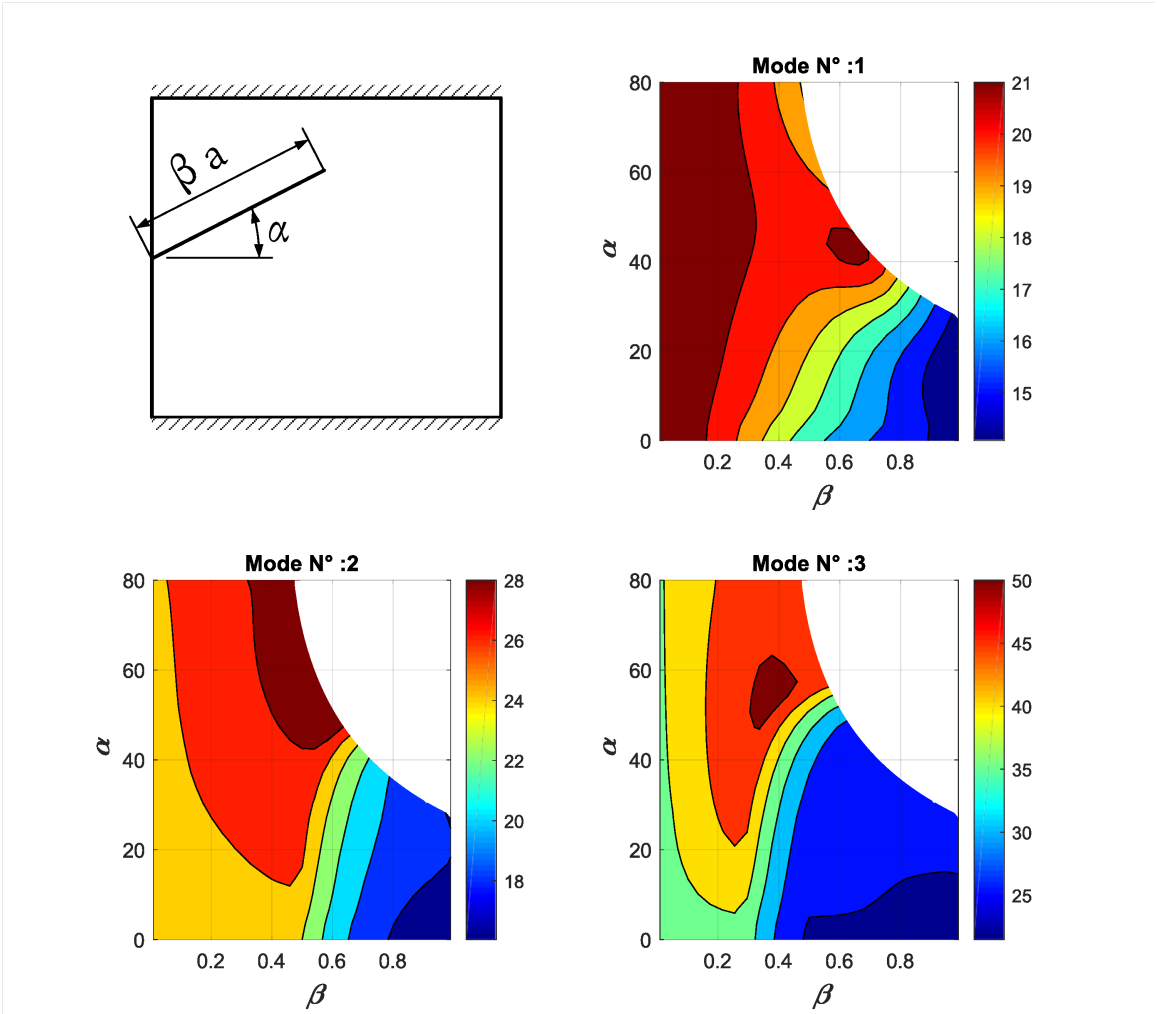

Figure 3.10: contour plots of the first three frequency parameters $\overline{\omega}$ versus crack angle α and crack length ratio β for an *C-F-C-F* nanoplate $\mu = 0.1nm^2$ with a *side crack*.

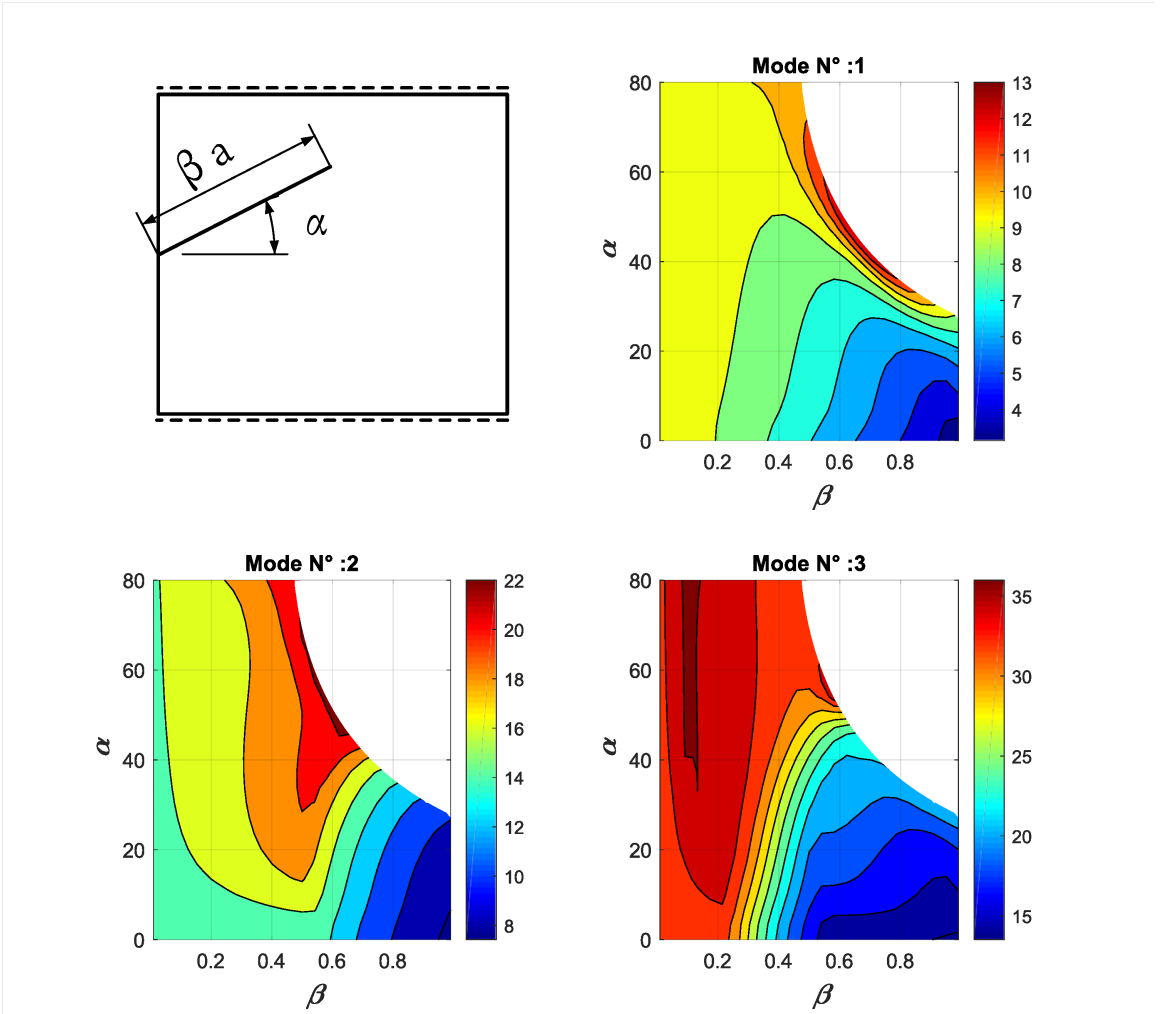

Figure 3.11: contour plots of the first three frequency parameters $\overline{\omega}$ versus crack angle α and crack length ratio β for an *S-F-S-F* nanoplate $\mu = 0.1nm^2$ with a *side crack*.

It is concluded from the analysis of the presented results that the presence of a horizontal side crack $\alpha = 0$ reduces the flexural stiffness as the crack length increases which results in lower frequency parameters. However, the presence of an inclined central crack $\alpha \neq 0$ increases the flexural stiffness that results in higher frequency parameters.

3.2.2 Central crack

Here, we investigate crack parameters influence (crack length and angle), we consider a plate with aspect ratio $a/b = 1$, as shown in Figure 3.1b, a 3×2 mesh is used for plates with central crack, the interpolation order is $p = 16$ for each element. The effect of crack length ratio β and crack angle α, is studied with different values of non-local parameter $\mu \in \{0nm^2, 0.06nm^2, 0.1nm^2\}$ for several cases of boundary conditions *(S-S-S-S, C-F-C-F and S-F-S-F).*

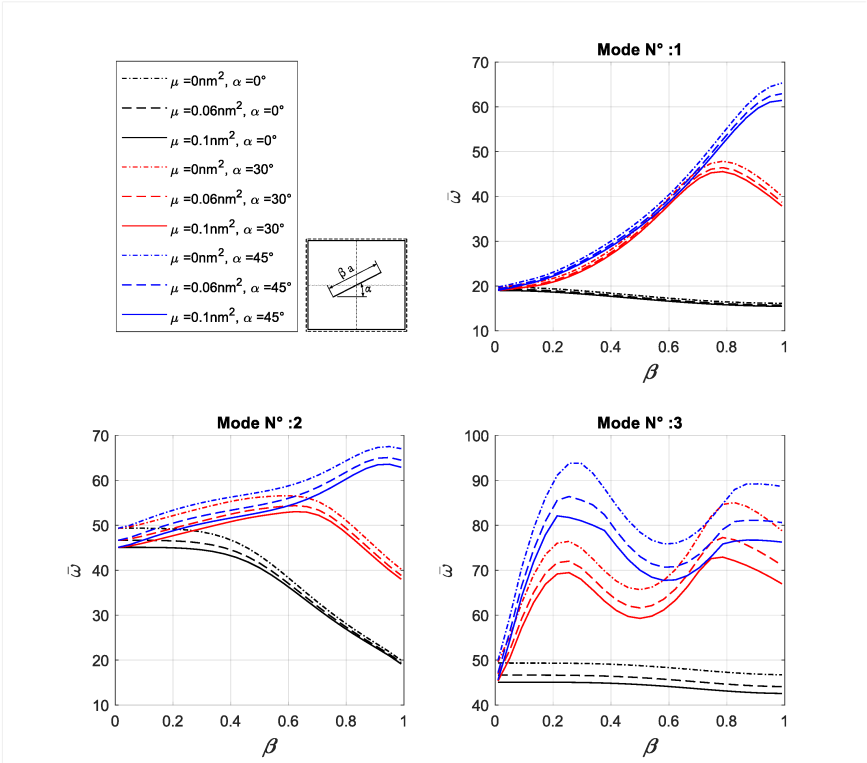

Figure 3.12: plots of the first three frequency parameters $\overline{\omega}$ versus crack length ratio β for an *S-S-S-S* nanoplate with a *central crack* and different values of crack angle α and non-local parameter μ.

Figures (3.12, 3.13 and 3.14) represent the variation of the three first frequency parameters as a function of the crack length ratio β for a square nanoplate with a central

crack, subjected to *(S-S-S-S, C-F-C-F and S-F-S-F)* boundary conditions respectively. It is noticeable that the frequency parameters decrease with the increasing values of non-local parameter μ for nanoplates with central crack for all cases of boundary conditions and for all values of crack length ratio β and crack angle α. Also it is observed that for crack angle $\alpha = 0$, the frequency parameters are decreasing with the increase of crack length ratio β.

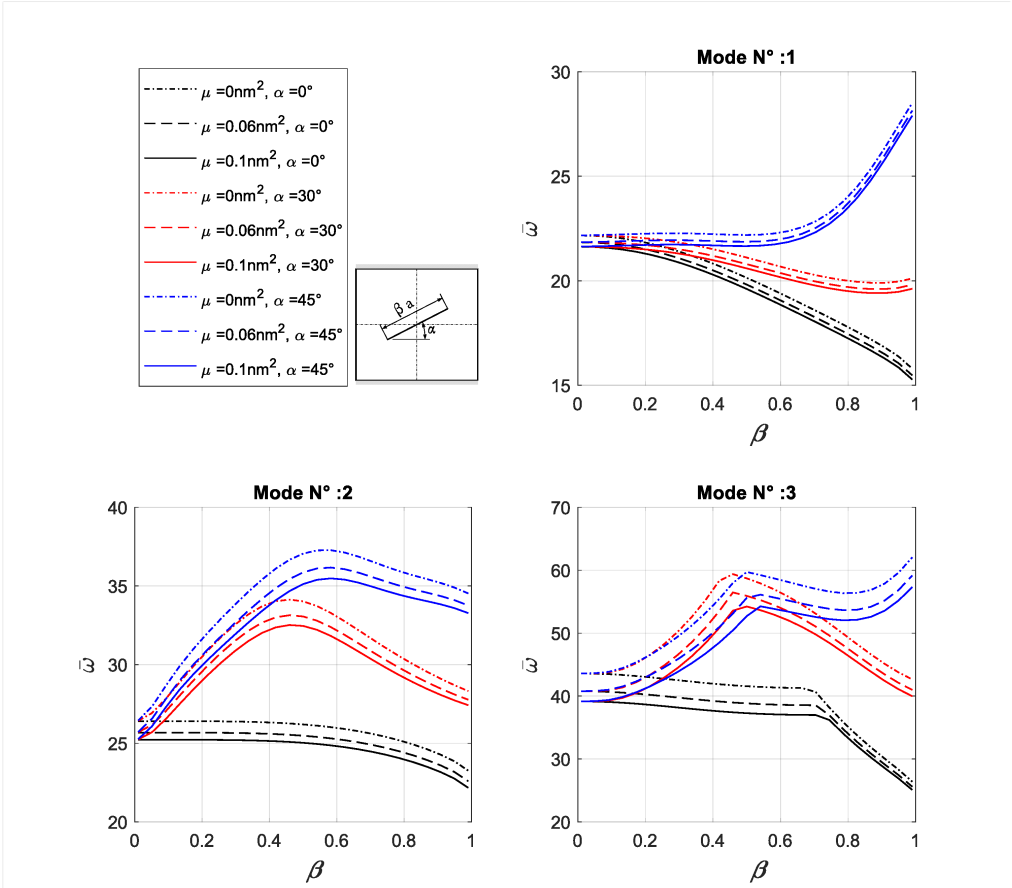

Figure 3.13: plots of the first three frequency parameters $\overline{\omega}$ versus crack length ratio β for an *C-F-C-F* nanoplate with a *central crack* and different values of crack angle α and non-local parameter μ.

For inclined central crack $(\alpha = 30^{\circ})$ and *(S-S-S-S)* boundary condition, it is noticed that the fundamental frequency parameter exhibits an increasing behavior for crack length ratio

$\beta \in [0:0.77]$, then decreases for $\beta > 0.77$. Also the second frequency parameter exhibits an increasing behavior for crack length ratio $\beta \in [0:0.65]$, then decreases for $\beta > 0.65$. However, the fundamental frequency parameter is decreasing with a low rate with respect to crack length ratio β for *(C-F-C-F)* configuration, and with a slightly higher rate for *(S-F-S-F)* configuration, then it changes behavior to increasing at $\beta \geq 0.85$.

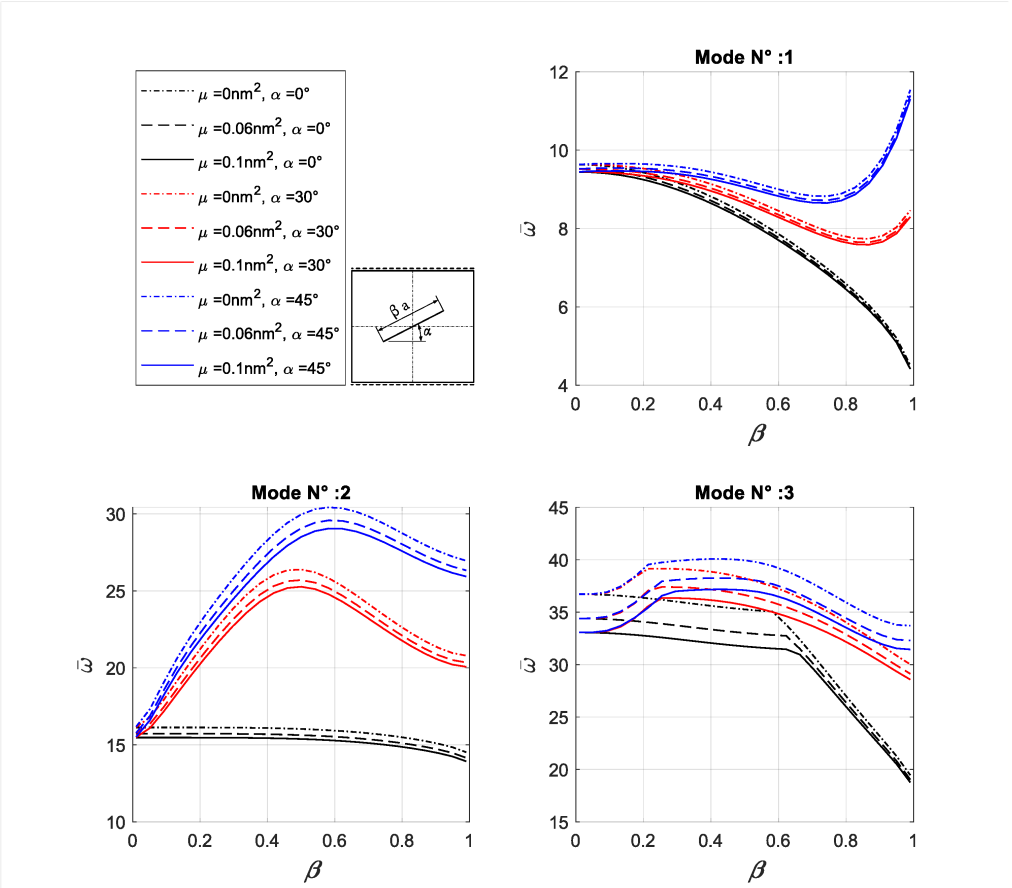

Figure 3.14: plots of the first three frequency parameters $\overline{\omega}$ versus crack length ratio β for an *S-F-S-F* nanoplate with a *central crack* and different values of crack angle α and non-local parameter μ.

For inclined central crack $(\alpha = 60^\circ)$ and *(S-S-S-S)* boundary condition, it is observed that the first and second frequency parameter monotonically increases with respect to crack

length ratio β, whereas for *(C-F-C-F)* configuration, the fundamental frequency parameter is at constant value and start increasing with higher and higher rates from $\beta \geq 0.5$. However for the *(S-F-S-F)* configuration, it is decreasing with low rates and starts increasing with higher and higher rates from $\beta \geq 0.7$.

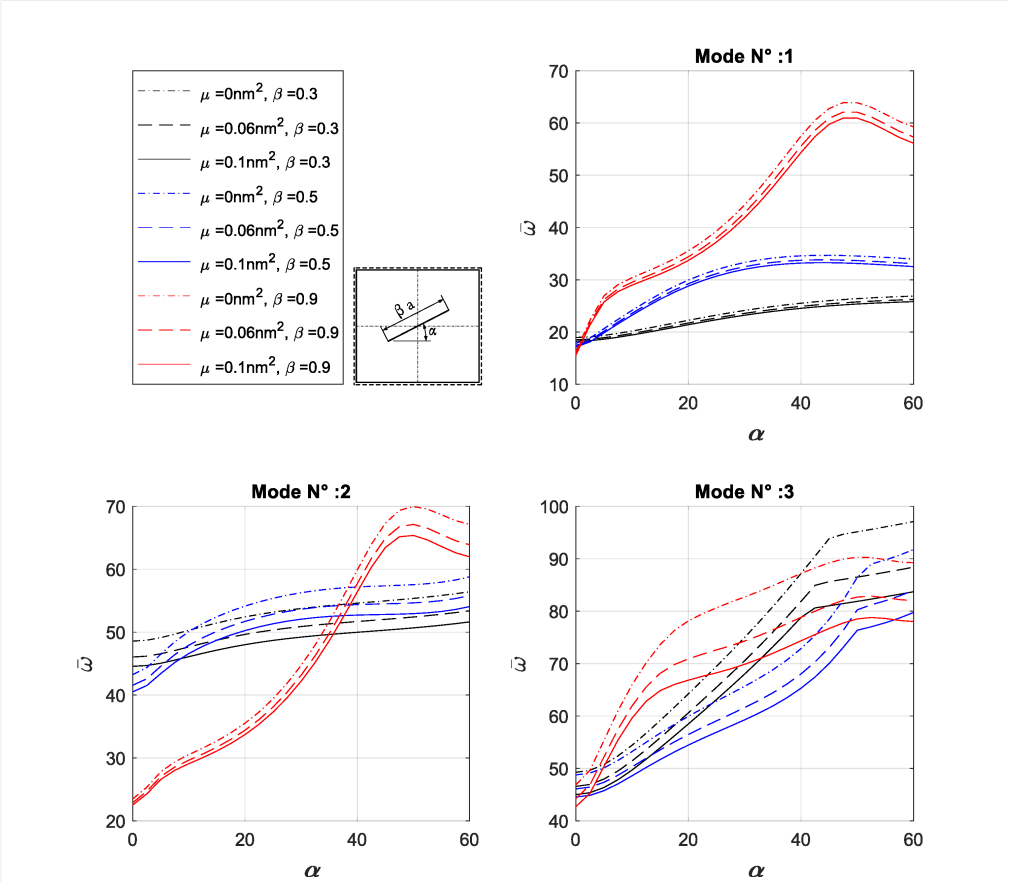

Figure 3.15: plots of the first three frequency parameters $\overline{\omega}$ versus crack angle α for an *S-S-S-S* nanoplate with a *central crack* and different values of crack length ratio β and non-local parameter μ.

On the other hand for *(S-S-S-S, C-F-C-F* and *S-F-S-F)* boundary condition, the third frequency parameter manifests a fluctuating behavior as a function of crack length ratio β for both configurations of crack angle $(\alpha = 30^\circ)$ and $(\alpha = 60^\circ)$. Also the second frequency parameter is increasing with a high rate then decreases with relatively lower rate

with respect to crack length ratio β for *(C-F-C-F* and *S-F-S-F)* configuration in both cases of crack angle $(\alpha = 30^\circ)$ and $(\alpha = 60^\circ)$.

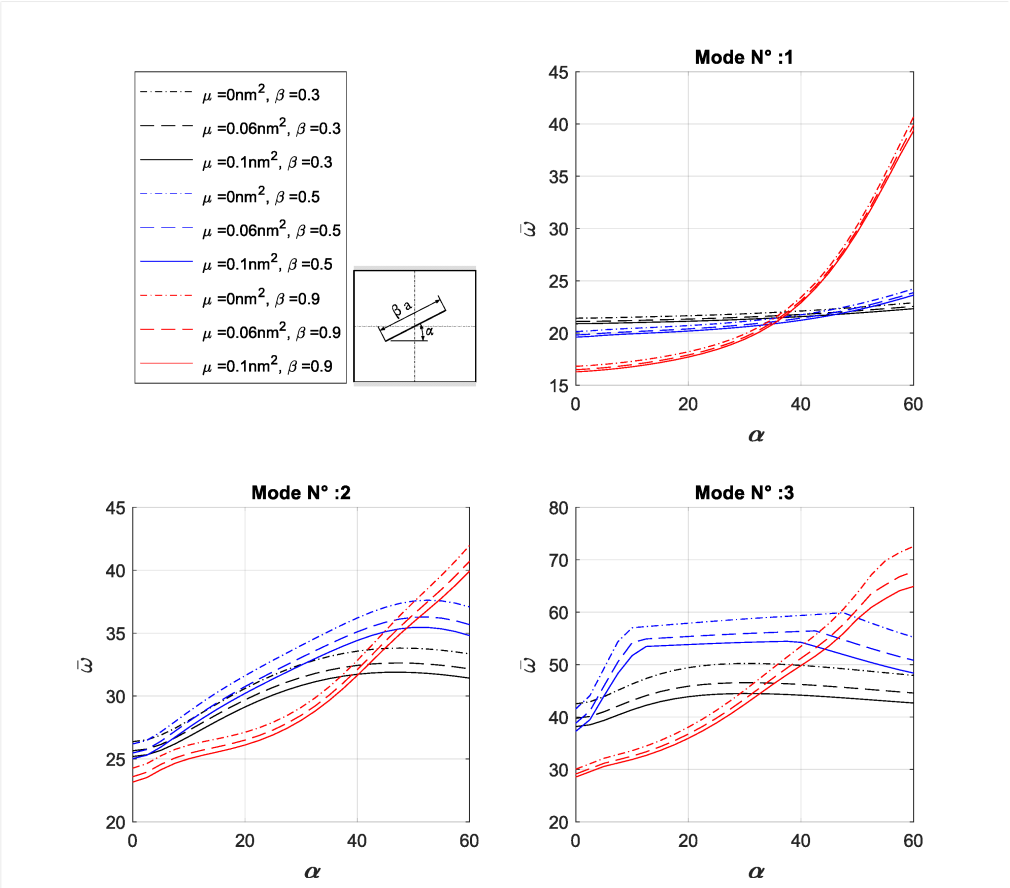

Figure 3.16: plots of the first three frequency parameters $\overline{\omega}$ versus crack angle α for an *C-F-C-F* nanoplate with a *central crack* and different values of crack length ratio β and non-local parameter μ.

The three first frequency parameters as a function of the crack angle α for a square nanoplate with a central crack, subjected to *(S-S-S-S, C-F-C-F and S-F-S-F)* boundary conditions are shown in Figures (3.15, 3.16 and 3.17) respectively. It is clear that for all boundary conditions configurations, frequency parameters are generally increasing with respect to crack angle α, whereas the rate of increase is higher for higher values of crack

length ratios β. Again the non-local parameter μ is causing frequency parameters to drop for all cases of boundary conditions and for all values of crack length ratio β and crack angle α.

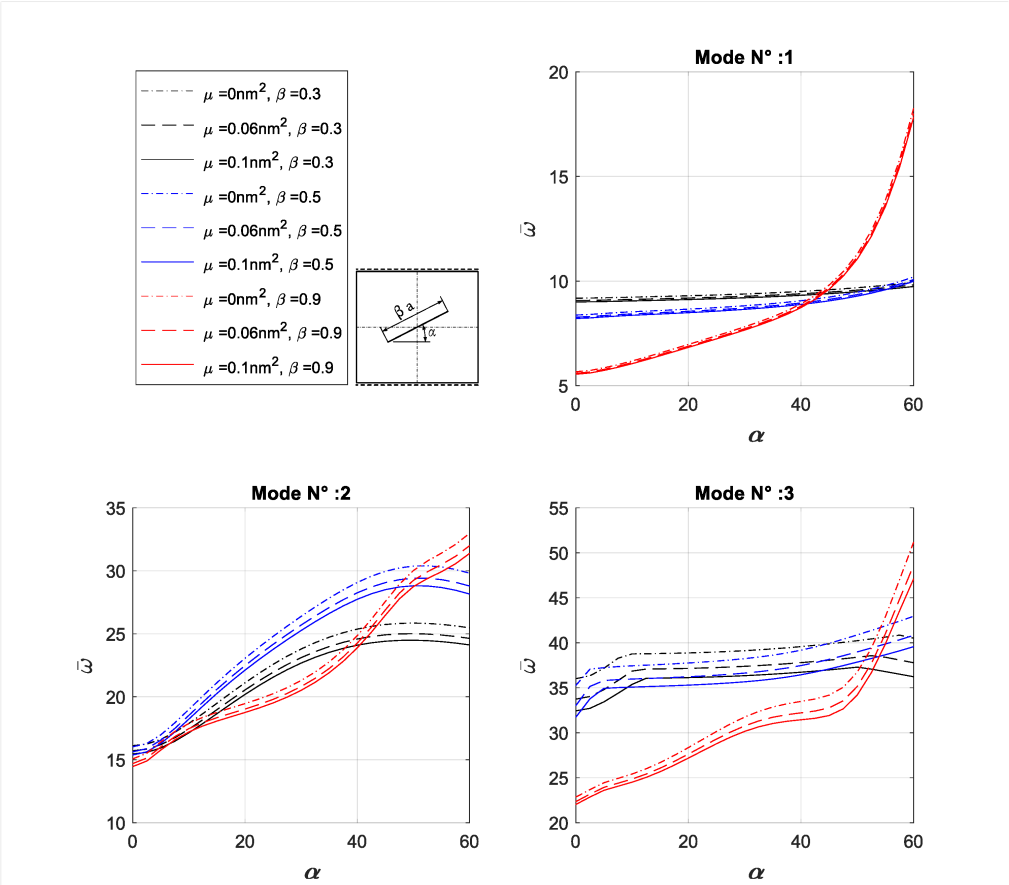

Figure 3.17: plots of the first three frequency parameters $\overline{\omega}$ versus crack angle α for an *S-F-S-F* nanoplate with a *central crack* and different values of crack length ratio β and non-local parameter μ.

The three first frequency parameters as function of crack length ratio β and crack angle α for square nanoplates $\mu = 0.1nm^2$ with central crack, are presented as contour plots for *(S-S-S-S, C-F-C-F and S-F-S-F)* boundary conditions in Figures (3.18, 3.19 and 3.20) respectively.

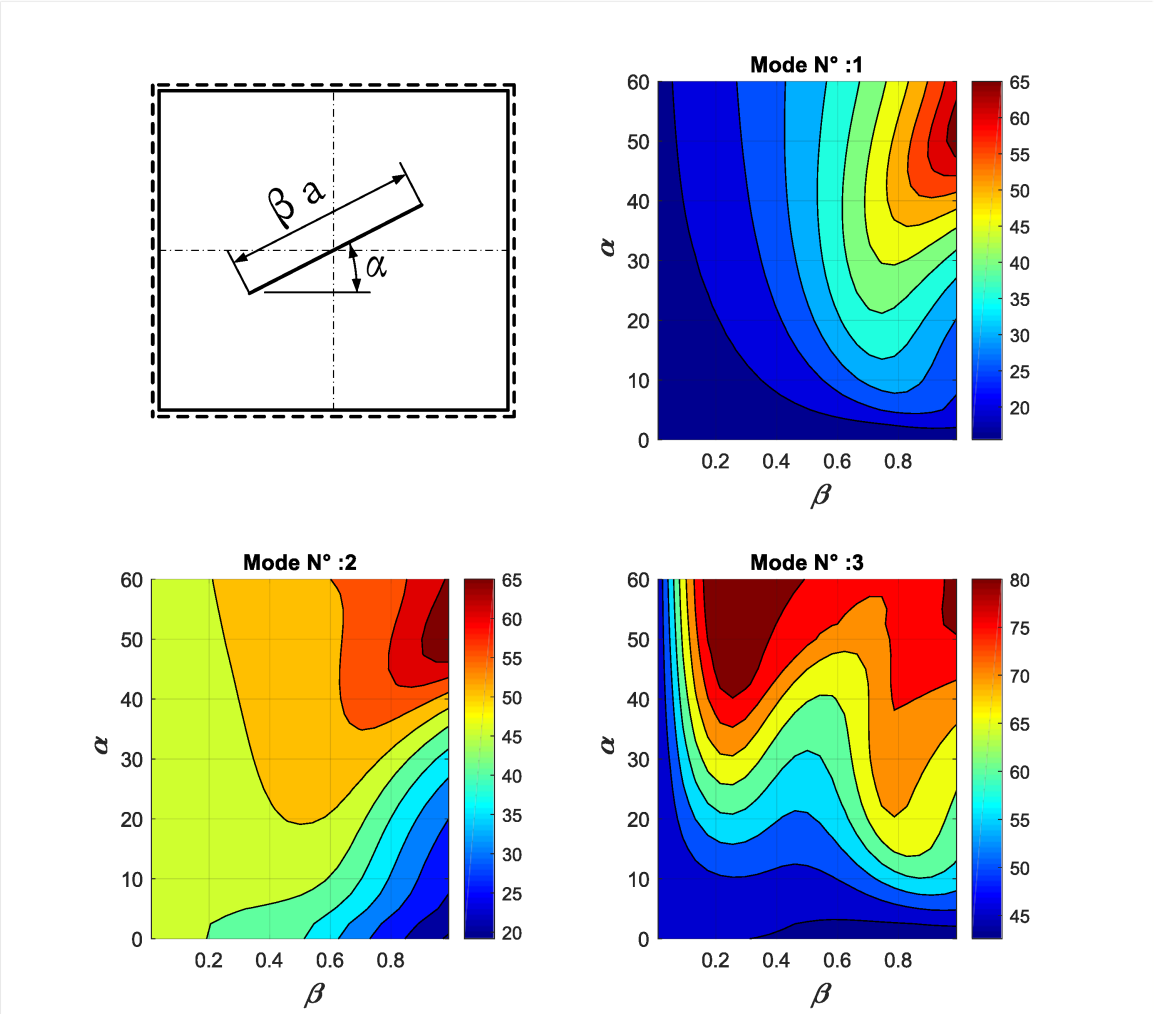

Figure 3.18: contour plots of the first three frequency parameters $\overline{\omega}$ versus crack angle α and crack length ratio β for an *S-S-S-S* nanoplate $\mu = 0.1nm^2$ with a *central crack*.

This representation gives a more complete insight into the combined effect of crack length ratio β and crack angle α, it can be noted that increasing crack angle α often causes frequency parameters to increase. On the other hand increasing crack length ratio causes frequencies to drop for crack angle $\alpha = 0$, but for crack angle $\alpha \neq 0$, it is noticed that increasing crack length ratio β often amplifies the effect of crack angle α on the frequency parameters.

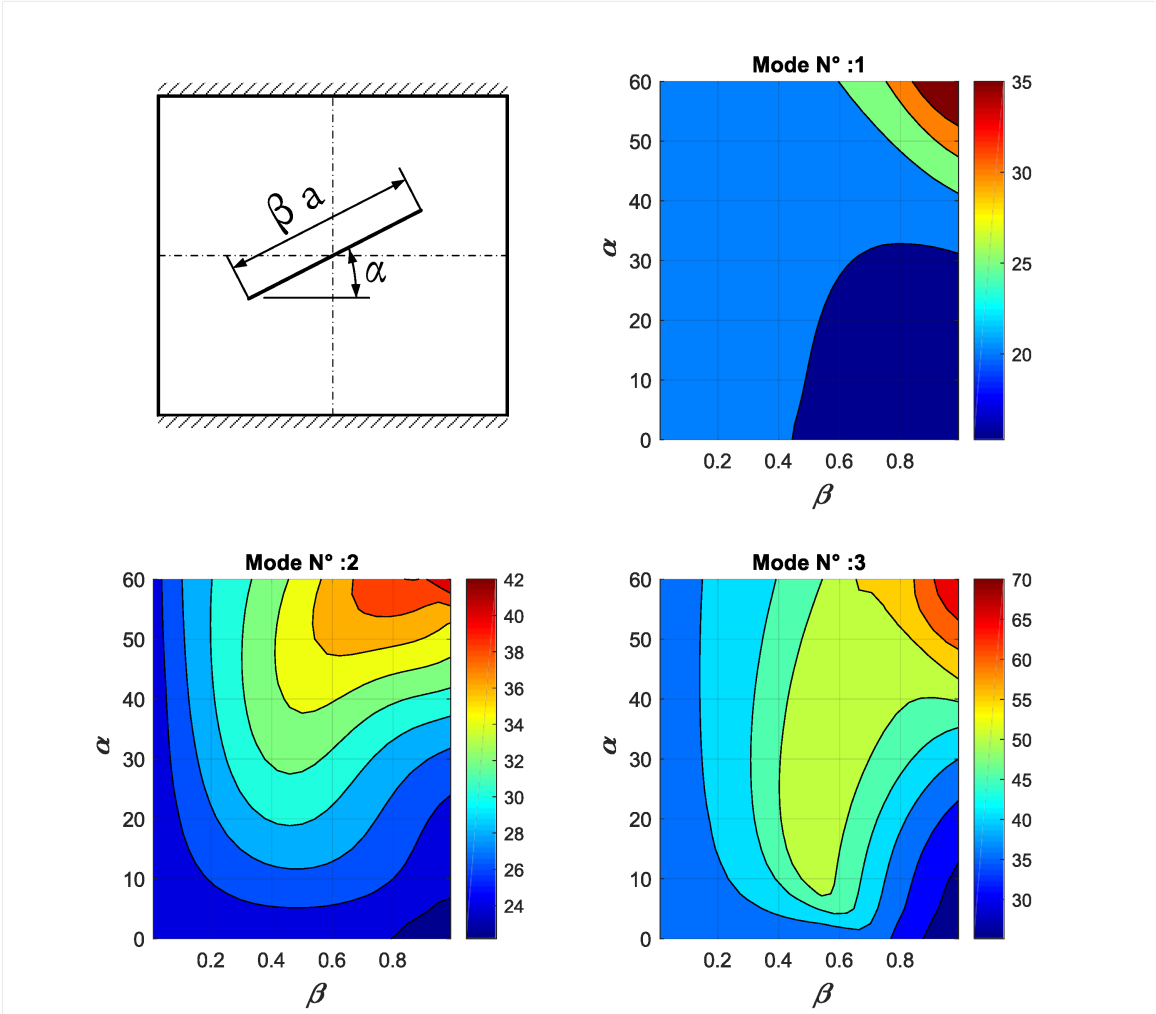

Figure 3.19: contour plots of the first three frequency parameters $\overline{\omega}$ versus crack angle α and crack length ratio β for an *C-F-C-F* nanoplate $\mu = 0.1nm^2$ with a *central crack*.

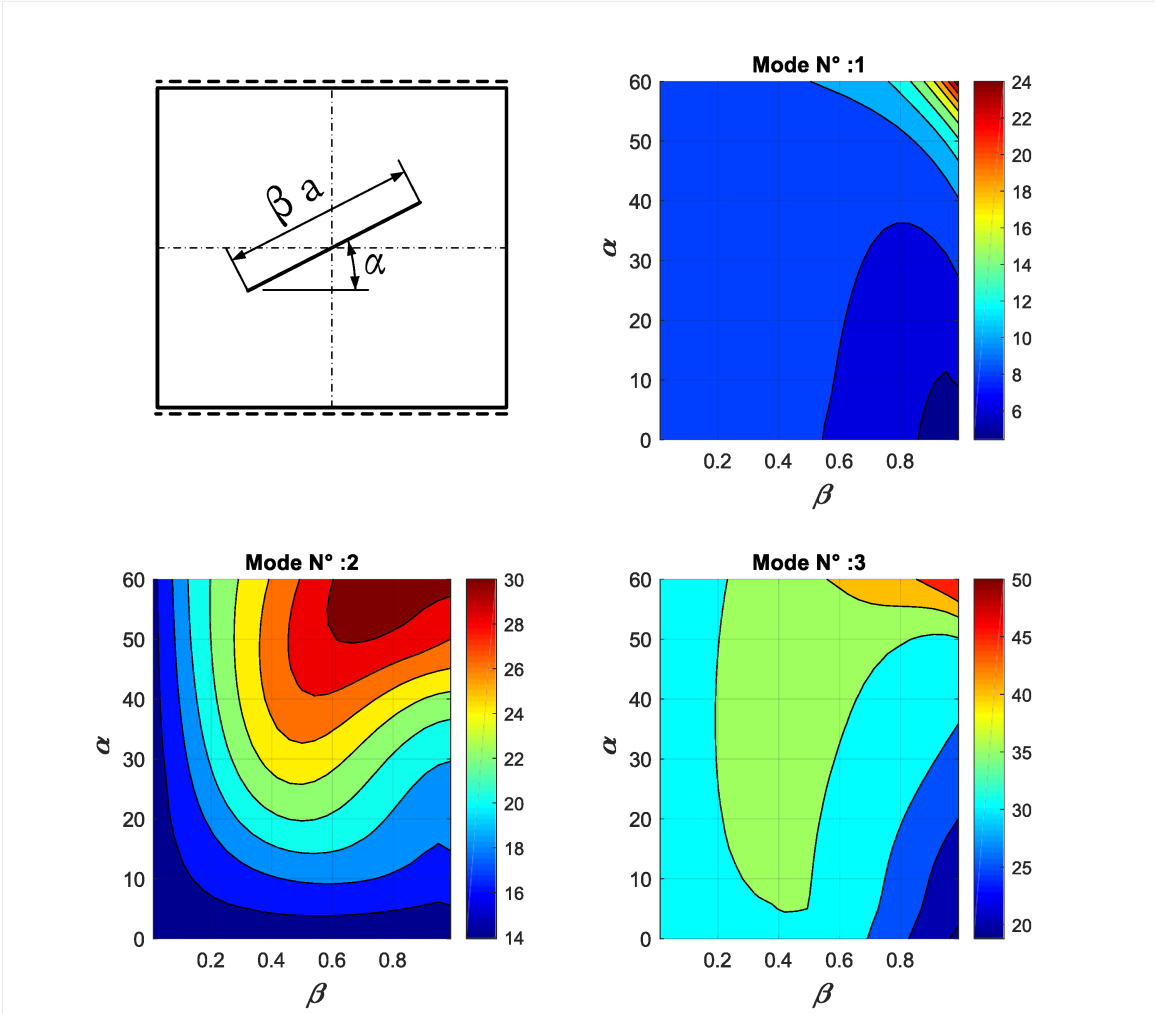

Figure 3.20: contour plots of the first three frequency parameters $\overline{\omega}$ versus crack angle α and crack length ratio β for an *S-F-S-F* nanoplate $\mu = 0.1nm^2$ with a *central crack*.

Similar to the results of the side crack, the presented results of a horizontal central crack $\alpha = 0$ suggest that the crack reduces the flexural stiffness as the crack length increases, hence lowering frequency parameters. However the an inclined central crack $\alpha \neq 0$ increases the flexural stiffness resulting in higher frequency parameters.

3.3 Summary

In this chapter, we considered linear vibration of isotropic cracked nanoplates based on non-local elasticity and first-order shear deformation theory. The cracked plate is modeled using the *h-p* version of the finite element method. The advantage of this modeling approach is that it requires significantly less preprocessing and no human intervention when refinement is needed or when crack parameters are changed. The developed numerical approach is shown to be accurate when compared to results in literature for intact nanoplates and cracked local plates, thus the model is suitable to study cracked nanoplates. The investigation of the effect of crack parameters (length, orientation), plate geometry, boundary conditions and the non-local parameter on frequency parameter revealed that the non-local parameter has a softening effect that leads to the decrease of frequency. Also, the frequency parameter increases as a function of plate aspect ratio and side to thickness ratios. With regard to crack parameters, it is concluded that a horizontal crack softens the nanoplate as the crack length increases which results in lower frequencies. However, an inclined crack increases the flexural stiffness and increases frequency parameters. In the following chapter, linear free vibrations of functionally graded material (FGM) cracked nanoplates will be considered.

Chapter 4

Linear Vibration of cracked FGM nanoplates

In the previous chapter, the influence of crack parameters and the non-local effect on linear free vibration of isotropic cracked nanoplates has been investigated and discussed. The aim of this chapter is to investigate the linear free vibrations of functionally graded nano-plates by studying the influence of material parameters (i.e. volume fraction exponent n) along with crack parameters.

In this chapter we:

- Investigate convergence for intact and cracked FGM plates.
- Conduct a comparison with results in literature to verify the accuracy of the present model for intact FGM plates.
- Present and discuss original results for cracked non-local FGM plates, subjected to several cases of boundary conditions, in order to investigate the influence of volume fraction exponent n, crack length ratio β, crack angle α and non-local parameter μ.
- Study the influence of crack position γ and volume fraction exponent on linear free vibrations of cracked FGM nanoplates.

Table 4.1: Material constants of Ti–6Al–4V and Aluminum oxide at T=300K

	P_0	P_{-1}	P_1	P_2	P_3	P @ 300K
Aluminum oxide						
E	349.55 e9	0.0	-3.853 e-4	4.027 e-7	-1.673 e-10	3.2024 e11
ν	0.26	0.0	0.0	0.0	0.0	0.26
ρ	3750	0.0	0.0	0.0	0.0	3750
Ti–6Al–4V						
E	122.56 e9	0.0	-4.586 e-4	0.0	0.0	1.057 e11
ν	0.2884	0.0	1.12 e-4	0.0	0.0	0.2981
ρ	4429	0.0	0.0	0.0	0.0	4429

4.1 Convergence and Comparison

In this section, convergence of the linear solution is verified for a centrally cracked $\beta = 0.3$ simply supported square plate modeled using one p-element (3×2 mesh in the serendipity polynomial space). Materials properties used in this chapter are listed in Table 4.1.

Table 4.3 depicts results of first three modes for a *moderately thick plate* $\frac{a}{h} = 10$, for increasing p-refinement. It is clear that reasonable convergence of the linear solution is achieved at low values of p.

Table 4.2: Comparison of the first frequency parameter $\overline{\omega} = \omega h\sqrt{\frac{\rho_c}{E_c}}$ of simply supported square Al/Al_2O_3 FG plates

a/h	Source	n				
		0	0.5	1	4	10
5	ref [92]	0.2121	0.1819	0.1640	0.1383	0.1306
	ref [93]	0.2055	0.1757	0.1587	0.1356	0.1284
	present	0.2112	0.1862	0.1756	0.1473	0.1289
10	ref [92]	0.0577	0.0492	0.0443	0.0381	0.0364
	ref [93]	0.0567	0.0482	0.0435	0.0376	0.0359
	present	0.0577	0.0507	0.0480	0.0405	0.0354

Table 4.3: Convergence of first three frequency parameters $\overline{\omega} = \omega h\sqrt{\frac{\rho_c}{E_c}}$ for a simply supported square FG (Al/Al_2O_3) plates with central crack $\beta = 0.3$

n	mode n°	$p^\dagger$								
		4	5	6	7	8	9	10	11	12
0	1^{st}	0.0558	0.0550	0.0547	0.0545	0.0544	0.0544	0.0543	0.0543	0.0543
	2^{nd}	0.1353	0.1339	0.1330	0.1327	0.1325	0.1324	0.1322	0.1321	0.1321
	3^{rd}	0.1378	0.1374	0.1373	0.1373	0.1372	0.1372	0.1372	0.1372	0.1372
0.5	1^{st}	0.0491	0.0484	0.0481	0.0479	0.0479	0.0478	0.0478	0.0477	0.0477
	2^{nd}	0.1192	0.1180	0.1172	0.1169	0.1168	0.1166	0.1165	0.1164	0.1163
	3^{rd}	0.1213	0.1210	0.1209	0.1209	0.1208	0.1208	0.1208	0.1208	0.1208
1.0	1^{st}	0.0464	0.0458	0.0455	0.0453	0.0453	0.0452	0.0452	0.0451	0.0451
	2^{nd}	0.1125	0.1114	0.1106	0.1104	0.1102	0.1101	0.1100	0.1099	0.1098
	3^{rd}	0.1146	0.1143	0.1142	0.1142	0.1141	0.1141	0.1141	0.1141	0.1141
5	1^{st}	0.0409	0.0404	0.0401	0.0400	0.0400	0.0399	0.0399	0.0399	0.0398
	2^{nd}	0.0981	0.0970	0.0964	0.0962	0.0960	0.0959	0.0958	0.0957	0.0956
	3^{rd}	0.1002	0.1000	0.0999	0.0999	0.0999	0.0998	0.0998	0.0998	0.0998
10	1^{st}	0.0376	0.0371	0.0369	0.0368	0.0368	0.0367	0.0367	0.0367	0.0367
	2^{nd}	0.0902	0.0892	0.0886	0.0884	0.0883	0.0881	0.0880	0.0880	0.0879
	3^{rd}	0.0922	0.0920	0.0919	0.0919	0.0919	0.0918	0.0918	0.0918	0.0918

$a/b = 1, a/h = 10$

†: Serendipity polynomial space

In order to verify the accuracy of the present model for FGM plates a comparison is carried out for linear free vibration of intact plates results available in literature. In Table 4.2 the fundamental frequency parameters $\overline{\omega} = \omega h\sqrt{\frac{\rho_c}{E_c}}$ of simply supported square plates are compared with numerical results of Matsunga [92] and Zhao [93]. It is clear that the results of the present model are in good agreement with those of references.

4.2 Parametric study of cracked FGM nano-plates

The effect of volume fraction exponent n and crack length ratio β is presented in Table 4.4 for a side and central horizontal crack $\alpha = 0$ in simply supported nanoplate. It is observed in both cases of side and central crack that, the frequency parameters in all modes decrease with the growth of crack length, whereas for plates with a certain crack length, the frequency parameters decrease with the increase of volume fraction exponent n.

Table 4.4: Effect of volume fraction exponent n and crack length ratio β on the first three frequency parameters $\overline{\omega} = \omega \frac{a^2}{h}\sqrt{\frac{12(1-\nu_m^2)\rho_m}{E_m}}$, for an *S*-*S*-*S*-*S* square nanoplates with side and central crack $(\nu = 0.3,\ \alpha = 0,\ \mu = 0.1nm^2,\ a/h = 10^3)$

β	0.25			0.5			0.75		
mode n°	1	2	3	1	2	3	1	2	3
	Side crack								
0.0	42.735	101.326	101.692	40.985	92.353	99.469	37.710	60.911	99.110
0.2	34.824	82.551	82.880	33.344	75.166	80.927	30.591	49.423	80.613
0.5	29.761	70.537	70.839	28.460	64.177	69.077	26.053	42.098	68.793
0.8	27.289	64.671	64.958	26.078	58.814	63.295	23.844	38.531	63.028
1.0	26.243	62.190	62.471	25.070	56.547	60.851	22.911	37.025	60.590
1.5	24.606	58.304	58.575	23.493	52.997	57.023	21.450	34.666	56.774
2.0	23.649	56.035	56.300	22.572	50.922	54.787	20.595	33.287	54.544
10.0	20.463	48.469	48.724	19.487	43.983	47.299	17.712	28.634	47.070
100.0	19.108	45.246	45.506	18.160	41.005	44.078	16.452	26.600	43.849
	Central crack								
0.0	41.789	101.198	101.754	39.254	91.968	100.915	36.906	67.286	98.930
0.2	34.024	82.474	82.927	31.887	74.869	82.190	29.919	54.625	80.451
0.5	29.058	70.490	70.877	27.186	63.935	70.212	25.468	46.549	68.644
0.8	26.635	64.637	64.992	24.894	58.599	64.364	23.302	42.615	62.886
1.0	25.609	62.161	62.502	23.926	56.342	61.890	22.387	40.953	60.451
1.5	24.004	58.284	58.604	22.409	52.809	58.017	20.955	38.351	56.639
2.0	23.067	56.019	56.327	21.523	50.744	55.755	20.118	36.829	54.411
10.0	19.935	48.478	48.745	18.543	43.845	48.204	17.287	31.705	46.941
100.0	18.596	45.274	45.523	17.251	40.890	44.981	16.045	29.471	43.717

4.2.1 Side crack

Here, we consider a square plate $a/b = 1$ with side crack, a 2×2 elements mesh is used as shown in Figure 3.1a, the degree of interpolation is $p = 16$ for each element. The effect of volume fraction exponent n, crack length ratio β and crack angle α on the non-dimensional frequency parameters $\overline{\omega} = \omega \frac{a^2}{h}\sqrt{\frac{12\left(1-\nu_m^2\right)\rho_m}{E_m}}$, is studied for different values of non-local parameter μ and several cases of boundary conditions *(C-C-C-C, S-S-S-S, C-S-C-S, S-C-S-C, C-F-C-F, F-C-F-C, S-F-S-F* and *F-S-F-S).*

The effects of the crack length ratio β, volume fraction exponent n and crack angle α on the two first frequency parameters for a clamped *(C-C-C-C)* square nanoplate with a side crack is presented in Figure 4.1 for different values non local parameter μ. The obtained results show that the fundamental frequency decreases with a relatively low rate for horizontal crack $\alpha = 0$ as a function of crack length ratio β, however it increases with a high rate for an inclined side crack $\alpha = 60°$ and fluctuates for lower crack angles $\alpha = 20°, 40°$ but mostly the fundamental frequency is higher than that of an intact plate. Furthermore the second frequency parameter for a horizontal crack decreases with a low rate for $\beta < 0.5$ then with high rate as the crack length ratioβ is higher than 0.5, this is also mostly true for slightly inclined crack $\alpha = 20°$ however some minor fluctuations can be observed a low crack lengths $0 < \beta < 0.3$, in addition for moderately inclined crack $\alpha = 40°$ significant fluctuations are exhibited yet the second frequency is often higher than that of an intact plate. For highly inclined crack $\alpha = 60°$ the second frequency parameter increases monotonically with a relatively low rate.

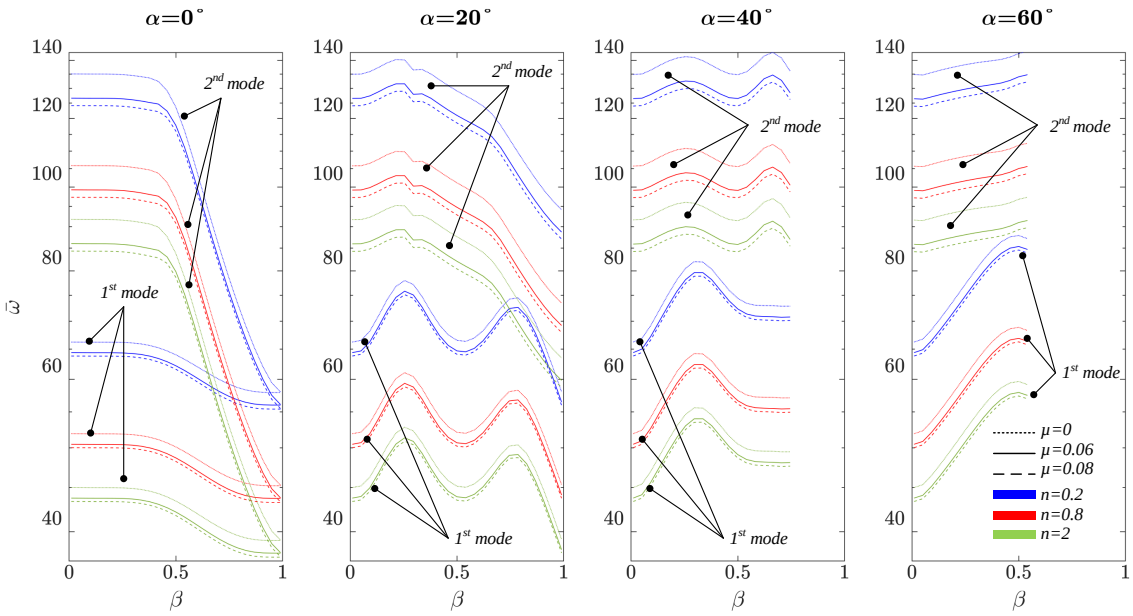

Figure 4.1: Plots of the first and second frequency parameters $\overline{\omega}$ versus crack length ratio β of a FGM nanoplate with a *side crack* for different values of volume fraction exponent n, crack angle α and non-local parameter μ, subjected to *C-C-C-C* boundary conditions.

Figure 4.1 presents the effects of the crack length ratio β on the two first frequency parameters for a simply supported *(S-S-S-S)* square nanoplate with a side crack and different values of volume fraction exponent n, crack angle α and non local parameter μ. These results show generally similar trends when compared to clamped plate especially for horizontal crack $\alpha = 0$. However some differences can be noted, for example the fluctuations of frequency parameters for inclined side cracks are much more intense than those of clamped plates and the fluctuating frequencies are always higher than those of intact plates.

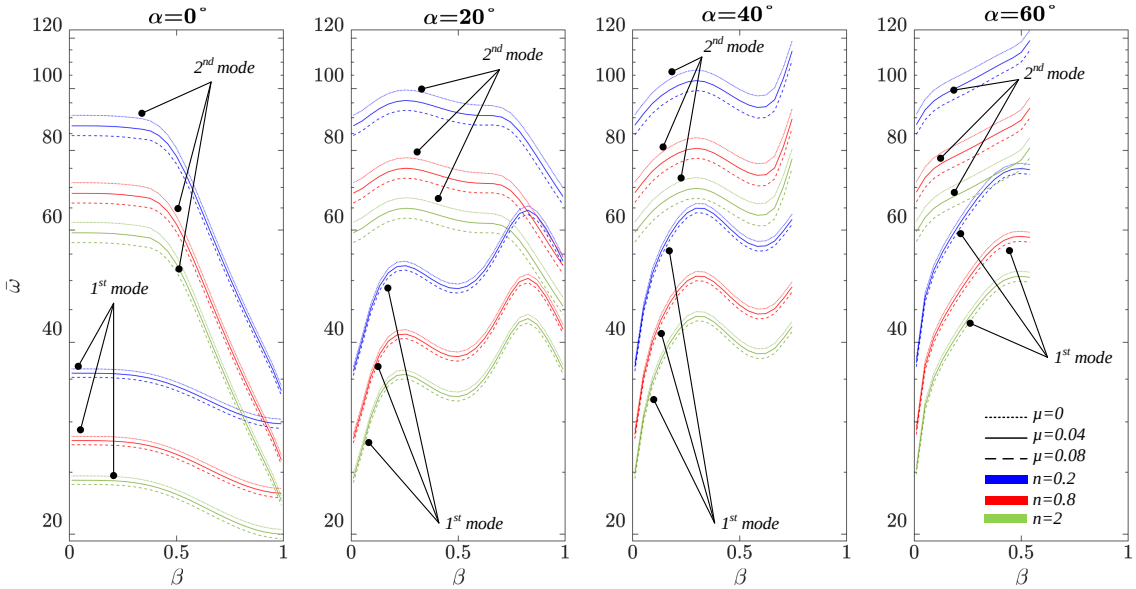

Figure 4.2: Plots of the first and second frequency parameters $\overline{\omega}$ versus crack length ratio β of a FGM nanoplate with a *side crack* for different values of volume fraction exponent n, crack angle α and non-local parameter μ, subjected to *S-S-S-S* boundary conditions.

The effects of the crack length ratio β on the two first frequency parameters of a *(C-S-C-S)* square nanoplate with a side crack is presented in Figure 4.1 for different values non local parameter μ, volume fraction exponent n and crack angle α. The obtained results show identical trends when compared to the results of clamped *(C-C-C-C)* plates.

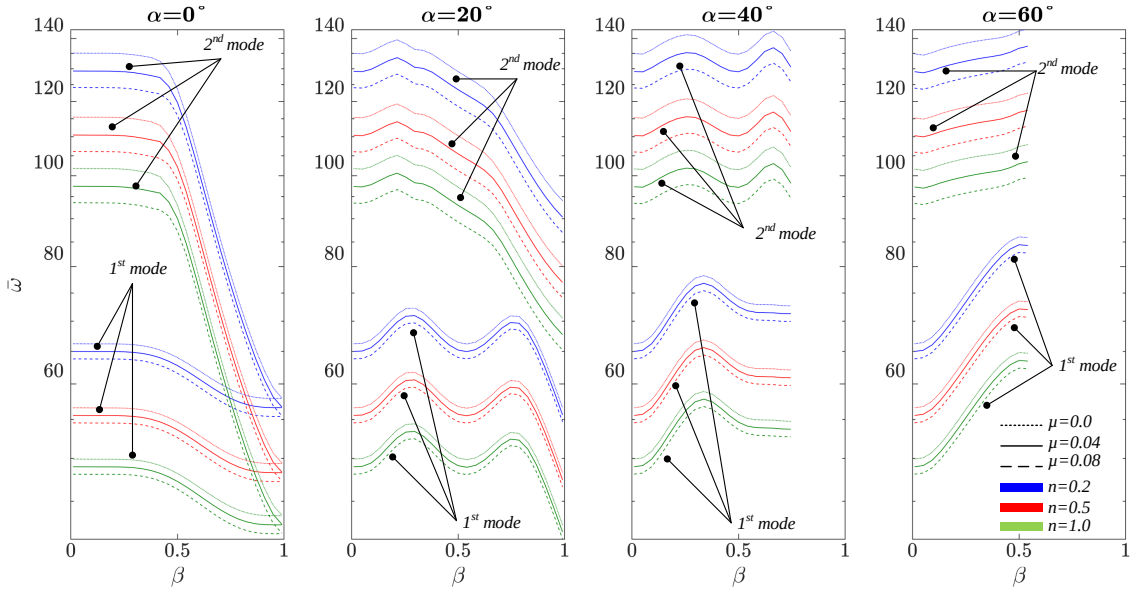

Figure 4.3: Plots of the first and second frequency parameters $\overline{\omega}$ versus crack length ratio β of a FGM nanoplate with a *side crack* for different values of volume fraction exponent n, crack angle α and non-local parameter μ, subjected to *C-S-C-S* boundary conditions.

Figure 4.4 presents the effects of the crack length ratio β on the two first frequency parameters for square nanoplates with a side crack subjected to *(S-C-S-C)* boundary conditions and different values of volume fraction exponent n, crack angle α and non local parameter μ.

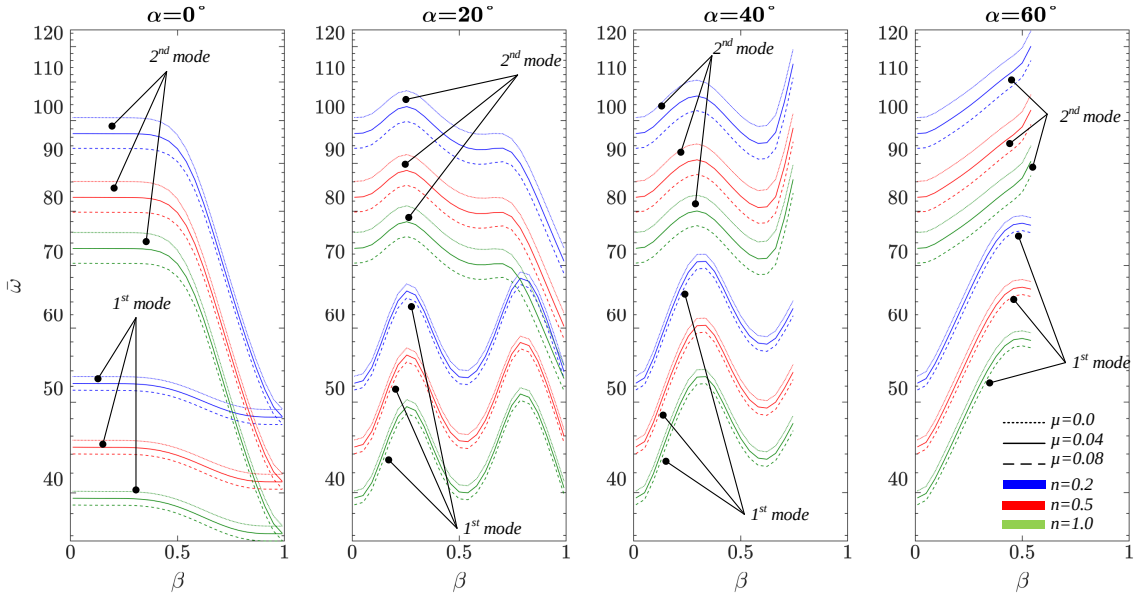

Figure 4.4: Plots of the first and second frequency parameters $\overline{\omega}$ versus crack length ratio β of a FGM nanoplate with a *side crack* for different values of volume fraction exponent n, crack angle α and non-local parameter μ, subjected to *S-C-S-C* boundary conditions.

The previously presented results considered different combinations of clamped and simply supported boundary conditions, showing slight to moderate differences in vibrational behavior of side crack FGM nanoplates. Subsequently various combinations of free edges with clamped or simply supported boundary conditions are studied and discussed. Figure 4.5 shows the effects of the crack length ratio β on the two first frequency parameters for a square FGM nanoplate with a side crack for different values of volume fraction exponent n, crack angle α and non local parameter μ, subjected to *(C-F-C-F)* boundary conditions. it is observed that the fundamental frequency parameter is decreasing as the crack length increases, the decreasing rate is high for horizontal an slightly inclined cracks $\alpha = 0°, 20°$ and relatively low rate of decrease is observed for higher angles $\alpha = 40°, 60°$ with a minor fluctuation for crack angle $\alpha = 40°$. Additionally the second frequency parameter for a horizontal side crack decreases with a low rate for crack length ratio $\beta < 0.5$ and a high rate for $\beta > 0.5$. For low and moderate crack angles $\alpha = 20°, 40°$ the second

frequency parameter increases if crack length ratio $\beta < 0.5$ and then decreases with a high rate. At high crack angle $\alpha = 60°$ the second frequency parameter increases with high rate.

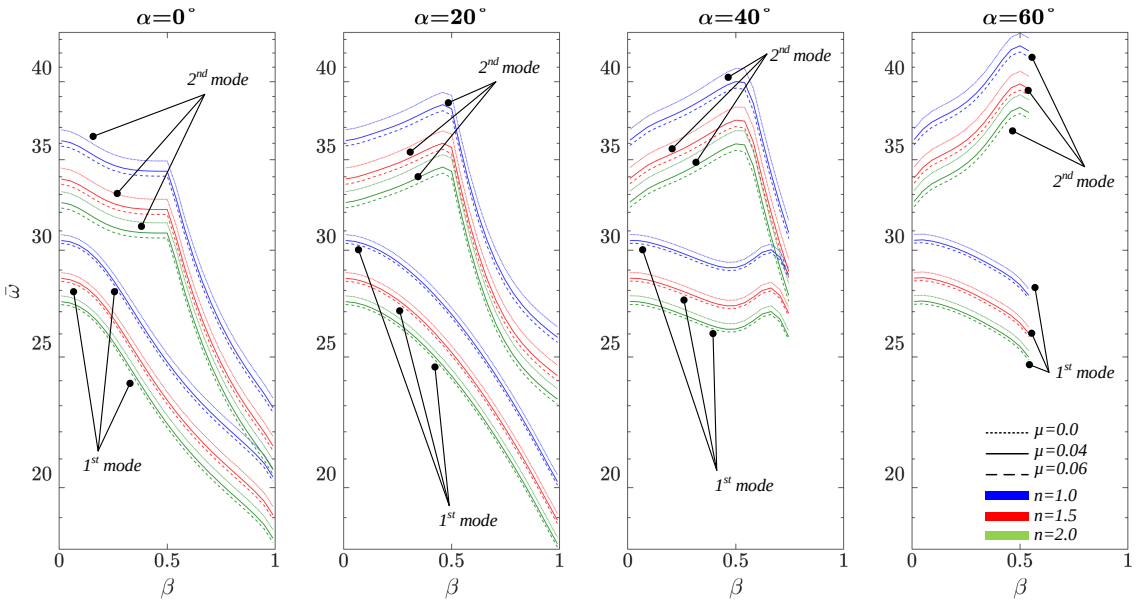

Figure 4.5: Plots of the first and second frequency parameters $\overline{\omega}$ versus crack length ratio β of a FGM nanoplate with a *side crack* for different values of volume fraction exponent n, crack angle α and non-local parameter μ, subjected to *C-F-C-F* boundary conditions.

Figure 4.6 presents the effects of the crack length ratio β on the two first frequency parameters of a square nanoplate with a side crack for different values non local parameter μ, volume fraction exponent n and crack angle α subjected to *(F-C-F-C)* boundary conditions (i.e., the crack is emanating from a clamped edge). The obtained results are very different when compared to the results of *(C-F-C-F)* plates where the crack is emanating from a free edge. The fundamental frequency parameter is decreasing slightly in the case of a horizontal crack $\alpha = 0$, increasing with high rate in the case of high crack angle $\alpha = 60°$ and exhibits intense fluctuations with frequency values higher than those of intact plates in the case of crack angles $\alpha = 20°, 40°$. The second frequency parameter for a horizontal side crack decreases with a low rate for crack length ratio $\beta < 0.5$ and a high rate for $\beta > 0.5$. For low and moderate crack angles $\alpha = 20°, 40°$ the second frequency parameter fluctuates

yet its value remains higher than that of an intact plate. At high crack angle $\alpha = 60°$ the second frequency parameter increases with high rate.

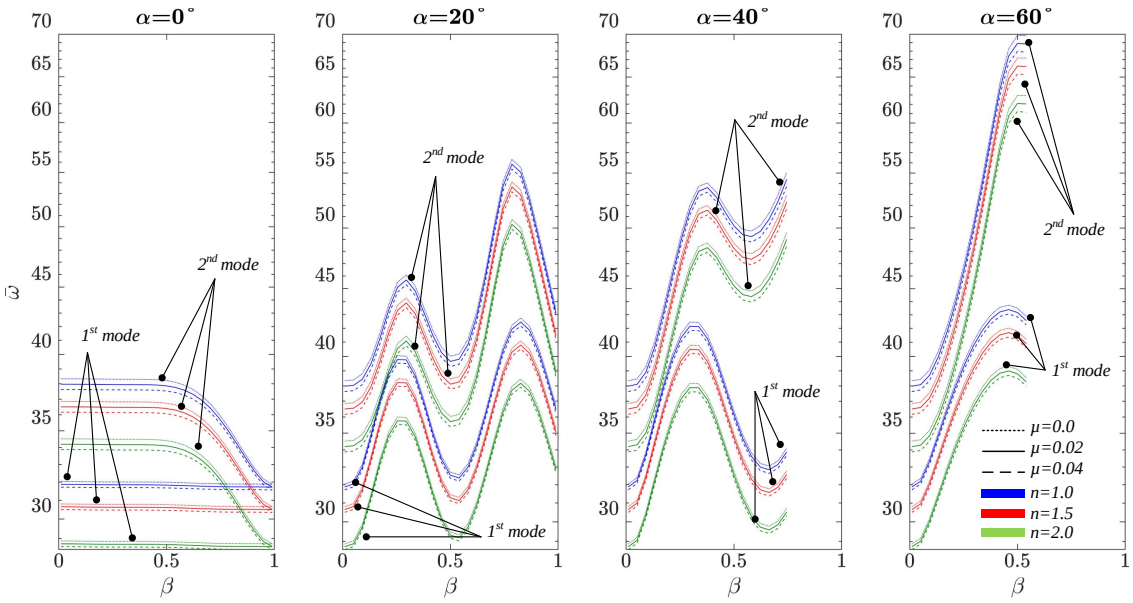

Figure 4.6: Plots of the first and second frequency parameters $\overline{\omega}$ versus crack length ratio β of a FGM nanoplate with a *side crack* for different values of volume fraction exponent n, crack angle α and non-local parameter μ, subjected to *F-C-F-C* boundary conditions.

Formerly two combinations of free and simply supported boundary conditions (*C-F-C-F, F-C-F-C*) and the results clearly suggest significant differences in vibrational behavior of side cracked FGM nanoplate depending on whether the crack is emanating from a free or clamped edge. Hence two combinations of free and simply supported boundary conditions (*S-F-S-F, F-S-F-S*) are studied and discussed. Figure 4.7 presents the effects of the crack length ratio β on the two first frequency parameters of a square nanoplate with a side crack for different values non local parameter μ, volume fraction exponent n and crack angle α subjected to *(S-F-S-F)* boundary conditions (i.e., the crack is emanating from a simply supported edge). The first frequency parameter is decreasing with a high rate in the case of a horizontal crack $\alpha = 0$, in the case of crack angle $\alpha = 20°$ it is decreasing with a relatively moderate rate until $\beta \simeq 0.8$ then it starts to increase but it remains lower than the

value of an intact plate. In the case of moderate and high crack angles $\alpha = 40°, 60°$, the first frequency parameter decreases with low rate until the crack length ratio β reaches a certain value then it increases with high rate and becomes higher than the value of an intact plate. the second frequency parameter behavior is quite similar to that of a plate subjected to *(C-F-C-F)* boundary conditions.

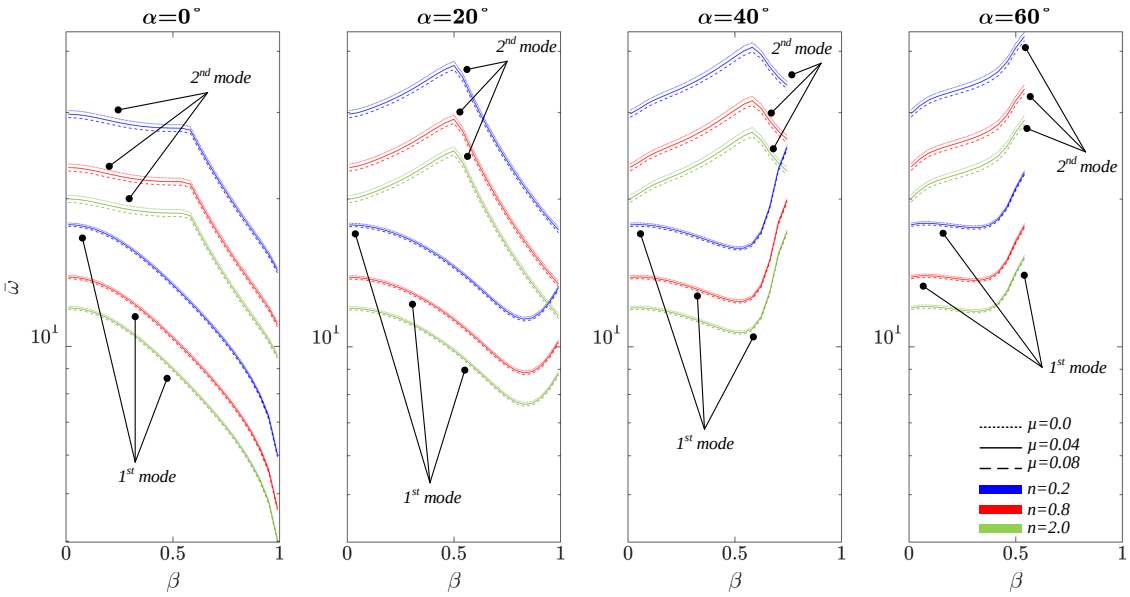

Figure 4.7: Plots of the first and second frequency parameters $\overline{\omega}$ versus crack length ratio β of a FGM nanoplate with a *side crack* for different values of volume fraction exponent n, crack angle α and non-local parameter μ, subjected to *S-F-S-F* boundary conditions.

Figure 4.8 presents the effects of the crack length ratio β on the two first frequency parameters of a square nanoplate with a side crack for different values non local parameter μ, volume fraction exponent n and crack angle α subjected to *(F-S-F-S)* boundary conditions (i.e., the crack is emanating from a free edge). it is observed that in the case of a horizontal crac $\alpha = 0$ similar trends are exhibited when comparing with a side cracked plate subjected to (*F-C-F-C*) boundary conditions. For inclined cracks although the fluctuations in frequency parameters are also present, however the drops are much less intense, allowing for much higher frequencies to be attained.

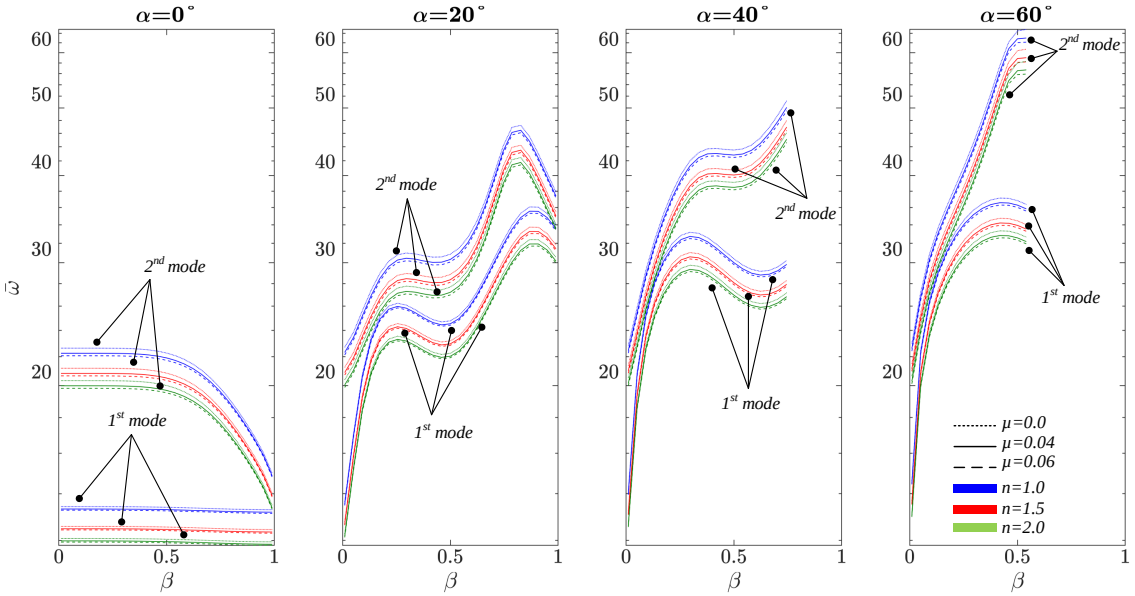

Figure 4.8: Plots of the first and second frequency parameters $\overline{\omega}$ versus crack length ratio β of a FGM nanoplate with a *side crack* for different values of volume fraction exponent n, crack angle α and non-local parameter μ, subjected to *F-S-F-S* boundary conditions.

In the analysis of previous results, the influence of side crack parameters and boundary conditions on free vibrations of FGM nanoplates has been presented. Concerning the influence of volume fraction exponent n and non local parameter μ, it is clear from the results that the obtained curves are identical but shifted as the values of volume fraction exponent n or non local parameter μ are changed, this observation means that the influence of these two material parameters is independent of the crack length ratio β and the crack angle α.

4.2.2 Central crack

In this study, vibrational behavior of a square plate $a/b = 1$ with central crack is investigated, a 3×2 elements mesh is used as shown in Figure 3.1b, the degree of interpolation is $p = 16$ for each element. The effect of volume fraction exponent n, crack length ratio β and crack angle α on the non-dimensional frequency parameters $\overline{\omega} = \omega \frac{a^2}{h}\sqrt{\frac{12\left(1-\nu_m^2\right)\rho_m}{E_m}}$, is

studied for different values of non-local parameter μ and several cases of boundary conditions *(C-C-C-C, S-S-S-S, C-S-C-S, S-C-S-C, C-F-C-F, F-C-F-C, S-F-S-F* and *F-S-F-S).*

Figure 4.9 presents the effects of the crack length ratio β on the two first frequency parameters for a clamped *(C-C-C-C)* square nanoplate with a central crack for different values of volume fraction exponent n, crack angle α and non local parameter μ. It is observed in the case a horizontal central crack $\alpha = 0$, the first and second frequency parameters decrease as the crack length ratio β evolves and become equals as $\beta \approx 1$. In the case of moderately inclined central crack $\alpha = 15°, 30°$, the first frequency parameter increases then decreases as β reaches a certain value $0.6 \backsim 0.7$ depending on the angle α, the second frequency parameter is generally decreasing with a low rate then the rate of decrease becomes high as $\beta > 0.5 \sim 0.6$ depending on the angle α, it is also observed that at certain crack length ratio $\beta > 0.75 \sim 0.8$, the first and second frequency parameters are equals. In the case of highly inclined central crack $\alpha = 45°, 60°$, the first frequency parameter is increasing monotonically with a high rate, the second frequency parameter exhibits minor fluctuations around the value of the second frequency of an intact plate, also the first and second frequency parameters become equals as $\beta \approx 1$.

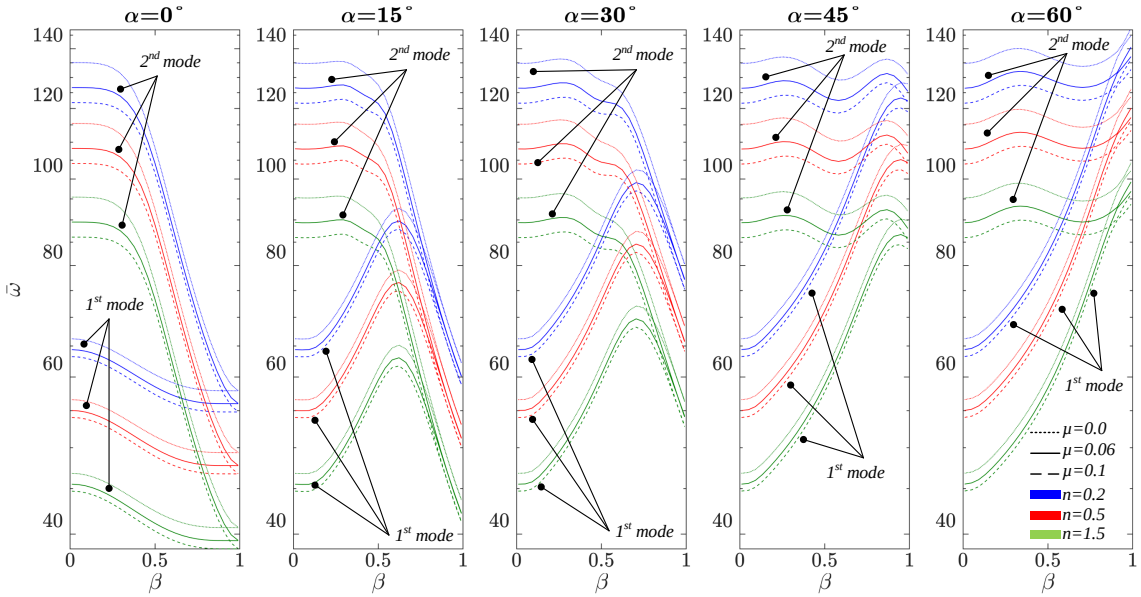

Figure 4.9: Plots of the first and second frequency parameters $\overline{\omega}$ versus crack length ratio β of a FGM nanoplate with a *central crack* for different values of volume fraction exponent n, crack angle α and non-local parameter μ, subjected to *C-C-C-C* boundary conditions.

The effects of the crack length ratio β on the two first frequency parameters of a simply-supported square nanoplate with a central crack is presented in Figure 4.10 for different values non local parameter μ, volume fraction exponent n and crack angle α. The obtained results show almost similar trends when compared to the results of clamped *(C-C-C-C)* plates especially for the first frequency parameter, however some differences concerning the second frequency parameter emerges whereas, for moderately inclined central crack $\alpha = 15°, 30°$ increases at low rate then decreases and for highly inclined central crack $\alpha = 45°, 60°$ increases with a low rate contrary to fluctuating behavior in the case of clamped plate.

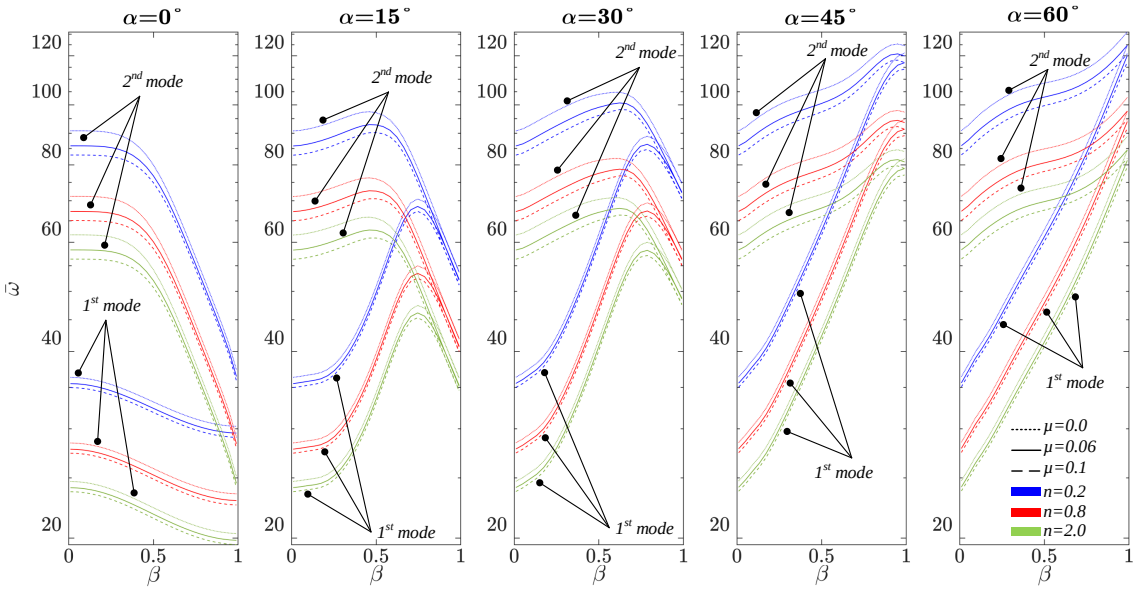

Figure 4.10: Plots of the first and second frequency parameters $\overline{\omega}$ versus crack length ratio β of a FGM nanoplate with a *central crack* for different values of volume fraction exponent n, crack angle α and non-local parameter μ, subjected to *S-S-S-S* boundary conditions.

Figure 4.11 presents the effects of the crack length ratio β on the two first frequency parameters of a square nanoplate with a central crack for different values of volume fraction exponent n, crack angle α and non local parameter μ subjected to *(C-S-C-S)* boundary conditions. the obtained results show similar trends when compared to results of a clamped plate.

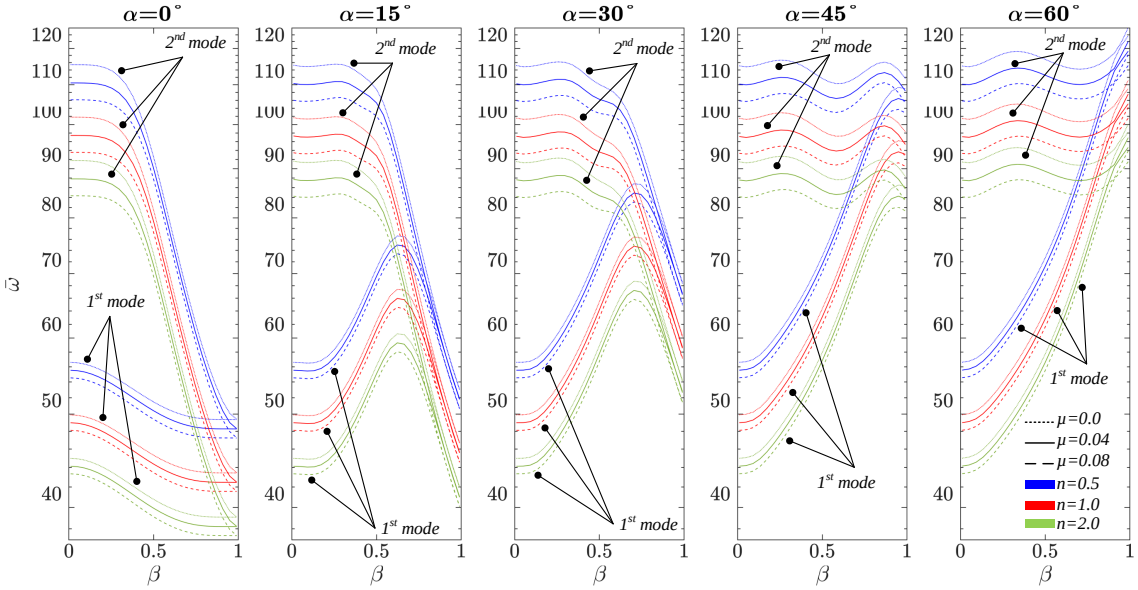

Figure 4.11: Plots of the first and second frequency parameters $\overline{\omega}$ versus crack length ratio β of a FGM nanoplate with a *central crack* for different values of volume fraction exponent n, crack angle α and non-local parameter μ, subjected to *C-S-C-S* boundary conditions.

Figure 4.12 presents the effects of the crack length ratio β on the two first frequency parameters of a square nanoplate with a central crack for different values of volume fraction exponent n, crack angle α and non local parameter μ subjected to *(S-C-S-C)* boundary conditions. the obtained results show similar trends when compared to results of a simply supported plate.

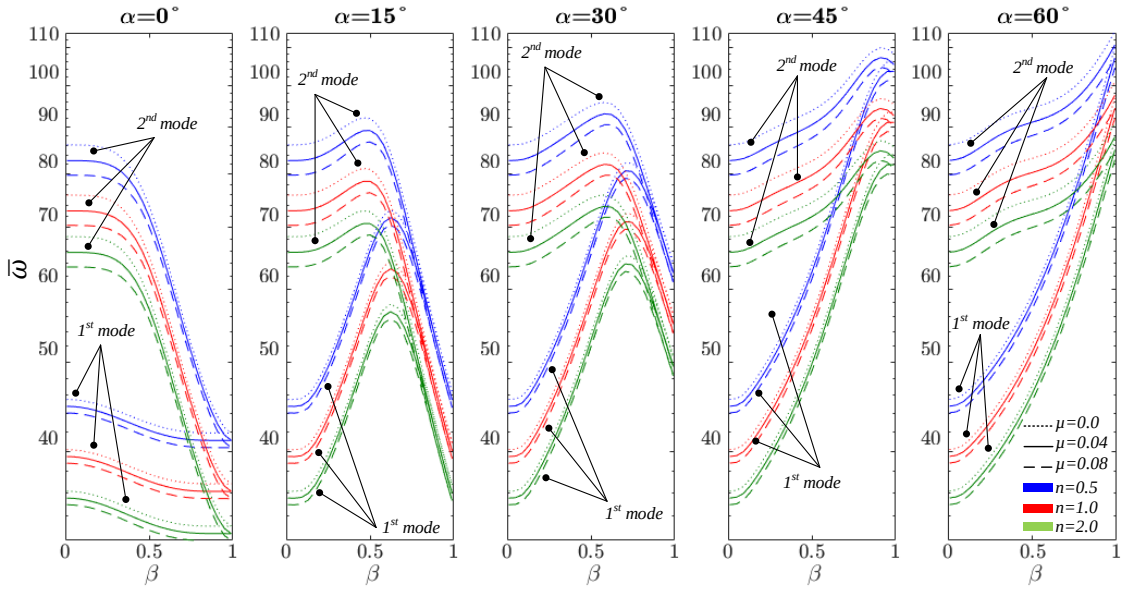

Figure 4.12: Plots of the first and second frequency parameters $\overline{\omega}$ versus crack length ratio β of a FGM nanoplate with a *central crack* for different values of volume fraction exponent n, crack angle α and non-local parameter μ, subjected to *S-C-S-C* boundary conditions.

After discussing the results where four different combinations of clamped and simply supported boundary conditions are considered and observing an overall slight influence of these boundary conditions on vibrational behavior of centrally cracked FGM nanoplates. Subsequently various combinations of free edges with clamped or simply supported boundary conditions are studied and discussed. Figure 4.13 presents the effects of the crack length ratio β on the two first frequency parameters for a square FGM nanoplate with a side crack for different values of volume fraction exponent n, crack angle α and non local parameter μ, subjected to *(C-F-C-F)* boundary conditions. it is observed that the first frequency parameter is decreasing as the crack length increases for horizontal an slightly inclined cracks $\alpha = 0°, 15°, 30°$ and rate of decrease becomes low as the crack angle α increases, however for higher angles $\alpha = 45°, 60°$ the first frequency parameter increases as a function of crack length ratio β and high rates of increase are observed as the crack angle increases. The second frequency parameter for a horizontal side crack decreases with for crack length ratio $\beta < 0.5$ and a high rate for $\beta > 0.5$. For inclined crack $\alpha = 15°, 30°, 45°$ the second

frequency parameter increases if crack length ratio $\beta < 0.5$ and then decreases and keeping frequency higher than that of an intact plate. At high crack angle $\alpha = 60°$ the second frequency parameter increases with high rate.

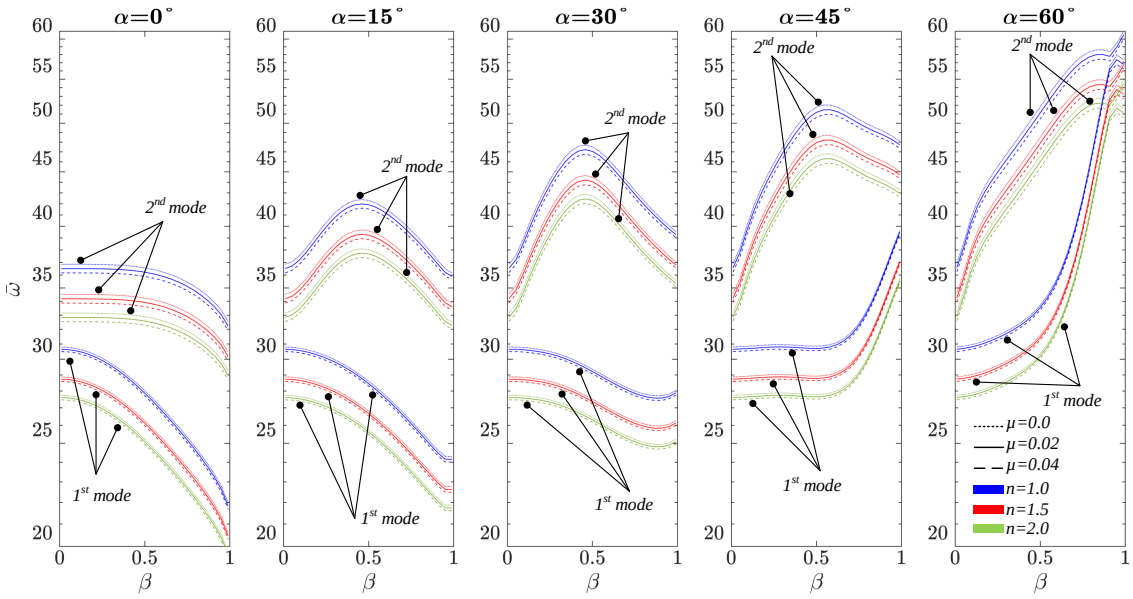

Figure 4.13: Plots of the first and second frequency parameters $\overline{\omega}$ versus crack length ratio β of a FGM nanoplate with a *central crack* for different values of volume fraction exponent n, crack angle α and non-local parameter μ, subjected to *C-F-C-F* boundary conditions.

Figure 4.14 presents the effects of the crack length ratio β on the two first frequency parameters of a square nanoplate with a central crack for different values non local parameter μ, volume fraction exponent n and crack angle α subjected to *(F-C-F-C)* boundary conditions. The obtained results are very different when compared to the results of *(C-F-C-F)* plates especially in the case of inclined crack. It is observed in the case a horizontal central crack $\alpha = 0$, the first and second frequency parameters decrease as the crack length ratio β evolves and become equals as $\beta \approx 1$. The first and second frequency parameters are increasing with a high rate and become equals after a certain crack length β. At low and moderate crack angles $\alpha = 15°, 30°$ the first and second frequency parameters decrease after some value of crack length ratio β.

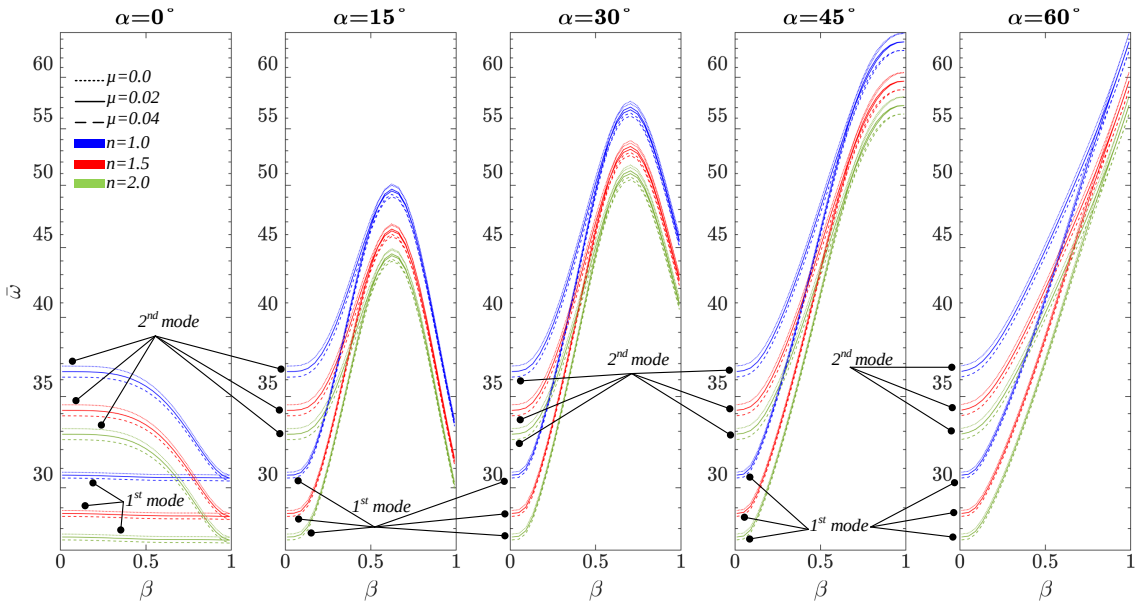

Figure 4.14: Plots of the first and second frequency parameters $\overline{\omega}$ versus crack length ratio β of a FGM nanoplate with a *central crack* for different values of volume fraction exponent n, crack angle α and non-local parameter μ, subjected to *F-C-F-C* boundary conditions.

Previously, (*C-F-C-F, F-C-F-C*) boundary conditions has been discussed and the results clearly suggest significant differences in vibrational behavior of the centrally cracked FGM nanoplate depending on whether the crack is growing toward a free or clamped edge. Therefore boundary conditions (*S-F-S-F, F-S-F-S*) are presented and discussed. The effects of the crack length ratio β on the two first frequency parameters of a *(S-F-S-F)* square nanoplate with a side crack is presented in Figure 4.15 for different values non local parameter μ, volume fraction exponent n and crack angle α. The obtained results show similar trends when compared to the results of plates subjected to *(C-F-C-F)* boundary conditions.

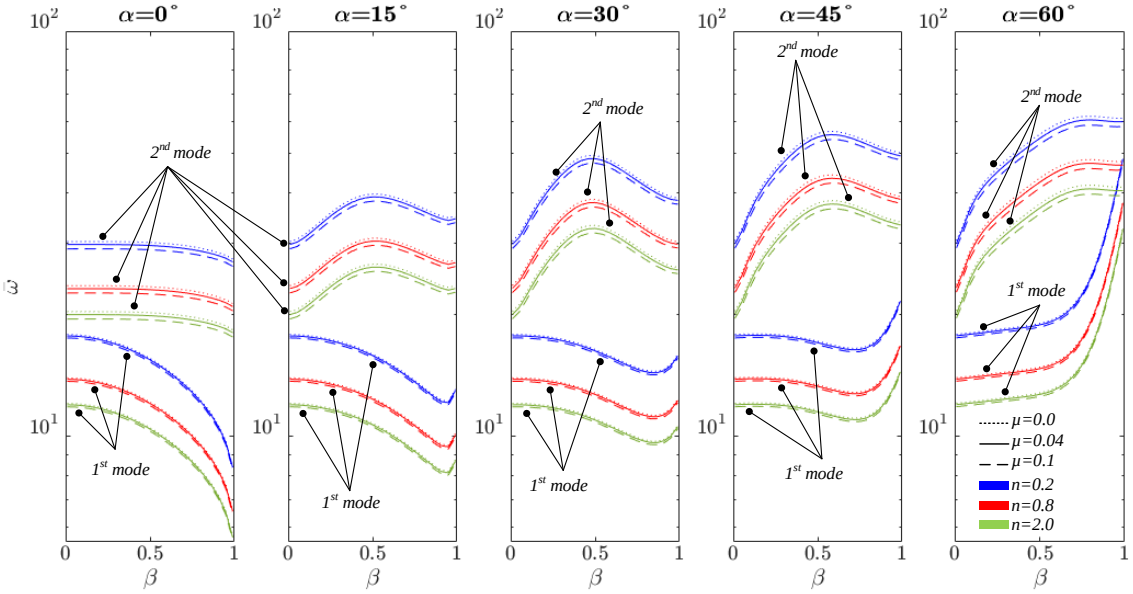

Figure 4.15: Plots of the first and second frequency parameters $\overline{\omega}$ versus crack length ratio β of a FGM nanoplate with a *central crack* for different values of volume fraction exponent n, crack angle α and non-local parameter μ, subjected to *S-F-S-F* boundary conditions.

Figure 4.15 presents the effects of the crack length ratio β on the two first frequency parameters of a *(F-S-F-S)* square nanoplate with a side crack for different values non local parameter μ, volume fraction exponent n and crack angle α. The obtained results show similar trends when compared to the results of plates subjected to *(F-C-F-C)* boundary conditions.

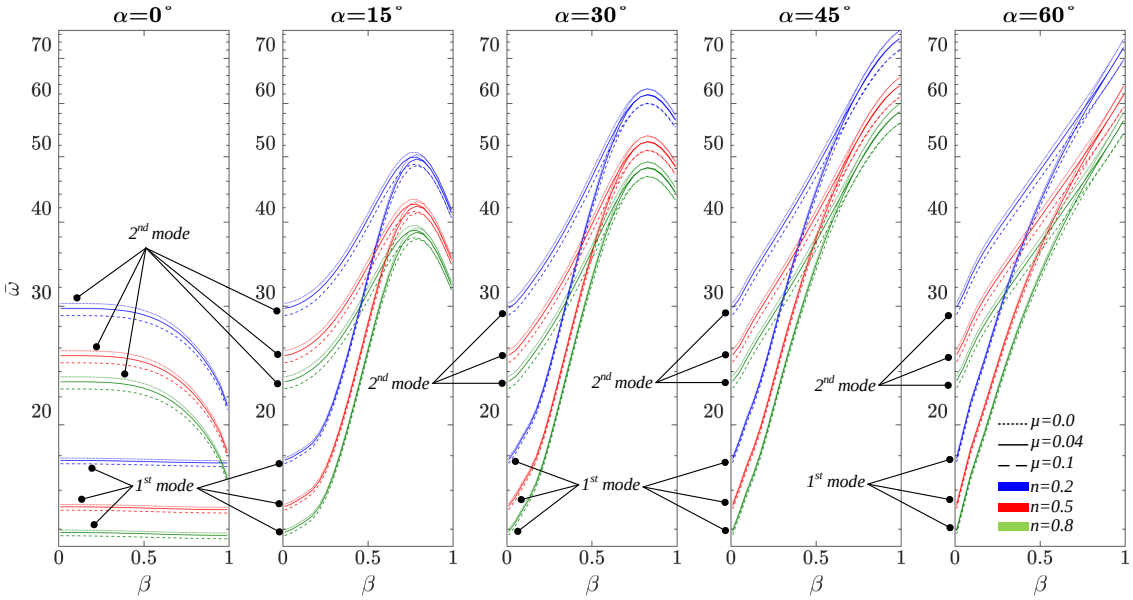

Figure 4.16: Plots of the first and second frequency parameters $\overline{\omega}$ versus crack length ratio β of a FGM nanoplate with a *central crack* for different values of volume fraction exponent n, crack angle α and non-local parameter μ, subjected to *F-S-F-S* boundary conditions.

In the analysis of above results, the influence of central crack parameters and boundary conditions on free vibrations of FGM nanoplates has been presented. Concerning the influence of volume fraction exponent n and non local parameter μ, once again it is clear from the results that the obtained curves are identical but shifted as the values of volume fraction exponent n or non local parameter μ are changed, this observation means that the influence of these two material parameters is independent of the crack length ratio β, the crack angle α and also independent of the crack position (central crack, side crack). In order to further study the influence of crack position combined with the influence of volume fraction exponent n and non local parameter μ on the vibrational behavior of cracked FGM nanoplates, the next section 4.2.3 will consider a side crack at different positions on the edge from which the crack is emanating.

4.2.3 Crack position

Earlier on, side and central cracks influence on vibrational behavior of FGM nano-plates has been studied and discussed. In order to further explore the effect of crack position beyond only side and central positions, in this study, vibrational behavior of a square plate $a/b = 1$ with side crack positioned arbitrarily on an edge is investigated, a 2×2 elements mesh is used as shown in Figure 4.17, the degree of interpolation is $p = 16$ for each element. The effect of crack position ratio γ, crack length ratio β, crack angle α and volume fraction exponent n on the non-dimensional fundamental frequency parameter $\overline{\omega} = \omega \frac{a^2}{h} \sqrt{\frac{12(1-\nu_m^2)\rho_m}{E_m}}$, is studied for two values of non-local parameter $\mu = 0, 0.1$ and several cases of boundary conditions *(C-C-C-C, S-S-S-S, C-S-C-S, S-C-S-C, C-F-C-F, F-C-F-C, S-F-S-F* and *F-S-F-S).*

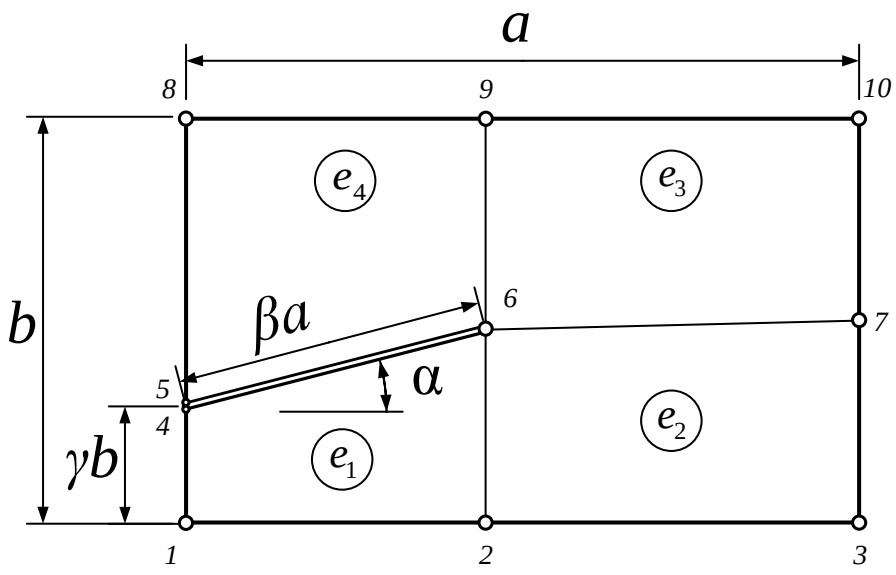

Figure 4.17: Crack position to plate length ratio γ and mesh configuration for side cracked plates

Figure 4.18 presents the effects of the crack position ratio γ on the fundamental frequency parameters of a local and non-local FGM clamped square plate with a side crack

for different values crack length ratio β, crack angle α and volume fraction exponent n. For a horizontal crack $\alpha = 0°$, it is observed that the fundamental frequency parameter curve is symmetric about $\gamma = 0.5$ axis and value of frequency decreases as the crack position is moved toward the middle of the edge, Also the rate of decrease is higher as the position is closer to the center of the edge. In the case of crack angle $\alpha = 40$, the curve symmetry axis is translated to a lower value $\gamma \approx 0.25$.

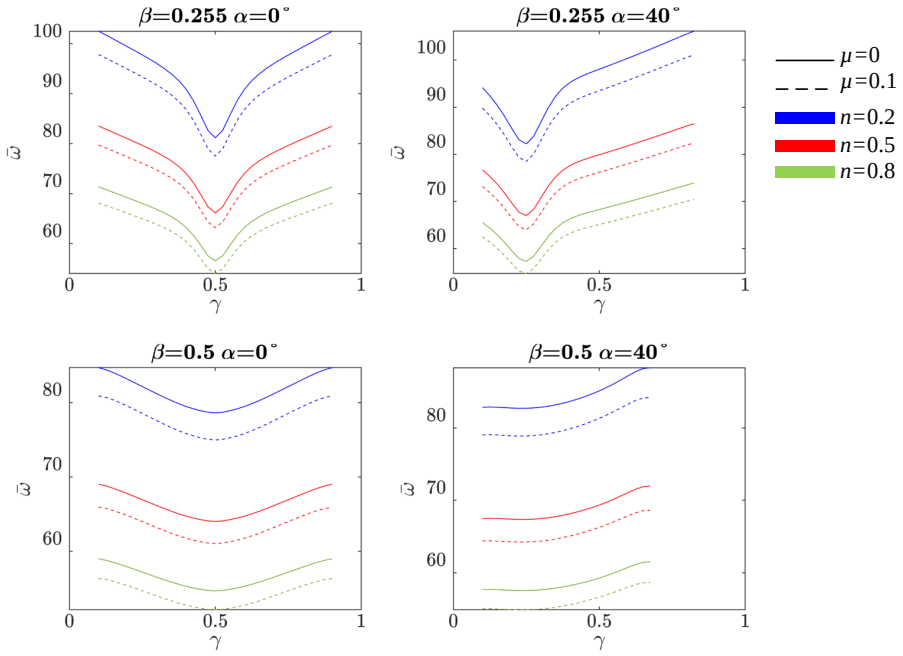

Figure 4.18: Plots of the fundamental frequency parameter $\overline{\omega}$ versus crack position ratio γ of a FGM local and non-local plate with a *side crack* for different values of volume fraction exponent n, crack angle α and crack length ratio β, subjected to *C-C-C-C* boundary conditions.

The effects of the crack position ratio γ on the fundamental frequency parameter of a local and non-local FGM simply-supported square plate with a side crack is presented in Figure 4.19 for different values crack length ratio β, crack angle α and volume fraction exponent n. Obviously similar trends are shown when comparing with the previous results of the clamped plate, however the drops in frequency are much higher.

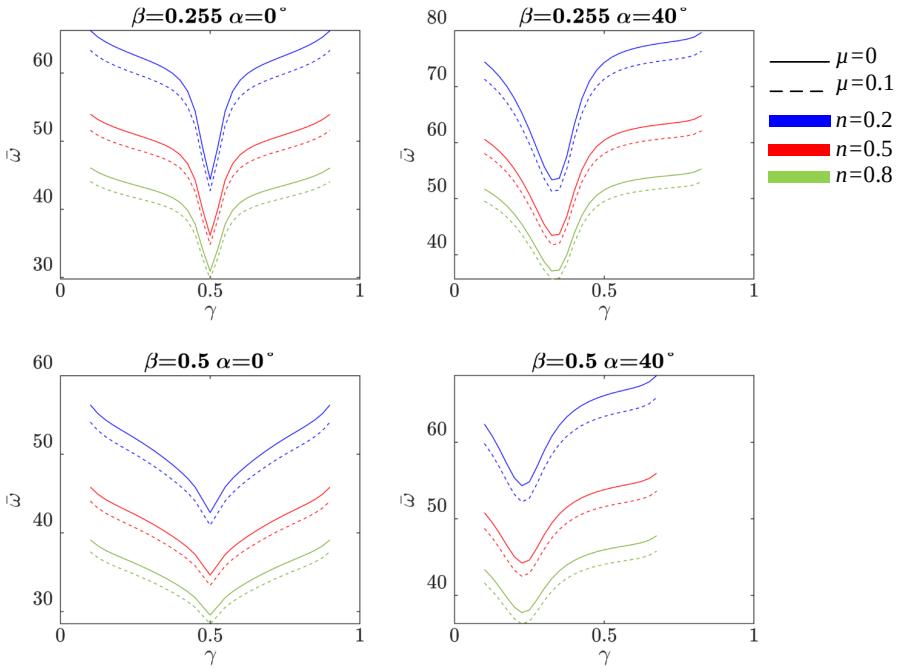

Figure 4.19: Plots of the fundamental frequency parameter $\overline{\omega}$ versus crack position ratio γ of a FGM local and non-local plate with a *side crack* for different values of volume fraction exponent n, crack angle α and crack length ratio β, subjected to *S*-*S*-*S*-*S* boundary conditions.

Figure 4.20 presents the effects of the crack position ratio γ on the fundamental frequency parameters of a local and non-local FGM square plate with a side crack for different values crack length ratio β, crack angle α and volume fraction exponent n subjected to (*C*-*S*-*C*-*S*) boundary conditions. For a horizontal crack $\alpha = 0°$, it is observed that the fundamental frequency parameter curve is symmetric about $\gamma = 0.5$ axis and value of frequency decreases as the crack position is moved toward the middle of the edge, however contrary to the simply supported and clamped plates the rate of decrease is much more uniform. In the case of crack angle $\alpha = 40$, the curve symmetry axis is translated to a lower value $\gamma \approx 0.25$.

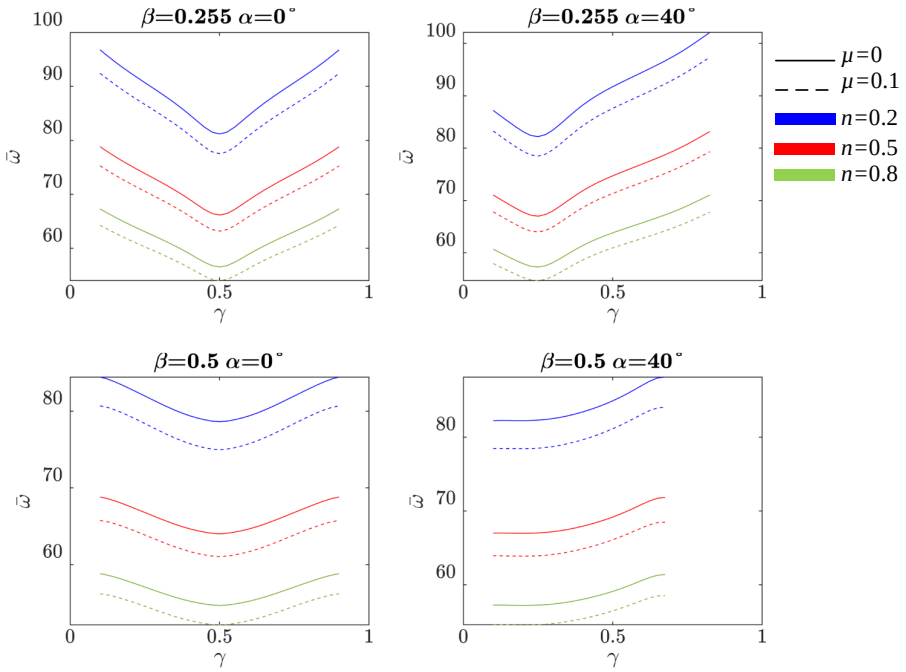

Figure 4.20: Plots of the fundamental frequency parameter $\overline{\omega}$ versus crack position ratio γ of a FGM local and non-local plate with a *side crack* for different values of volume fraction exponent n, crack angle α and crack length ratio β, subjected to *C-S-C-S* boundary conditions.

Figure 4.21 presents the effects of the crack position ratio γ on the fundamental frequency parameter of a local and non-local FGM square plate with a side crack subjected to (*S-C-S-C*) boundary conditions for different values crack length ratio β, crack angle α and volume fraction exponent n. it is clear that similar trends are exhibited when comparing with the results of the clamped and simply supported plates.

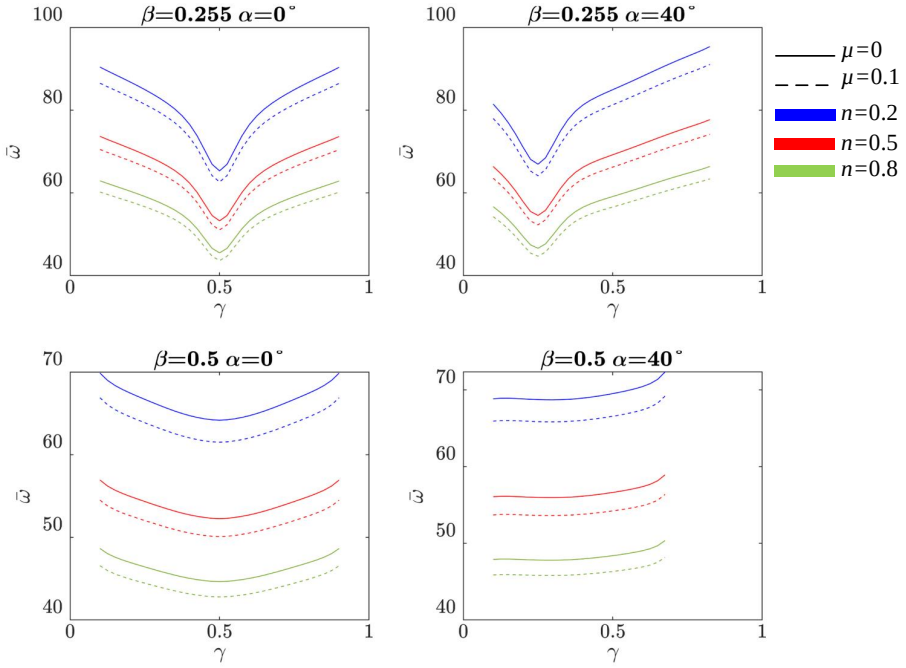

Figure 4.21: Plots of the fundamental frequency parameter $\overline{\omega}$ versus crack position ratio γ of a FGM local and non-local plate with a *side crack* for different values of volume fraction exponent n, crack angle α and crack length ratio β, subjected to *S-C-S-C* boundary conditions.

From the results of different combinations of clamped and simply supported boundary conditions, it is observed that slight differences are occurring in vibrational behavior of side crack FGM nanoplates under different boundary conditions. Hence various combinations of free edges with clamped or simply supported boundary conditions are studied and discussed. Figure 4.22 shows the effects of the crack position ratio γ on the fundamental frequency parameters a of a local and non-local FGM square plates with a side crack for different values of volume fraction exponent n, crack angle α and crack length ratioβ, subjected to *(C-F-C-F)* boundary conditions (i.e., crack emanating from a clamped edge). It is observed that the trends are significantly different from those of plates subjected to simply-supported and clamped combinations. For a horizontal crack $\alpha = 0$ the fundamental frequency parameter curves are symmetric about $\gamma = 0.5$ axis and the value of frequency increases as the crack position is moved toward the middle of the edge for a crack length

$\beta = 0.5$, however for a crack length ratio $\beta = 0.255$ the fundamental frequency parameter starts to slightly decrease as the crack position approaches the middle of the edge. For inclined crack $\alpha = 40°$ and crack length ratio $\beta = 0.5$ the fundamental frequency parameter increases as the crack position ratio increases

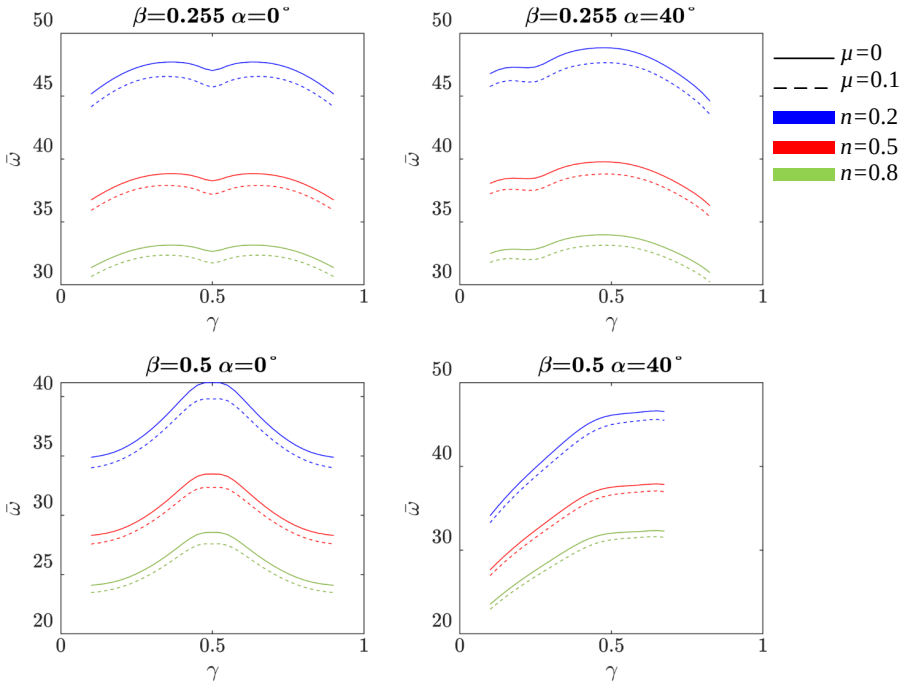

Figure 4.22: Plots of the fundamental frequency parameter $\overline{\omega}$ versus crack position ratio γ of a FGM local and non-local plate with a *side crack* for different values of volume fraction exponent n, crack angle α and crack length ratio β, subjected to *C-F-C-F* boundary conditions.

Figure 4.24 shows the effects of the crack position ratio γ on the fundamental frequency parameters a of a local and non-local FGM square plates with a side crack for different values of volume fraction exponent n, crack angle α and crack length ratioβ, subjected to *(F-C-F-C)* boundary conditions (i.e., crack emanating from a free edge). It is observed that the trends are very similar to those of plates subjected to simply-supported and clamped combinations.

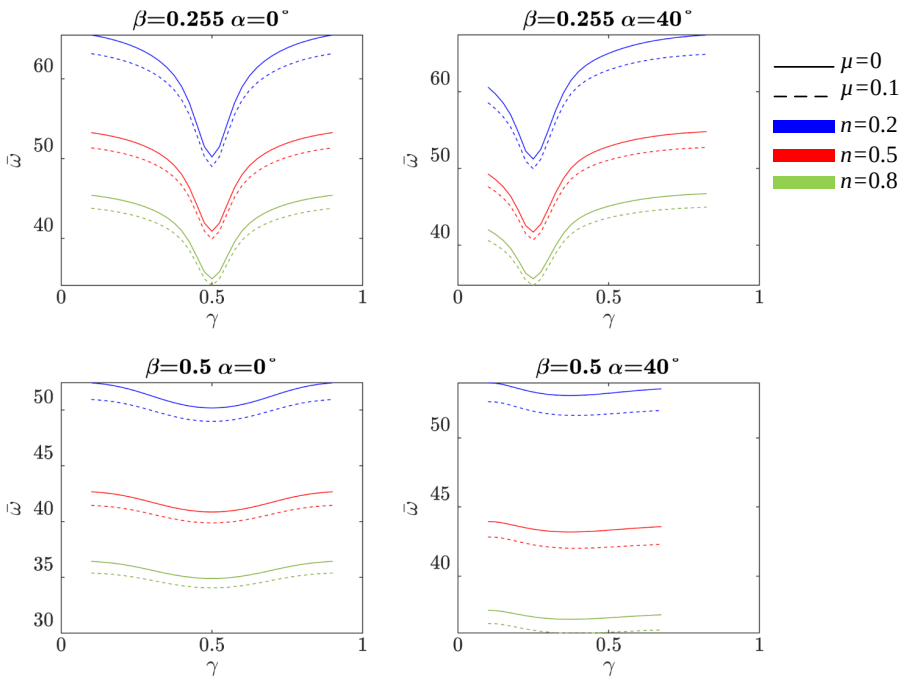

Figure 4.23: Plots of the fundamental frequency parameter $\overline{\omega}$ versus crack position ratio γ of a FGM local and non-local plate with a *side crack* for different values of volume fraction exponent n, crack angle α and crack length ratio β, subjected to *F-C-F-C* boundary conditions.

The effects of the crack position ratio γ on the fundamental frequency parameter of a local and non-local FGM square plate with a side crack subjected to *(S-F-S-F)* boundary conditions (i.e., crack emanating from a simply-supported edge) is presented in Figure 4.24 for different values crack length ratio β, crack angle α and volume fraction exponent n. For a horizontal crack $\alpha = 0$ the fundamental frequency parameter curves are symmetric about $\gamma = 0.5$ axis and the value of frequency decreases for crack position ratio $0.1 < \gamma < 0.2$ then increases for $0.2 < \gamma < 0.4$ and slightly decreases for $0.4 < \gamma < 0.5$. For inclined crack $\alpha = 40^\circ$ the fundamental frequency parameter increases as the crack position ratio γ increases.

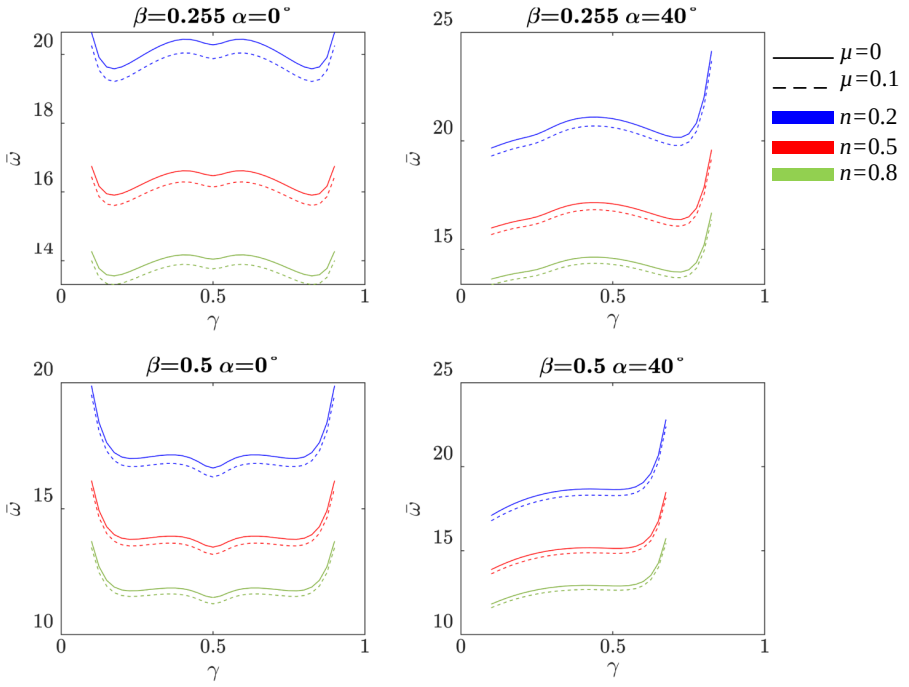

Figure 4.24: Plots of the fundamental frequency parameter $\overline{\omega}$ versus crack position ratio γ of a FGM local and non-local plate with a *side crack* for different values of volume fraction exponent n, crack angle α and crack length ratio β, subjected to *S-F-S-F* boundary conditions.

Figure 4.25 shows the effects of the crack position ratio γ on the fundamental frequency parameters a of a local and non-local FGM square plates with a side crack for different values of volume fraction exponent n, crack angle α and crack length ratioβ, subjected to *(F-S-F-S)* boundary conditions (i.e., crack emanating from a free edge). It is observed that the trends are very similar to those of plates subjected to simply-supported and clamped combinations.

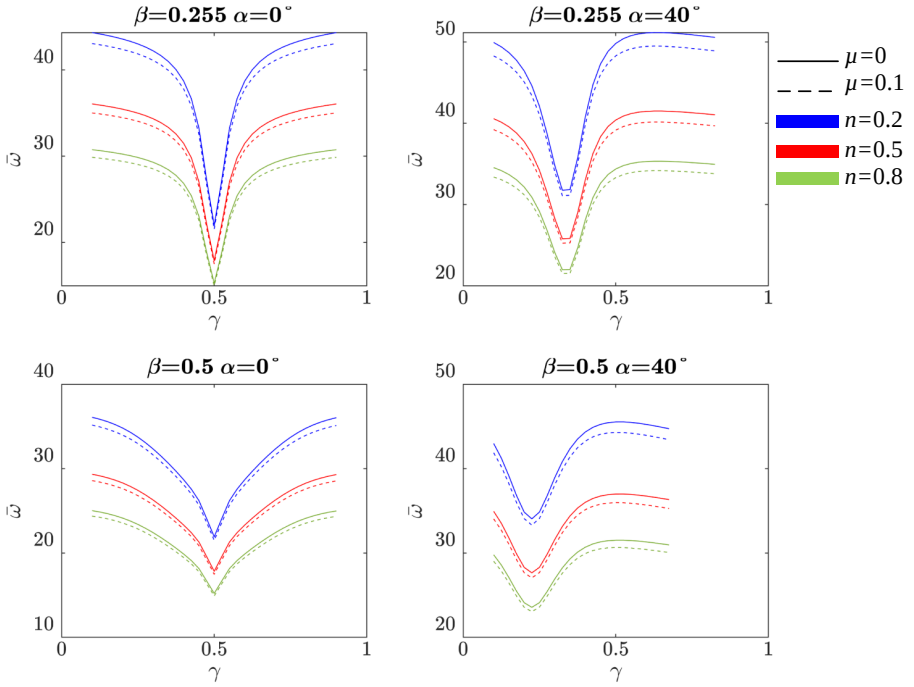

Figure 4.25: Plots of the fundamental frequency parameter $\overline{\omega}$ versus crack position ratio γ of a FGM local and non-local plate with a *side crack* for different values of volume fraction exponent n, crack angle α and crack length ratio β, subjected to *F-S-F-S* boundary conditions.

4.3 Summary

In this chapter, we investigated linear free vibration of FGM cracked nanoplates based on non-local elasticity and first-order shear deformation theory, by employing the modeling approach used in the previous chapter 3. A good agreement has been found between the results obtained by the present approach and results in literature for intact FGM plates. The investigation of the influence of material volume fraction exponent n along with crack parameters (length, orientation), plate geometry, boundary conditions and the non-local parameter on frequency parameter further confirmed the softening effect of the non-local parameter expressed by the decrease of frequency.

Concerning the crack parameters, it is concluded that, for any value of material volume fraction exponent n or any value of non-local parameter μ, the increase in crack length for a horizontal crack (side or central crack) softens the nanoplate resulting in lower frequencies, unlike the horizontal crack, an inclined crack at certain values of α can increase the stiffness of the plate resulting in higher frequencies than those of an intact plate. Regarding the crack position, it is concluded that as the crack is positioned closer to the middle of the plate, the stiffness of the plate is decreased resulting in reduced frequency. In the next chapter, the influence of crack parameters on nonlinear free vibrations of cracked nanoplates will investigated.

Chapter 5

Non-Linear Vibration of cracked nanoplates

In the previous chapters, linear free vibration of isotropic/FGM cracked nanoplates has been investigated and discussed. In this chapter we consider the nonlinear free vibrations of cracked nanoplates. The chapter begins by introducing a convergence study of non-linear free vibrations of simply supported plates, then a comparison study is carried out to investigate the accuracy of the model with nonlinear results found in literature. After that parametric studies are conducted where, the effects of crack parameters (length, position) and non-local parameter on the nonlinear free vibration of cracked nanoplates are the key point of interest.

In this chapter we:

- Study the convergence of the linear and non-linear solutions of intact and cracked plates obtained using full and selective *p*-refinement.
- Present a comparison to verify the accuracy of nonlinear solutions of the present model for intact isotropic/FGM plates.
- Study the influence of horizontal crack length and non-local parameter on non-linear free vibrations of cracked nanoplates subjected to different boundary conditions.

- Study the effect of horizontal crack position and non-local parameter on non-linear free vibrations of cracked nanoplates for several cases of boundary conditions.

5.1 Convergence and Comparison

In this section, convergence of the nonlinear solution is tested for an intact simply supported square plate modeled using one p-element (1×1 mesh in the product polynomial space), Table 5.1 depicts results of the fundamental mode at different plate thickness ratios $\frac{a}{h}$, for increasing p-refinement. It is clear that the linear solution converges at low values of p, and the nonlinear solution reaches a *reasonable* convergence but at higher values of p. Also it is observed that the number of iterations needed for the nonlinear iterative process to converge increases as the thickness of the plate increases.

Table 5.1: Convergence of the fundamental linear/nonlinear frequency of a simply supported isotropic square plate modeled with one p-element (shape function of the product polynomial space)

$\frac{a}{h}$	p					
	2	3	4	5	6	7
20	1.9639 *	1.9639	1.9637	1.9637	1.9636	1.9636
	2.2169(12)†	2.2148(12)	2.2140(12)	2.2131(12)	2.2127(12)	2.2113(12)
	1.1288‡	1.1278	1.1274	1.1270	1.1268	1.1262
50	1.9822	1.9834	1.9832	1.9831	1.9831	1.9831
	2.2674(11)	2.2677(11)	2.2671(11)	2.2666(11)	2.2663(11)	2.2660(11)
	1.1439	1.1433	1.1431	1.1430	1.1428	1.1426
100	1.9864	1.9907	1.9901	1.9902	1.9902	1.9902
	2.2771(7)	2.2811(7)	2.2800(7)	2.2797(7)	2.2795(7)	2.2793(7)
	1.1463	1.1459	1.1457	1.1455	1.1454	1.1453
250	1.9890	1.9998	1.9978	1.9992	1.9992	1.9992
	2.2834(7)	2.2959(7)	2.2923(7)	2.2935(7)	2.2933(7)	2.2932(7)
	1.1480	1.1480	1.1474	1.1472	1.1471	1.1470

$*$: linear first frequency parameter $\overline{\omega} = \omega \frac{a^2}{\pi^2}\sqrt{\frac{\rho h}{D_{22}}}$

$\dagger$: non-linear first frequency parameter $\overline{\omega}_{nl}$ at $\frac{w_{max}}{h} = 0.6$

$\ddagger$: non-linear to linear frequency ratio $\frac{\omega_{nl}}{\omega}$

$(\cdots)$: number of iterations for relative error $\frac{\Delta\omega}{\omega} < 10^{-5}$

Convergence analysis has been performed in Table 5.2 for the nonlinear solution of a simply supported rectangular plate with central crack $\beta = 0.3$ modeled using selective p-refinement (see Figure 5.1a), it is observed that the nonlinear solution is refined as p is increased, hence it can be considered that reasonable convergence is achieved. Concerning the convergence of the nonlinear iterative process, it is clear that increasing the amplitude $\frac{w_{max}}{h}$ increases the number of iterations needed to reach convergence.

Table 5.2: Convergence of the fundamental linear/nonlinear frequency of a simply supported isotropic rectangular plate with a horizontal central crack $\beta = 0.3$

$\frac{w_{max}}{h}$	$\frac{a}{b}$	$p^{\dagger}$				
		2	3	4	5	6
0.0	0.5	1.0000 (1)	1.0000 (1)	1.0000 (1)	1.0000 (1)	1.0000 (1)
	1.0	1.0000 (1)	1.0000 (1)	1.0000 (1)	1.0000 (1)	1.0000 (1)
0.2	0.5	1.0067 (5)	1.0066 (5)	1.0066 (5)	1.0066 (5)	1.0066 (5)
	1.0	1.0042 (5)	1.0041 (5)	1.0041 (5)	1.0040 (5)	1.0040 (5)
0.4	0.5	1.0264 (5)	1.0261 (5)	1.0261 (5)	1.0260 (5)	1.0260 (5)
	1.0	1.0163 (5)	1.0160 (5)	1.0158 (5)	1.0156 (5)	1.0153 (5)
0.6	0.5	1.0575 (6)	1.0567 (6)	1.0567 (6)	1.0565 (6)	1.0565 (6)
	1.0	1.0352 (6)	1.0345 (6)	1.0340 (6)	1.0332 (6)	1.0328 (9)
0.8 ‡	0.5	1.0980 (6)	1.0966 (11)	1.0964 (11)	1.0961 (11)	1.0960 (11)
	1.0	1.0590 (7)	1.0575 (7)	1.0564 (7)	1.0541 (11)	1.0537 (16)
1.0 ‡	0.5	1.0194 (9)	1.0192 (9)	1.0192 (11)	1.0192 (9)	1.0192 (9)
	1.0	1.0126 (11)	1.0125 (11)	1.0125 (11)	1.0125 (11)	1.0126 (15)

Side to thickness ratio $\frac{a}{h} = 50$, crack length ratio $\beta = 0.3$

†: shape functions in the product polynomial space

‡: results obtained using LUM method with averaging (see: paragraph 2.5.3)

$(\cdots)$: number of iterations for relative error $\frac{\Delta\omega}{\omega} < 10^{-5}$

In order to assess the accuracy of the present model and since the literature results are limited to intact plates, the comparison is carried out for nonlinear results of intact plates available in literature [94, 95, 96, 97]. In Table 5.3 the fundamental frequency ratio $\frac{\omega_{nl}}{\omega}$ of simply supported rectangular plates are compared with numerical results in literature. It is clear that the results of the present model are in good agreement with those of references.

Table 5.3: Comparison of the fundamental frequency ratio $\frac{\omega_{nl}}{\omega}$ of a simply supported isotropic rectangular plate

	ref[94]	ref [95]	ref[96]	ref [97]	Present	
$\frac{w_{max}}{h}$	h-FEM	Elliptic function	Pertur-bation	Rayleigh-Ritz	w/ IDI[a]	w/o IDI
			Square plate $(a/h = 240)$			
0.2	1.0185	1.0195	1.0196	1.0149	1.0193(2)[b]	1.0269(2)
0.4	1.0716	1.0757	1.0761	1.0583	1.0753(2)	1.1029(2)
0.6	1.1533	1.1625	1.1642	1.1270	1.1629(2)	1.2171(3)
0.8	1.2565	1.2734	1.2774	1.2166	1.2758(3)	1.3574(4)
1.0	1.3752	1.4024	1.4097	1.3230	1.4082(3)	1.5156(5)
			Rectangular plate $(a/b = 2.0,\ a/h = 480)$			
0.2	1.0238	1.0241	1.0241	1.0177	1.0247(2)	1.0340(3)
0.4	1.0918	1.0927	1.0933	1.0690	1.0959(2)	1.1292(2)
0.6	1.1957	1.1975	1.1998	1.1493	1.2065(3)	1.2703(2)
0.8	1.3264	1.3293	1.3347	1.2533	1.3490(4)	1.4437(2)
1.0	1.4762	1.4808	1.4903	1.3753	1.5153(6)	1.6346(6)

[a] IDI: Inplane deformation and inertia

[b] Number of iterations for relative error $\frac{\Delta\omega}{\omega} < 10^{-5}$

Table 5.4: Nonlinear to linear frequency ratio $\frac{\omega_{NL}}{\omega_L}$ of FGM simply supported square plate $(n = 2.0)$

$\frac{w_{max}}{h}$	0.0	0.2	0.4	0.6	0.8	1.0
	ZrO_2/Ti–$6Al$–$4V$					
ref[98]	1.000	1.021	1.082	1.176	1.296	1.436
present	1.000	1.038	1.109	1.206	1.325	1.459
error %	0.000	1.638	2.435	2.488	2.189	1.576
	$Si_3N_4/SUS304$					
ref[98]	1.000	1.021	1.081	1.174	1.293	1.432
present	1.000	1.037	1.106	1.202	1.320	1.453
error %	0.000	1.543	2.260	2.330	2.046	1.445

In Table 5.4 the fundamental frequency ratio $\frac{\omega_{nl}}{\omega}$ of simply supported FGM square plates are presented along with numerical results of Huang and Shen [98]. A good agreement is observed between the results of the present model and those of the reference.

5.2 Parametric study of cracked nano-plates

In this study, the influence of a horizontal crack $\alpha = 0$ parameters such as length ratio β and crack position (side, central and vertical position γ), on the backbone curves is studied under different cases of boundary conditions, unless stated otherwise all studied plates are square $a/b = 1$ with $a = 10\mu m$ and $a/h = 50$. A 20×20 mesh is used with selective p-refinement where only elements around the crack tip are refined Figure 5.1, this selective p-refinement strategy is adopted due to computational considerations. If full p-refinement is used like in studies of chapters 3 and 4 for nonlinear simulations where p must be as high as 16 to reach reasonable convergence, the computation time needed to establish the nonlinear stiffness matrices would be impractically high even when using parallel computation.

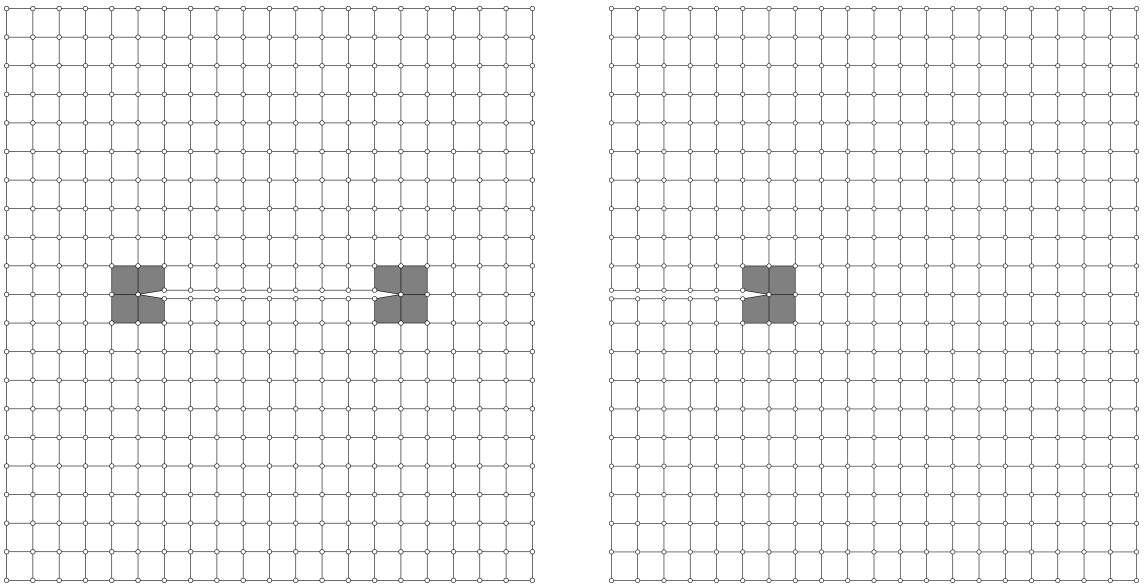

(a) Central crack (b) Side crack

Figure 5.1: Geometric parameters and mesh configuration for cracked plates, gray elements are selectively p-refined elements

5.2.1 Side crack

In this part of the study, backbone curves of the fundamental mode for *side cracked* nanoplates are presented and discussed for several cases of crack lengths β and nonlocal parameter μ under different boundary conditions (*S-S-S-S, C-C-C-C, F-C-F-C, F-S-F-S, C-F-C-F, S-F-S-F*).

Figure 5.2 presents backbone curves for non-local and local plates having a horizontal $\alpha = 0$ side crack subjected to simply supported / clamped boundary conditions for different values of crack length ratios β. The stiffening effect of large amplitude on free vibrations is clearly observed for intact local and non-local plate, however as the crack length ratio β is increased the non-linear effect is decreased $\frac{\omega_{nl}}{\omega} \sim 1$, further increase in crack length ratio β or vibration amplitude $\frac{w_{max}}{h}$ causes a softening effect $\frac{\omega_{nl}}{\omega} < 1$.

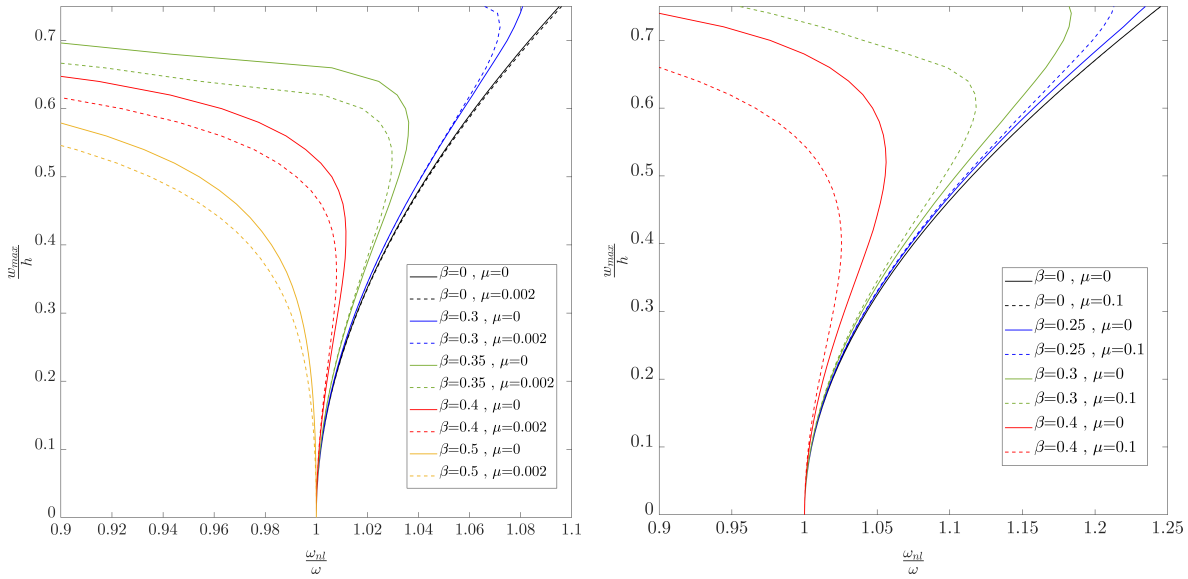

(a) Clamped plate (b) Simply supported plate

Figure 5.2: Backbone curves for the first mode of isotropic, square plates with a side crack for different values of crack length ratios β and and non-local parameter μ. subjected to clamped 5.2a and simply supported 5.2b boundary conditions.

Figure 5.3 presents backbone curves for non-local and local plates having a horizontal $\alpha = 0$ side crack subjected to *F-C-F-C 5.3a* / *F-S-F-S5.3b* boundary conditions for different values of crack length ratios β. Similar to previous results the stiffening effect is clearly

observed for intact local and non-local plate, however the softening effect is less significant and require higher crack length ratios β and higher vibration amplitudes $\frac{w_{max}}{h}$ to be clearly observed.

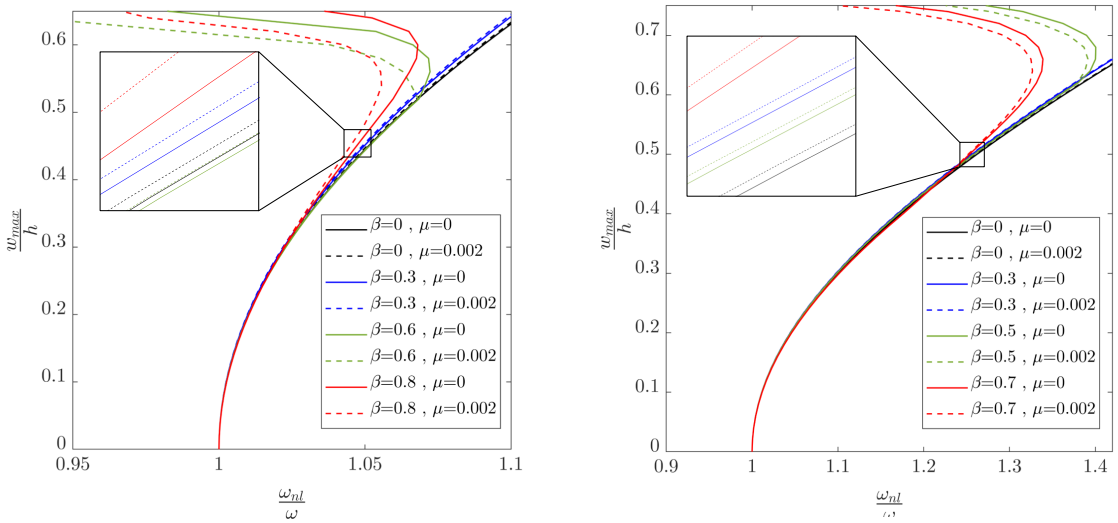

(a) *F-C-F-C* boundary conditions.

(b) *F-S-F-S* boundary conditions.

Figure 5.3: Backbone curves for the first mode of isotropic, square plates with a side crack for different values of crack length ratios β and and non-local parameter μ. subjected to *F-C-F-C* 5.2a and *F-S-F-S* 5.2b boundary conditions.

Figure 5.4 presents backbone curves for non-local and local plates having a horizontal $\alpha = 0$ side crack subjected to *C-F-C-F 5.4a* / *S-F-S-F5.4b* boundary conditions for different values of crack length ratios β. Similar to previous results the stiffening effect is clearly observed for intact local and non-local plate, however the softening effect is much more significant then that observed for simply supported or clamped plates. Also, it can be observed that the backbone curve will be almost a straight vertical line $\frac{\omega_{nl}}{\omega} = 1$ at vibration amplitudes $\frac{w_{max}}{h} < 0.5$ and crack length ratios $0.3 < \beta < 0.4$, suggesting that the vibration will only be carried out linearly.

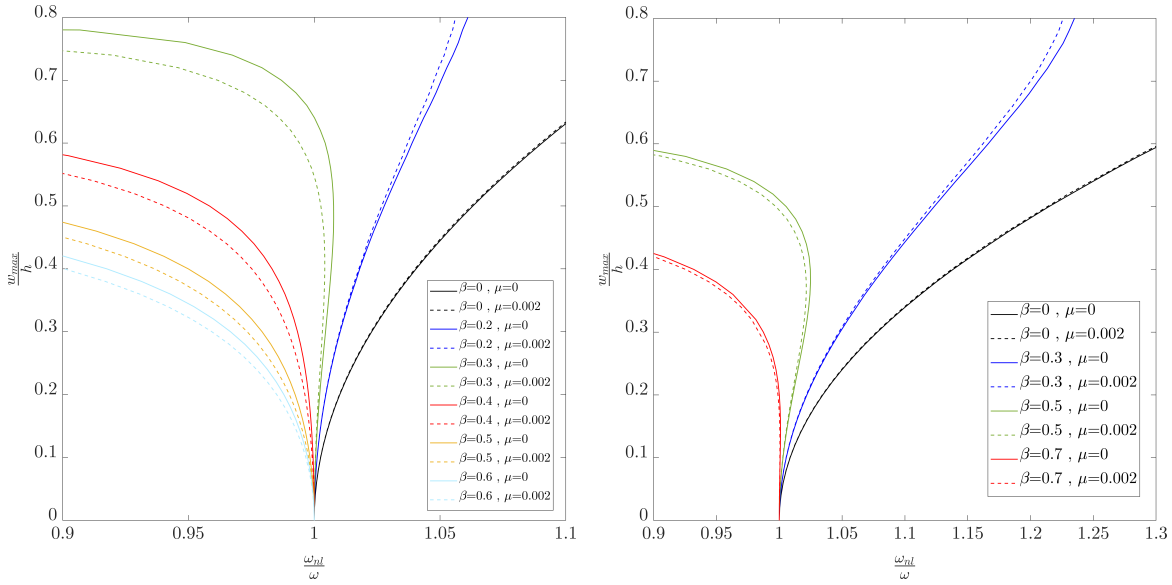

(a) *C-F-C*-F boundary conditions. (b) *S-F-S*-F boundary conditions.

Figure 5.4: Backbone curves for the first mode of isotropic, square plates with a side crack for different values of crack length ratios β and and non-local parameter μ. subjected to *C-F-C*-F 5.2a and *S-F-S*-F 5.2b boundary conditions.

5.2.2 Central crack

In this section, the effect of crack lengths β and nonlocal parameter μ under different boundary conditions (*S-S-S-S, C-C-C-C, C-F-C-F, S-F-S-F*) on the backbone curves of the fundamental mode for *centrally cracked* nanoplates is investigated and discussed .

Figure 5.5 depicts the backbone curves for the fundamental mode vibration of clamped square local/non-local centrally cracked plates $\alpha = 0$ for different values of crack length ratio β, it is observed from this results that the softening effect is significant as the crack length β increases, and for a small crack length ratio $\beta = 0.2$ the non-linear to linear frequency ratio $\frac{\omega_{nl}}{\omega} \approx 1$ which means the vibrational behavior is linear (i.e the non-linear effect is negligible).

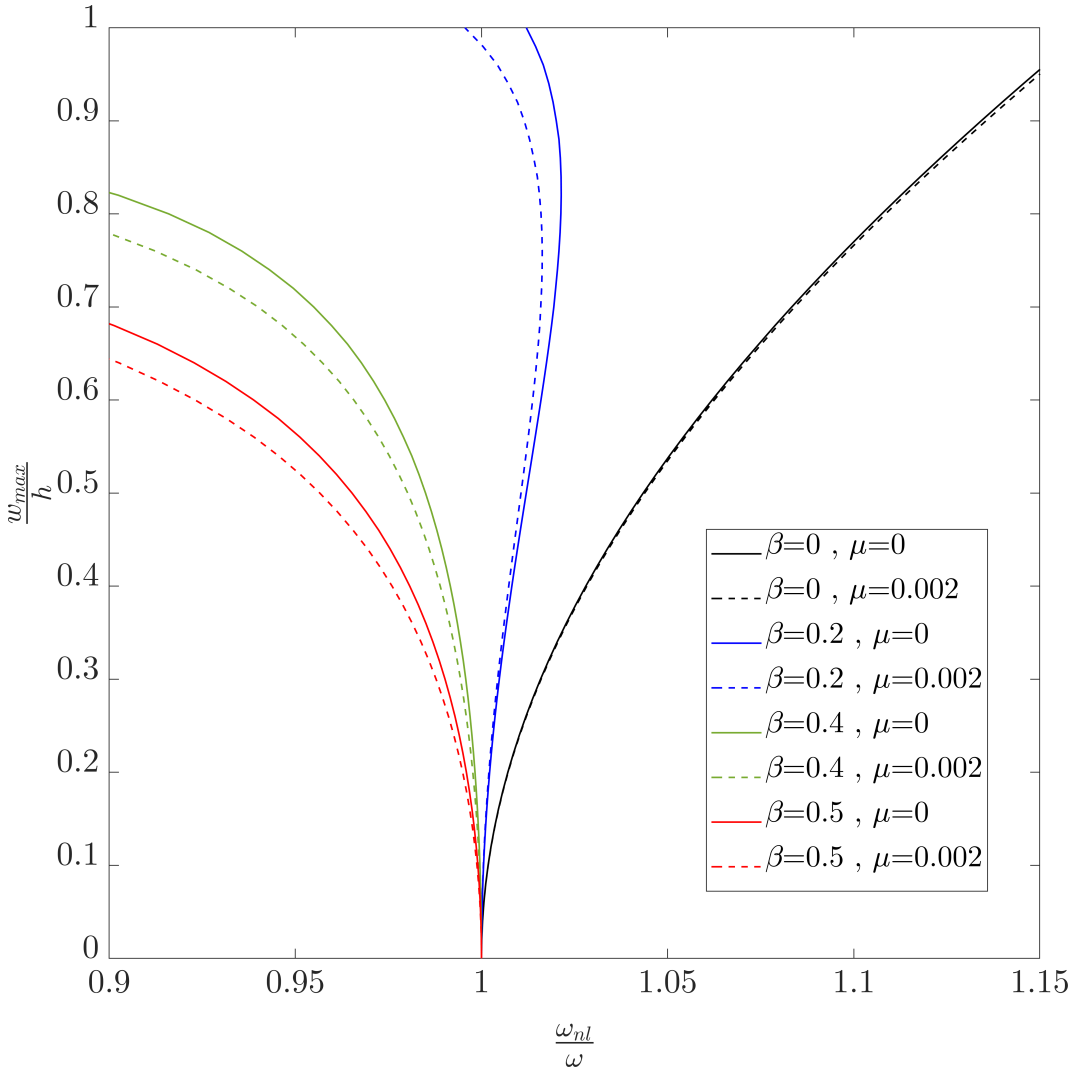

Figure 5.5: Backbone curves for the first mode of isotropic, clamped, centrally cracked square plates with different values of crack length ratios β and and non-local parameter μ.

The backbone curves for the fundamental mode vibration of simply-supported square local/non-local centrally cracked plates $\alpha = 0$ for different values of crack length ratio β is presented in Figure 5.6, it is observed that the presence of the crack $0 < \beta < 0.4$ decrease the stiffening effect observed in intact plate, and at higher crack length ratios $\beta > 0.4$ a softening effect is observed.

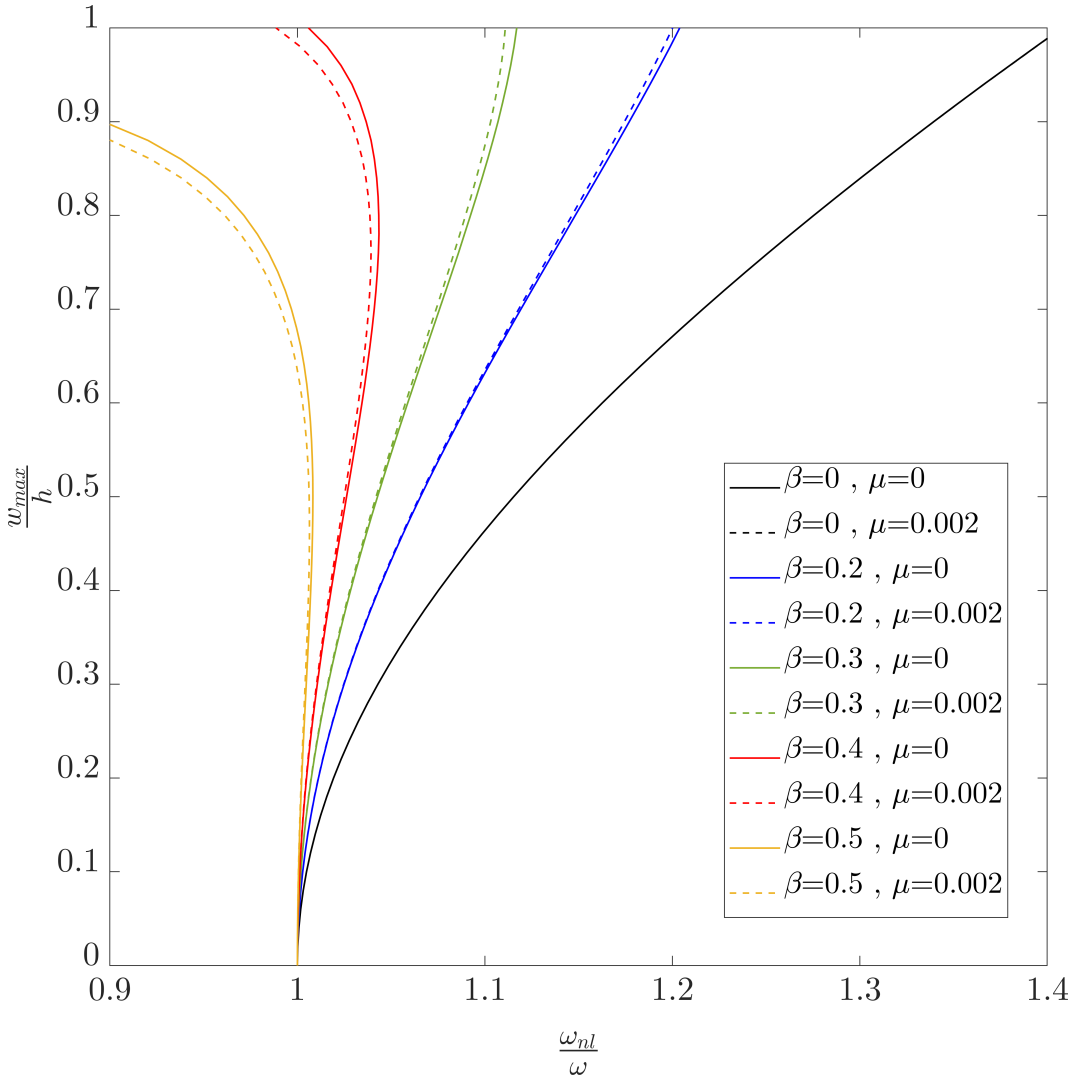

Figure 5.6: Backbone curves for the first mode of the isotropic, simply supported, centrally cracked square plates with different values of crack length ratios β and and non-local parameter μ.

Figures 5.7 and 5.8 depicts the backbone curves for the fundamental mode vibration local/non-local centrally cracked plates $\alpha = 0$ for several values of crack length ratios β subjected to *C-F-C-F* / *S-F-S-F* boundary conditions, again it is observed that the stiffening effect is decreasing as the crack length ratio β increases, and the stiffening effect is much more significant for the plates subjected to *S-F-S-F* boundary conditions.

Regarding the influence of the non-local parameter μ it is observed that it decreases the stiffening effect for all cases of central or side crack.

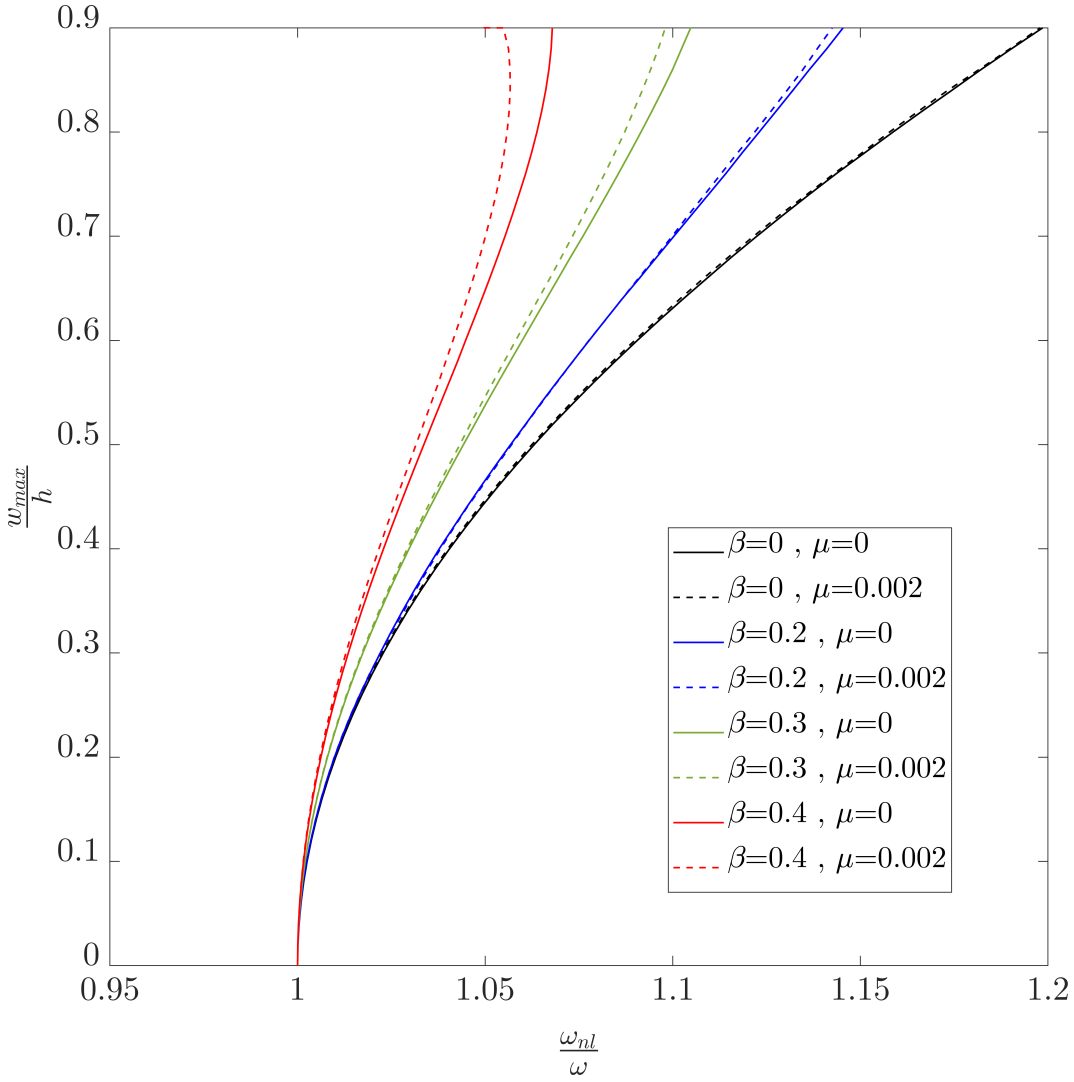

Figure 5.7: Backbone curves for the first mode of isotropic, centrally cracked square plates with different values of crack length ratios β and and non-local parameter μ, subjected to *C-F-C-F* boundary conditions.

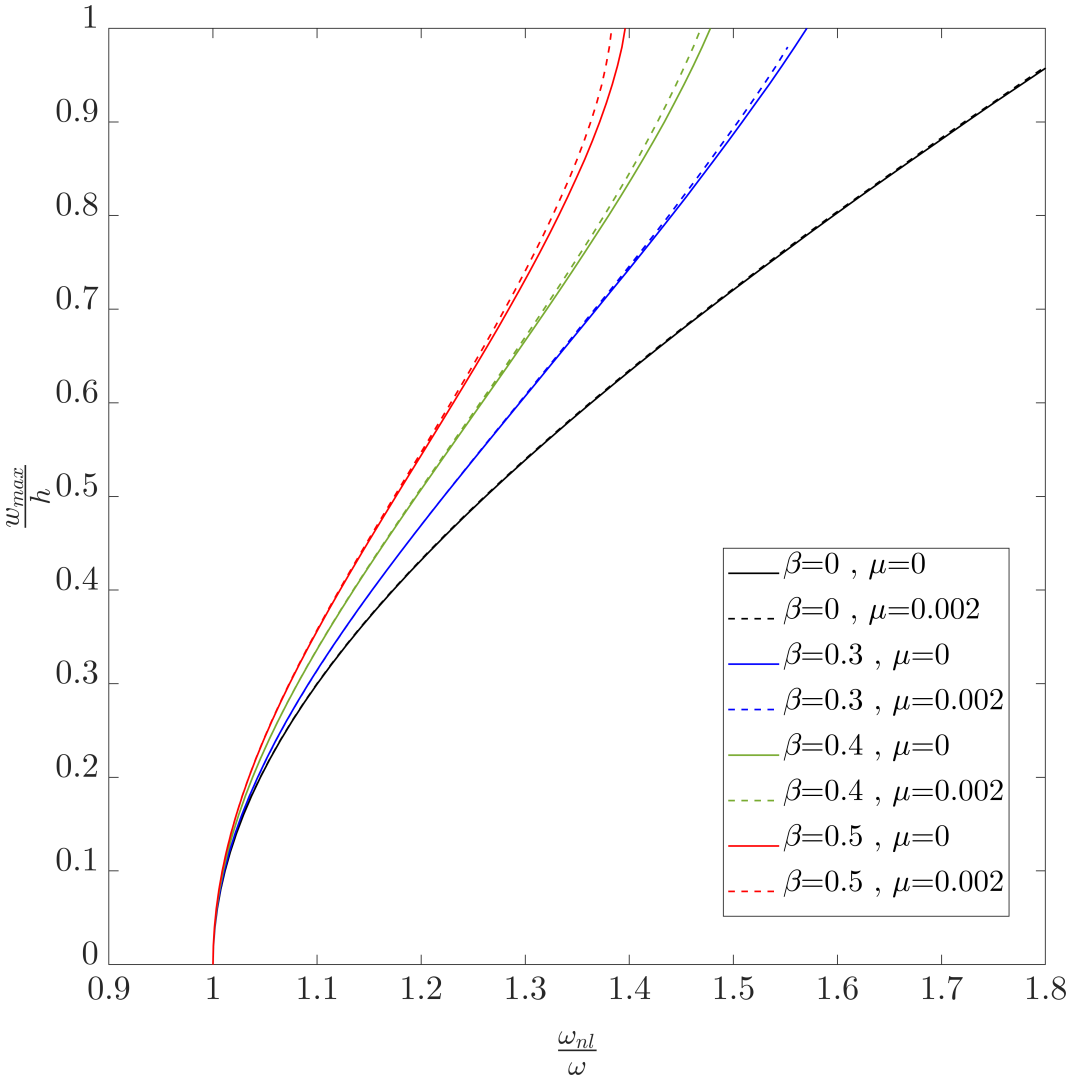

Figure 5.8: Backbone curves for the first mode of isotropic, centrally cracked square plates with different values of crack length ratios β and and non-local parameter μ, subjected to *S-F-S-F* boundary conditions.

5.2.3 Crack position

in this part of the study, we investigated the influence of position γ of a horizontal central crack (see Figure 5.9) in local plates $\mu = 0$ and nonlocal plates $\mu = 0.2$ under different boundary conditions (*S-S-S-S, C-C-C-C*, *S-F-S-F*, *C-F-C-F*).

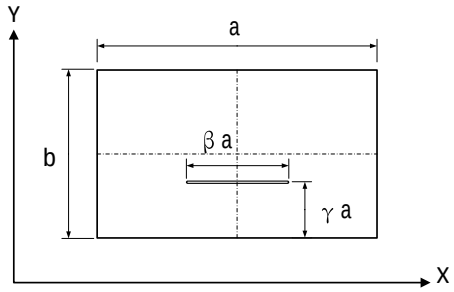

Figure 5.9: Crack position to plate length ratio γ and a centrally cracked plates

Figure 5.10 presents backbone curves for non-local and local plates having a horizontal $\alpha = 0$ central crack $\beta = 0.3$ subjected to simply supported boundary conditions for different values of crack position ratios γ. It is clear that the stiffening effect of large amplitude on free vibrations is decreased as the crack is positioned closer to the middle of the plate.

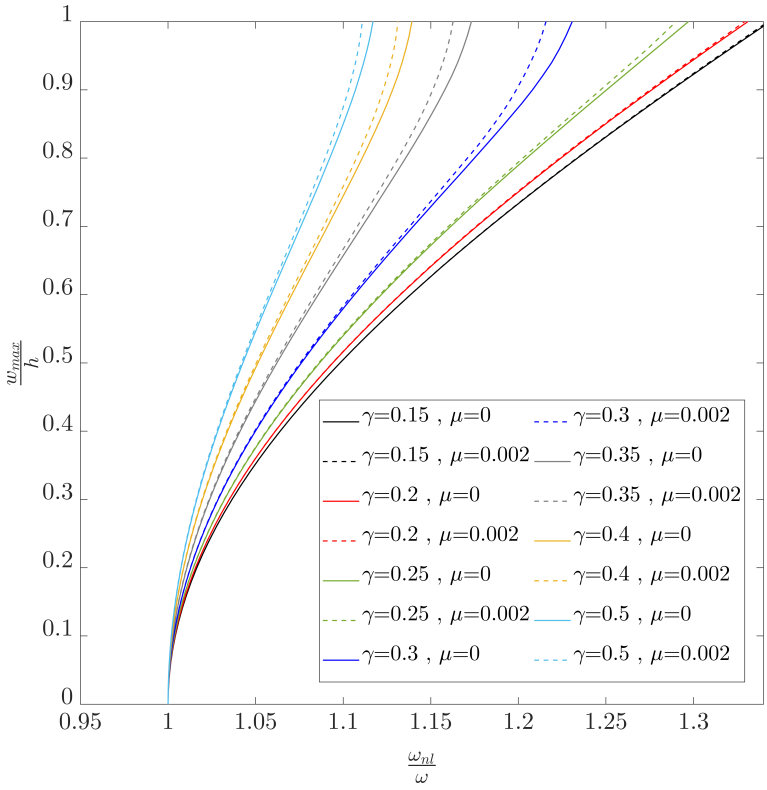

Figure 5.10: Backbone curves for the first mode of isotropic, centrally cracked $\beta = 0.3$, $\alpha = 0°$ simply-supported square plates with different values of crack position ratio γ and and non-local parameter μ.

Figure 5.11 depicts the backbone curves for the fundamental mode vibration of clamped square local/non-local centrally cracked plates $\alpha = 0$, $\beta = 0.3$ for different values of crack position ratio γ, Similarly to the simply-supported plates, it is observed that the stiffening effect of large amplitude on free vibrations is decreased noticeably as the crack is positioned closer to the middle of the plate $0.2 < \gamma < 0.4$. for crack position ratios $0.4 < \gamma < 0.5$ and amplitudes $\frac{w_{max}}{h} < 0.7$ the backbone curves are almost vertical straight lines $\frac{\omega_{nl}}{\omega} \approx 1$ (i.e. the vibration is carried out linearly), for amplitudes $\frac{w_{max}}{h} > 0.7$ a softening effect appears $\frac{\omega_{nl}}{\omega} < 1$.

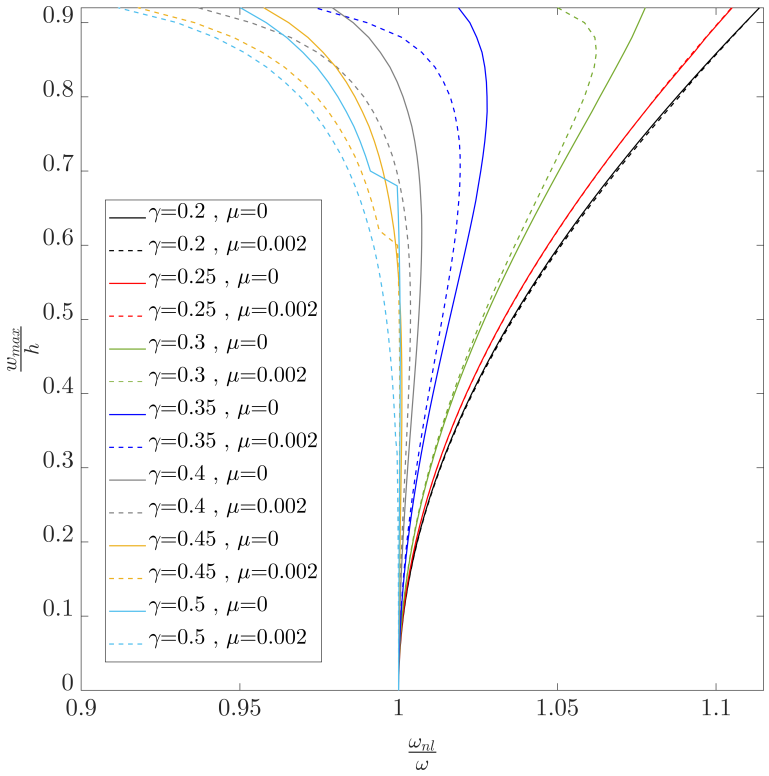

Figure 5.11: Backbone curves for the first mode of isotropic, centrally cracked $\beta = 0.3$, $\alpha = 0°$ clamped square plates with different values of crack position ratio γ and and non-local parameter μ.

The backbone curves for the fundamental mode vibration of square local/non-local centrally cracked plates $\alpha = 0$, $\beta = 0.3$ for different values of crack position ratio γ subjected

to *S-F-S-F* are presented in Figure 5.12, it is observed that the stiffening effect of large amplitude on free vibrations is increased for crack position ratios $0 < \gamma < 0.3$ and decreased for $0.3 < \gamma < 0.5$.

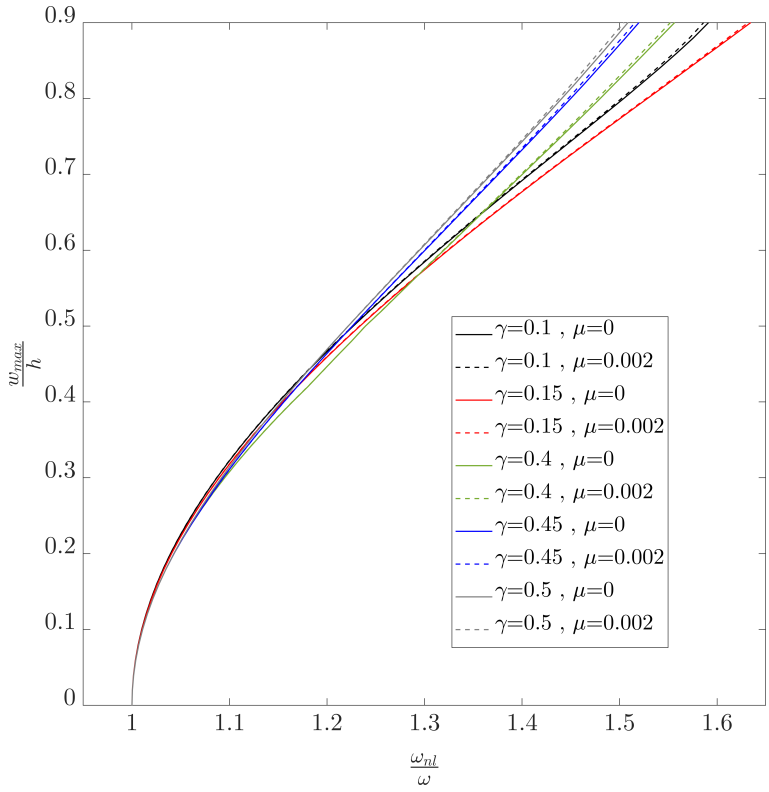

Figure 5.12: Backbone curves for the first mode of isotropic, centrally cracked $\beta = 0.3$, $\alpha = 0°$ square plates with different values of crack position ratio γ and and non-local parameter μ, subjected to *S-F-S-F* boundary conditions.

Figure 5.13 depicts the backbone curves for the fundamental mode vibration of *C-F-C-F* square local/non-local centrally cracked plates $\alpha = 0$, $\beta = 0.3$ for different values of crack position ratio γ, Similarly to the plates subjected to *S-F-S-F* boundary conditions, it is observed that the stiffening effect of large amplitude on free vibrations is increased for crack position ratios $0 < \gamma < 0.25$ and decreased for $0.25 < \gamma < 0.5$.

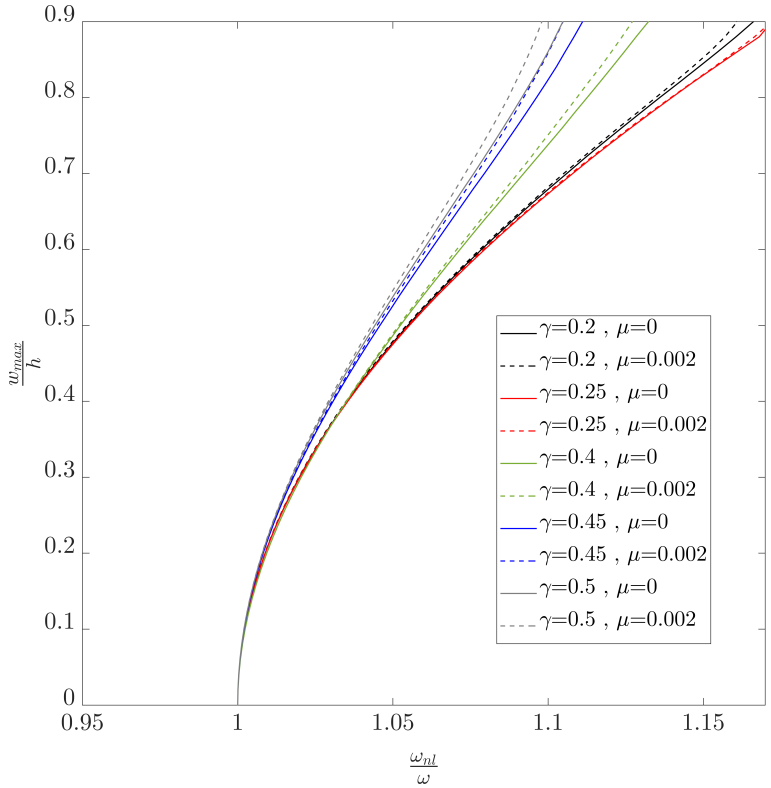

Figure 5.13: Backbone curves for the first mode of isotropic, centrally cracked $\beta = 0.3$, $\alpha = 0°$ square plates with different values of crack position ratio γ and and non-local parameter μ, subjected to *C-F-C-F* boundary conditions.

5.3 Summary

In this chapter, the non-linear free vibration of cracked nanoplates has been studied, based on non-local elasticity and first-order shear deformation theory, using *h-p* FEM with selective *p*-refinement. The obtained results for intact isotropic/FGM plates, are shown to be in very good agreement with the results literature. The investigation of the effect of horizontal crack length, boundary conditions and the non-local parameter on first mode backbone curves revealed that, the non-local parameter has a softening effect for all cases of boundary conditions and all values of crack length or crack position. The increase of crack length decreases the stiffening effect of large amplitude on free vibrations and at certain values of length ratio the vibration carried out linearly. Concerning the crack position, it is concluded

that as the crack is positioned closer to the middle of the plate, the stiffening effects of large amplitude vibrations is decreased.

Conclusion and future work

This thesis presented linear and nonlinear free vibrations of cracked nanoplates. Nonlocal elasticity theory has been applied in conjunction with first order shear deformation theory to derive equations of motion describing free vibrations of nanoplates. An *h-p* FEM model has been developed in order to accurately and efficiently handle the above mentioned problems. Several parametric studies has been established on the subject of linear/nonlinear free vibrations of isotropic/FGM cracked nanoplates, detailed conclusions were drawn at the end of each chapter. In the following sections, some important conclusions are summarized with respect to the numerical model, its implementation and results of parametric studies mentioned in previous chapters, recommendations for future work are also included.

Conclusions

The *h-p* FEM model that has been developed to handle problems of linear/nonlinear free vibrations of cracked nanoplates, has been used with computer implementation techniques such as parallel computing and sparse matrices storage scheme in order to efficiently conduct calculations on machines, along with two different meshing strategies, the first strategy was based on using few number of simple elements with full refinement (i.e,. all elements are *p-refined*), this strategy allowed full automation of mesh generation and refinement in other words parametric studies can be carried out without human intervention each time a crack parameter is changed. However a drawback of this strategy is the need for a relatively high *p-refinement* to reach convergence, this would be fine for linear analysis but for nonlinear analysis the integration step would be impractically slow even with parallel integration. The second meshing strategy addresses this problem by using an *h-refinement*

dominated mesh (i.e., selective *p-refinement*) where only elements around the crack tip are *p-refined* with a low degree p. This approach with parallel computing provided practical calculation time. However, it lacks full automation of mesh generation especially when changing crack orientation.

In the analysis of linear vibration of isotropic cracked nanoplates, the numerical model is shown to be accurate and efficient compared to results in literature for intact nanoplates and cracked local plates. The study of the effect of crack parameters (length, orientation), plate geometry, boundary conditions and the non-local parameter on frequency suggests that the non-local parameter has a softening effect that leads to the decrease of frequency. As for to crack parameters, a horizontal crack softens the nanoplate as the crack length increases (i.e., lower frequencies). However, an inclined crack mostly would increase the flexural stiffness.

In the analysis of linear free vibration of FGM cracked nanoplates. A good agreement has been found between our results and results in literature for intact FGM plates. The study of the influence of material volume fraction exponent n along with crack parameters (length, orientation), plate geometry, boundary conditions and the non-local parameter on frequency parameter further confirmed the softening effect of the non-local parameter. With regard to the crack parameters, for any value of material volume fraction exponent n or any value of non-local parameter μ, the increase in crack length for a horizontal crack (side or central crack) softens the nanoplate. Nevertheless, an inclined crack can increase the stiffness of the cracked plate. As for the crack position, as the crack is positioned closer to the middle of the plate, the stiffness of the plate is decreased.

For the analysis of non-linear free vibration of cracked nanoplates using *h-p* FEM with selective *p*-refinement around the crack tip. A very good agreement has been remarked between the obtained results and the results of literature for intact isotropic/FGM plates. From the parametric studies, it is concluded that the non-local parameter has a softening effect for any cases of boundary conditions and any values of crack length or crack position. The increase of crack length decreases the stiffening effect of large amplitude on free vibrations and at certain values of length ratio the vibration carried out linearly. As for the crack position, as the crack is positioned closer to the middle of the plate, the stiffening effects of large amplitude vibrations is decreased.

In this work, the main contributions for the simulation of cracks and nanoplates are:

1. The first endeavour to investigate linear free vibrations of cracked isotropic nanoplates based on nonlocal elasticity has been accomplished. Novel results characterizing the effect of different crack parameters such as length, orientation and position on linear vibrational behavior of isotropic nanoplates has been presented and discussed.

2. The achieved work has been further extended to linear free vibrations of FGM cracked nanoplates, where original results have been obtained relating the effect of material volume fraction exponent along with crack parameters and non-local parameter.

3. Original results for nonlinear free vibrations of cracked local plates (Classical elasticity) as well as nonlocal plates (nonlocal elasticity) have been presented and discussed.

4. Enrich the literature on the vibrations of cracked plates *using h-p FEM* since there is a paucity of research on the topic.

Suggestions for potential future work

The work in this thesis is limited and some improvements for the future may be considered:

- Extend the current numerical model to handle non-conforming meshes (i.e., irregular meshes) with hanging nodes, in the frame work *h-p version* of finite elements method (i.e., Coupling of *h* and *p* finite elements). This approach would allow better *h*-refinement around the crack tip and the transition out of the crack tip region would be carried out using few p-elements. The advantages of this approach are easy automation of mesh generation for any crack length or orientation, the ability to exploit *h-, p-* and *r-refinements* and obtain accurate results with fewer degrees of freedom.

- In nonlinear vibrations it is possible to encounter turning and bifurcation points at large amplitudes, translating into regions with multiple solutions (i.e., backbone

curve with secondary branches), which can not be handled using the LUM or Newton methods. Thus it is necessary to resort to *the continuation method* which is able to predict bifurcation points and construct secondary branches.

- The presented model can be further extended to other nanostructures (e.g., shells, 3D solids...) with multiple cracks and curved geometries.
- Another topic that can be considered for future research is forced linear/nonlinear vibrations of cracked nano-plates.
- Although the current state of literature is presenting non-local elasticity as a complete theory for nanostructures. However the data provided by different researchers on the value of the non-local parameter are not yet unitary and unambiguous. Thus the calibration of the non-local parameter is a pertinent factor for this theory to serve the engineering community in terms of predicting nanostructures behavior.

Appendix A

First Appendix

A.1 Hierarchic shape functions for quadrilateral elements

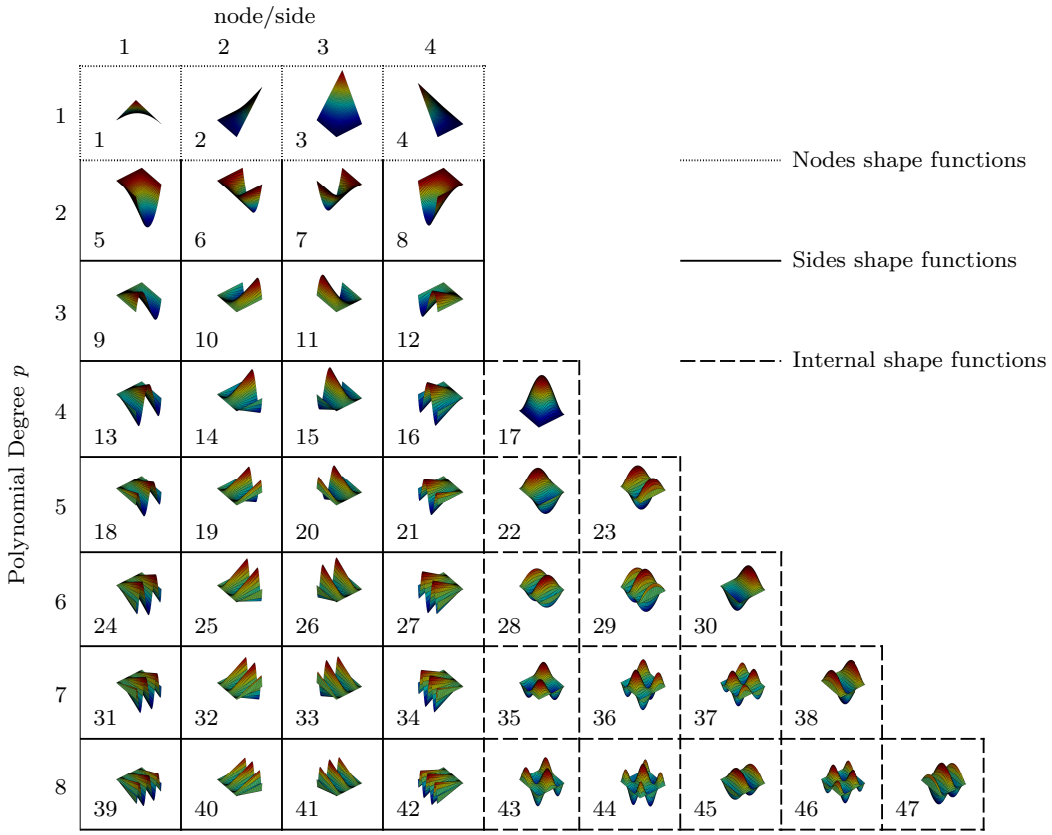

Figure A.1: Hierarchic shape functions for quadrilaterals

Bibliography

[1] Dimitri D Vvedensky. Multiscale modelling of nanostructures. *Journal of Physics: Condensed Matter*, 16(50):R1537–R1576, dec 2004. doi:10.1088/0953-8984/16/50/r01. 1

[2] Esmaeal Ghavanloo, Hashem Rafii-Tabar, and Seyed Ahmad Fazelzadeh. *Computational Continuum Mechanics of Nanoscopic Structures*. Springer, 2019. doi:10.1007/978-3-030-11650-7. 1, 20, 21

[3] KM Liew, Yang Zhang, and LW Zhang. Nonlocal elasticity theory for graphene modeling and simulation: prospects and challenges. *Journal of Modeling in Mechanics and Materials*, 1(1), 2017. doi:10.1515/jmmm-2016-0159. 1, 6

[4] A.C. Eringen, C.G. Speziale, and B.S. Kim. Crack-tip problem in non-local elasticity. *Journal of the Mechanics and Physics of Solids*, 25(5):339 – 355, 1977. ISSN 0022-5096. doi:10.1016/0022-5096(77)90002-3. 2, 19

[5] Ac Eringen and J Wegner. *Nonlocal Continuum Field Theories*, volume 56. 01 2003. doi:10.1115/1.1553434. 6, 18, 20

[6] R Ansari, S Sahmani, and B Arash. Nonlocal plate model for free vibrations of single-layered graphene sheets. *Physics Letters A*, 375(1):53–62, 2010. doi:10.1016/j.physleta.2010.10.028. 6

[7] SC Pradhan and A Kumar. Vibration analysis of orthotropic graphene sheets using nonlocal elasticity theory and differential quadrature method. *Composite Structures*, 93(2):774–779, 2011. doi:10.1016/j.compstruct.2010.08.004. 6

[8] Parviz Malekzadeh, AliReza Setoodeh, and Ali Alibeygi Beni. Small scale effect on the free vibration of orthotropic arbitrary straight-sided quadrilateral nanoplates. *Composite Structures - COMPOS STRUCT*, 93:1631–1639, 06 2011. doi:10.1016/j.compstruct.2011.01.008. 7

[9] C. Y. Wang, T. Murmu, and S. Adhikari. Mechanisms of nonlocal effect on the vibration of nanoplates. *Applied Physics Letters*, 98(15):153101, 2011. doi:10.1063/1.3579249. 7

[10] L. Y. HUANG, Q. HAN, and Y. J. LIANG. Calibration of nonlocal scale effect parameter for bending single-layered graphene sheet under molecular dynamics. *Nano*, 07(05):1250033, 2012. doi:10.1142/S1793292012500336. 7

[11] Chen Liu, Liao-Liang Ke, Yue-Sheng Wang, Jie Yang, and Sritawat Kitipornchai. Thermo-electro-mechanical vibration of piezoelectric nanoplates based on the nonlocal theory. *Composite Structures*, 106:167–174, 12 2013. doi:10.1016/j.compstruct.2013.05.031. 7

[12] Parviz Malekzadeh and Mohammad Shojaee. Free vibration of nanoplates based on a nonlocal two-variable refined plate theory. *Composite Structures*, 95:443–452, 01 2013. doi:10.1016/j.compstruct.2012.07.006. 7

[13] Shahrokh Hosseini-Hashemi, Mehdi Kermajani, and Reza Nazemnezhad. An analytical study on the buckling and free vibration of rectangular nanoplates using nonlocal third-order shear deformation plate theory. *European Journal of Mechanics - A/Solids*, 11 2014. doi:10.1016/j.euromechsol.2014.11.005. 7

[14] S.C. Pradhan and J.K. Phadikar. Nonlocal elasticity theory for vibration of nanoplates. *Journal of Sound and Vibration*, 325(1):206 – 223, 2009. ISSN 0022-460X. doi:10.1016/j.jsv.2009.03.007. 7

[15] Chen Liu, Liao-Liang Ke, Yue-Sheng Wang, Jie Yang, and Sritawat Kitipornchai. Thermo-electro-mechanical vibration of piezoelectric nanoplates based on the nonlocal theory. *Composite Structures*, 106:167 – 174, 2013. ISSN 0263-8223. doi:10.1016/j.compstruct.2013.05.031. 7

[16] H.R. Analooei, M. Azhari, and A. Heidarpour. Elastic buckling and vibration analyses of orthotropic nanoplates using nonlocal continuum mechanics and spline finite strip method. *Applied Mathematical Modelling*, 37(10):6703 – 6717, 2013. ISSN 0307-904X. doi:10.1016/j.apm.2013.01.051. 7

[17] Tolga Aksencer and Metin Aydogdu. Forced transverse vibration of nanoplates using nonlocal elasticity. *Physica E: Low-dimensional Systems and Nanostructures*, 44(7): 1752 – 1759, 2012. ISSN 1386-9477. doi:10.1016/j.physe.2011.12.004. 7

[18] Ramin Aghababaei and J.N. Reddy. Nonlocal third-order shear deformation plate theory with application to bending and vibration of plates. *Journal of Sound and Vibration*, 326(1):277 – 289, 2009. ISSN 0022-460X. doi:10.1016/j.jsv.2009.04.044. 7

[19] J. N. Reddy. A Simple Higher-Order Theory for Laminated Composite Plates. *Journal of Applied Mechanics*, 51(4):745–752, 12 1984. ISSN 0021-8936. doi:10.1115/1.3167719. 7

[20] K.F. Wang and B.L. Wang. Vibration of nanoscale plates with surface energy via nonlocal elasticity. *Physica E: Low-dimensional Systems and Nanostructures*, 44(2): 448 – 453, 2011. ISSN 1386-9477. doi:10.1016/j.physe.2011.09.019. 8

[21] S Chakraverty and Laxmi Behera. Free vibration of rectangular nanoplates using rayleigh-ritz method. 56:357–363, 02 2014. doi:10.1016/j.physe.2013.08.014. 8, 54, 55

[22] Abdelkrim Necira, Sid Ahmed Belalia, and Abdelkrim Boukhalfa. Size-dependent free vibration analysis of mindlin nano-plates with curvilinear plan-forms by a high order curved hierarchical finite element. *Mechanics of Advanced Materials and Structures*, pages 1–19, 06 2018. doi:10.1080/15376494.2018.1472342. 8

[23] Yang Zhang, Z.X. Lei, L.W. Zhang, K.M. Liew, and J.L. Yu. Nonlocal continuum model for vibration of single-layered graphene sheets based on the element-free kp-ritz method. *Engineering Analysis with Boundary Elements*, 56:90 – 97, 2015. ISSN 0955-7997. doi:10.1016/j.enganabound.2015.01.020. 8

[24] Keivan Kiani. Small-scale effect on the vibration of thin nanoplates subjected to a moving nanoparticle via nonlocal continuum theory. *Journal of Sound and Vibration*, 330(20):4896 – 4914, 2011. ISSN 0022-460X. doi:10.1016/j.jsv.2011.03.033. 8

[25] Yu Wang, Fengming Li, Xingjian Jing, and Yize Wang. Nonlinear vibration analysis of double-layered nanoplates with different boundary conditions. *Physics Letters A*, 379(24):1532 – 1537, 2015. ISSN 0375-9601. doi:10.1016/j.physleta.2015.04.002. 8

[26] Emad Jomehzadeh and A. Saidi. Study of small scale effect on nonlinear vibration of nano-plates. *Journal of Computational and Theoretical Nanoscience*, 9, 06 2012. doi:10.1166/jctn.2012.2108. 8

[27] S Natarajan, S Chakraborty, M Thangavel, Stéphane Bordas, and Timon Rabczuk. Size-dependent free flexural vibration behavior of functionally graded nanoplates. *Computational Materials Science*, 65:74–80, 2012. doi:10.1016/j.commatsci.2012.06.031. 8

[28] Mohammad Rahim Nami and Maziar Janghorban. Resonance behavior of fg rectangular micro/nano plate based on nonlocal elasticity theory and strain gradient theory with one gradient constant. *Composite Structures*, 111:349–353, 2014. doi:10.1016/j.compstruct.2014.01.012. 8

[29] Ismahene Belkorissat, Mohammed Sid Ahmed Houari, Abdelouahed Tounsi, EA Bedia, and SR Mahmoud. On vibration properties of functionally graded nano-plate using a new nonlocal refined four variable model. *Steel Compos. Struct*, 18(4):1063–1081, 2015. doi:10.12989/scs.2015.18.4.1063. 8

[30] R Ansari, M Faghih Shojaei, A Shahabodini, and M Bazdid-Vahdati. Three-dimensional bending and vibration analysis of functionally graded nanoplates by a novel differential quadrature-based approach. *Composite Structures*, 131:753–764, 2015. doi:10.1016/j.compstruct.2015.06.027. 9

[31] Zhi-Bin Shen, Hai-Li Tang, Dao-Kui Li, and Guo-Jin Tang. Vibration of single-layered graphene sheet-based nanomechanical sensor via nonlocal kirchhoff plate

theory. *Computational Materials Science*, 61:200 – 205, 2012. ISSN 0927-0256. doi:10.1016/j.commatsci.2012.04.003. 9

[32] S. Adhikari and R. Chowdhury. Zeptogram sensing from gigahertz vibration: Graphene based nanosensor. *Physica E: Low-dimensional Systems and Nanostructures*, 44(7):1528 – 1534, 2012. ISSN 1386-9477. doi:10.1016/j.physe.2012.03.021. 9

[33] A. Sakhaee-Pour, M.T. Ahmadian, and A. Vafai. Applications of single-layered graphene sheets as mass sensors and atomistic dust detectors. *Solid State Communications*, 145(4):168 – 172, 2008. ISSN 0038-1098. doi:10.1016/j.ssc.2007.10.032. 9

[34] S. Ahmad Fazelzadeh and Esmaeal Ghavanloo. Nanoscale mass sensing based on vibration of single-layered graphene sheet in thermal environments. *Acta Mechanica Sinica*, 30(1):84–91, Feb 2014. ISSN 1614-3116. doi:10.1007/s10409-013-0102-6. 9

[35] Zhi-Bin Shen, Ren-Wei Jiang, Liang Zhang, and Guo-Jin Tang. Nonlocal galerkin strip transfer function method for vibration of double-layered graphene mass sensor. *Acta Mechanica Solida Sinica*, 31(1):94–107, Feb 2018. ISSN 1860-2134. doi:10.1007/s10338-018-0003-0. 9

[36] T. Murmu and S. Adhikari. Nonlocal mass nanosensors based on vibrating monolayer graphene sheets. *Sensors and Actuators B: Chemical*, 188:1319 – 1327, 2013. ISSN 0925-4005. doi:10.1016/j.snb.2013.07.051. 9

[37] S. Kamal Jalali, M. Hassan Naei, and Nicola Maria Pugno. Graphene-based resonant sensors for detection of ultra-fine nanoparticles: Molecular dynamics and nonlocal elasticity investigations. *Nano*, 10(02):1550024, 2015. doi:10.1142/S1793292015500241. 9

[38] Jingyuan Li, Xiaofeng Wang, Lina Zhao, Xingfa Gao, Yuliang Zhao, and Ruhong Zhou. Rotation motion of designed nano-turbine. *Scientific reports*, 4:5846, 2014. 10

[39] Navvab Shafiei, Majid Ghadiri, Hesam Makvandi, and Seyyed Amirhosein Hosseini. Vibration analysis of nano-rotor's blade applying eringen nonlocal elasticity and generalized differential quadrature method. *Applied Mathematical Modelling*, 43:191 – 206, 2017. ISSN 0307-904X. doi:10.1016/j.apm.2016.10.061. 10

[40] Leon. Stahl, B & Keer. Vibration and stability of cracked rectangular plates. *International Journal of Solids and Structures*, 8:69–91, 1972. doi:10.1016/0020-7683(72)90052-2. 11, 54, 56

[41] Roman Solecki. Bending vibration of a simply supported rectangular plate with a crack parallel to one edge. *Engineering Fracture Mechanics*, 18(6):1111 – 1118, 1983. ISSN 0013-7944. doi:10.1016/0013-7944(83)90004-8. 11

[42] Yoshitaro HIRANO and Katsutoshi OKAZAKI. Vibrarfon of cracked rectangular plates. *Bulletin of JSME*, 23(179):732–740, 1980. 11

[43] K Liew, K C. Hung, and M K. Lim. Solution method for analysis of cracked plates under vibration. *Engineering Fracture Mechanics - ENG FRACTURE MECH*, 48: 393–404, 06 1994. doi:10.1016/0013-7944(94)90130-9. 11, 54, 56, 57

[44] H.P. Lee and S.P. Lim. Vibration of cracked rectangular plates including transverse shear deformation and rotary inertia. *Computers & Structures*, 49(4):715 – 718, 1993. ISSN 0045-7949. doi:10.1016/0045-7949(93)90074-N. 11

[45] C. S. Huang, A. W. Leissa, and M. J. Chang. Vibrations of skewed cantilevered triangular, trapezoidal and parallelogram mindlin plates with considering corner stress singularities. *International Journal for Numerical Methods in Engineering*, 62(13): 1789–1806, 2005. doi:10.1002/nme.1247. 11

[46] C.S. Huang and A.W. Leissa. Vibration analysis of rectangular plates with side cracks via the ritz method. *Journal of Sound and Vibration*, 323(3):974 – 988, 2009. ISSN 0022-460X. doi:10.1016/j.jsv.2009.01.018. 11

[47] Qian Guan-Liang, Gu Song-Nian, and Jiang Jie-Sheng. A finite element model of cracked plates and application to vibration problems. *Computers & Structures*, 39(5): 483 – 487, 1991. ISSN 0045-7949. doi:10.1016/0045-7949(91)90056-R. 11

[48] G.-L. Qian, S.-N. Gu, and J.-S. Jiang. The dynamic behaviour and crack detection of a beam with a crack. *Journal of Sound and Vibration*, 138(2):233 – 243, 1990. ISSN 0022-460X. doi:10.1016/0022-460X(90)90540-G. 11

[49] M. Krawczuk. Natural vibrations of rectangular plates with a through crack. *Archive of Applied Mechanics*, 63(7):491–504, Jul 1993. ISSN 1432-0681. doi:10.1007/BF00788047. 11

[50] B Zastrau. Vibration of cracked structures. *Archives of Mechanics*, 37(6):731–743, 1985. 12

[51] Karl Markstrom and Bertil Stoakers. Buckling of cracked members under tension. *International Journal of Solids and Structures*, 16(3):217 – 229, 1980. ISSN 0020-7683. doi:10.1016/0020-7683(80)90075-X. 12

[52] S. Natarajan, P.M. Baiz, M. Ganapathi, P. Kerfriden, and S. Bordas. Linear free flexural vibration of cracked functionally graded plates in thermal environment. *Computers & Structures*, 89(15):1535 – 1546, 2011. ISSN 0045-7949. doi:10.1016/j.compstruc.2011.04.002. 12

[53] R. D. Henshell and K. G. Shaw. Crack tip finite elements are unnecessary. *International Journal for Numerical Methods in Engineering*, 9(3):495–507, 1975. doi:10.1002/nme.1620090302. 12

[54] H. D. Hibbitt. Some properties of singular isoparametric elements. *International Journal for Numerical Methods in Engineering*, 11(1):180–184, 1977. doi:10.1002/nme.1620110117. 12

[55] Roshdy S. Barsoum. On the use of isoparametric finite elements in linear fracture mechanics. *International Journal for Numerical Methods in Engineering*, 10(1):25–37, 1976. doi:10.1002/nme.1620100103. 12

[56] M.-H.H. Shen and C. Pierre. Natural modes of bernoulli-euler beams with symmetric cracks. *Journal of Sound and Vibration*, 138(1):115 – 134, 1990. ISSN 0022-460X. doi:10.1016/0022-460X(90)90707-7. 12

[57] M. Bachene, R. Tiberkak, and S. Rechak. Vibration analysis of cracked plates using the extended finite element method. *Archive of Applied Mechanics*, 79(3):249–262, Mar 2009. ISSN 1432-0681. doi:10.1007/s00419-008-0224-7. 12

[58] Nicolas Moës, John Dolbow, and Ted Belytschko. A finite element method for crack growth without remeshing. *International Journal for Numerical Methods in Engineering*, 46(1):131–150, 1999. doi:10.1002/(SICI)1097-0207(19990910)46:1<131::AID-NME726>3.0.CO;2-J. 13

[59] M. Bachene, R. Tiberkak, S. Rechak, G. Maurice, and B. K. Hachi. *Enriched Finite Element for Modal Analysis of Cracked Plates*, pages 463–471. Springer Netherlands, Dordrecht, 2009. ISBN 978-90-481-2669-9. doi:10.1007/978-90-481-2669-9$_4$9. 13

[60] S. Natarajan, P.M. Baiz, S. Bordas, T. Rabczuk, and P. Kerfriden. Natural frequencies of cracked functionally graded material plates by the extended finite element method. *Composite Structures*, 93(11):3082 – 3092, 2011. ISSN 0263-8223. doi:10.1016/j.compstruct.2011.04.007. 13

[61] Kai-Uwe Bletzinger, Manfred Bischoff, and Ekkehard Ramm. A unified approach for shear-locking-free triangular and rectangular shell finite elements. *Computers & Structures*, 75(3):321 – 334, 2000. ISSN 0045-7949. doi:10.1016/S0045-7949(99)00140-6. 13

[62] Tiantang Yu, Tinh Quoc Bui, Peng Liu, and Sohichi Hirose. A stabilized discrete shear gap extended finite element for the analysis of cracked reissner–mindlin plate vibration problems involving distorted meshes. *International Journal of Mechanics and Materials in Design*, 12(1):85–107, Mar 2016. ISSN 1573-8841. doi:10.1007/s10999-014-9282-x. 13

[63] Loc V. Tran, Hung Anh Ly, Jaehong Lee, M. Abdel Wahab, and H. Nguyen-Xuan. Vibration analysis of cracked fgm plates using higher-order shear deformation theory and extended isogeometric approach. *International Journal of Mechanical Sciences*, 96-97:65 – 78, 2015. ISSN 0020-7403. doi:10.1016/j.ijmecsci.2015.03.003. 14

[64] Shuohui Yin, Tiantang Yu, Tinh Quoc Bui, Peng Liu, and Sohichi Hirose. Buckling and vibration extended isogeometric analysis of imperfect graded reissner-mindlin plates with internal defects using nurbs and level sets. *Computers & Structures*, 177: 23 – 38, 2016. ISSN 0045-7949. doi:10.1016/j.compstruc.2016.08.005. 14

[65] Tiantang Yu, Tinh Quoc Bui, Shuohui Yin, Duc Hong Doan, C.T. Wu, Thom Van Do, and Satoyuki Tanaka. On the thermal buckling analysis of functionally graded plates with internal defects using extended isogeometric analysis. *Composite Structures*, 136:684 – 695, 2016. ISSN 0263-8223. doi:10.1016/j.compstruct.2015.11.002. 14

[66] Pengfei Tan, Nhon Nguyen-Thanh, and Kun Zhou. Extended isogeometric analysis based on bézier extraction for an fgm plate by using the two-variable refined plate theory. *Theoretical and Applied Fracture Mechanics*, 89:127 – 138, 2017. ISSN 0167-8442. doi:10.1016/j.tafmec.2017.02.002. 14

[67] S.K. Singh, I.V. Singh, B.K. Mishra, G. Bhardwaj, and S.K. Singh. Analysis of cracked plate using higher-order shear deformation theory: Asymptotic crack-tip fields and xiga implementation. *Computer Methods in Applied Mechanics and Engineering*, 336:594 – 639, 2018. ISSN 0045-7825. doi:10.1016/j.cma.2018.03.009. 15

[68] B. A. Szabo and A. K. Mehta. p-convergent finite element approximations in fracture mechanics. *International Journal for Numerical Methods in Engineering*, 12(3):551–560, 1978. doi:10.1002/nme.1620120313. 15

[69] N.S. Bardell, J.M. Dunsdon, and R.S. Langley. Free vibration analysis of thin rectangular laminated plate assemblies using the h-p version of the finite element method. *Composite Structures*, 32(1):237 – 246, 1995. ISSN 0263-8223. doi:10.1016/0263-8223(95)00081-X. Eighth International Conference on Composite Structures. 15

[70] A. Hadjoui, H. Mebarek, and B. Bachir Bouiadjra. Free vibration analysis for cracked triangular orthotropic plates using h-p finite element method. *International Journal for Computational Methods in Engineering Science and Mechanics*, 12(2):59–74, 2011. doi:10.1080/15502287.2010.548003. 15

[71] Y. Povstenko. The nonlocal theory of elasticity and its applications to the description of defects in solid bodies. *Journal of Mathematical Sciences*, 97:3840–3845, 1999. doi:10.1007/BF02364923. 19

[72] ZdenÄk P. BaÅŸant and Milan JirÃ¡sek. Nonlocal integral formulations of plasticity and damage: Survey of progress. *Journal of Engineering Mechanics*, 128(11):1119–1149, 2002. doi:10.1061/(ASCE)0733-9399(2002)128:11(1119). 20

[73] Castrenze Polizzotto. Nonlocal elasticity and related variational principles. *International Journal of Solids and Structures*, 38(42):7359 – 7380, 2001. ISSN 0020-7683. doi:10.1016/S0020-7683(01)00039-7. 20

[74] R.C. Picu. The peierls stress in non-local elasticity. *Journal of the Mechanics and Physics of Solids*, 50(4):717 – 735, 2002. ISSN 0022-5096. doi:10.1016/S0022-5096(01)00096-5. 20

[75] A. Cemal Eringen. On differential equations of nonlocal elasticity and solutions of screw dislocation and surface waves. *Journal of Applied Physics*, 54(9):4703–4710, 1983. doi:10.1063/1.332803. 20

[76] Markus Lazar, GÃ©rard A. Maugin, and Elias C. Aifantis. On a theory of nonlocal elasticity of bi-helmholtz type and some applications. *International Journal of Solids and Structures*, 43(6):1404 – 1421, 2006. ISSN 0020-7683. doi:10.1016/j.ijsolstr.2005.04.027. 20

[77] J.N. Reddy. *Theory and Analysis of Elastic Plates and Shells, Second Edition*. Series in Systems and Control. Taylor & Francis, 2006. ISBN 9780849384158. 23

[78] J. N. Reddy and C. D. Chin. Thermomechanical analysis of functionally graded cylinders and plates. *Journal of Thermal Stresses*, 21(6):593–626, 1998. doi:10.1080/01495739808956165. 30

[79] YS Touloukian. Thermophysical properties of high temperature solid materials. volume 3: Ferrous alloys. Technical report, Thermophysical and Electronic Properties Information Analysis Center Lafayette, 1966. 30

[80] L. J. Gibson, M. F. Ashby, G. N. Karam, U. Wegst, and H. R. Shercliff. The mechanical properties of natural materials. ii. microstructures for mechanical efficiency. *Proceedings: Mathematical and Physical Sciences*, 450(1938):141–162, 1995. ISSN 09628444. URL `http://www.jstor.org/stable/52663`. 30

[81] Olek C Zienkiewicz, Robert L Taylor, and Jian Z Zhu. *The finite element method: its basis and fundamentals*. Elsevier, 2005. ISBN 978-1-85617-633-0. doi:10.1016/C2009-0-24909-9. 30, 39, 40

[82] B. E. Sandman and H. S. Walker. An Experimental Observation in Large Amplitude Plate Vibrations. *Journal of Applied Mechanics*, 40(2):633–634, 06 1973. ISSN 0021-8936. doi:10.1115/1.3423049. 32

[83] J. N. Reddy and W. C. Chao. Nonlinear Oscillations of Laminated, Anisotropic, Rectangular Plates. *Journal of Applied Mechanics*, 49(2):396–402, 06 1982. ISSN 0021-8936. doi:10.1115/1.3162100. 32

[84] Barna Szabó and Ivo Babuška. *Introduction to finite element analysis: formulation, verification and validation*, volume 35. John Wiley & Sons, 2011. 36, 37

[85] Junuthula Narasimha Reddy. *An Introduction to Nonlinear Finite Element Analysis: with applications to heat transfer, fluid mechanics, and solid mechanics*. OUP Oxford, 2014. ISBN 978-1-4419-1746-1. doi:10.1007/978-1-4419-1746-1. 37

[86] N. S. Bardell. The application of symbolic computing to the hierarchical finite element method. *International Journal for Numerical Methods in Engineering*, 28(5): 1181–1204, 1989. doi:10.1002/nme.1620280513. 38, 46

[87] Pedro Manuel Leal Ribeiro. Geometrical nonlinear vibration of beams and plates by the hierarchical finite element method. 1998. 45

[88] John R Gilbert, Cleve Moler, and Robert Schreiber. Sparse matrices in matlab: Design and implementation. *SIAM Journal on Matrix Analysis and Applications*, 13(1):333–356, 1992. 48

[89] Yousef Saad. *Numerical methods for large eigenvalue problems: revised edition*. SIAM, 2011. 48

[90] Viral Shah and John R. Gilbert. Sparse matrices in matlab*p: Design and implementation. In Luc Bougé and Viktor K. Prasanna, editors, *High Performance Computing - HiPC 2004*, pages 144–155, Berlin, Heidelberg, 2005. Springer Berlin Heidelberg. ISBN 978-3-540-30474-6. 48

[91] Sumi S Fujimoto, T. Vibration characteristics of center cracked plates under tension. 53:1124–1131, 1987. 54, 56, 57

[92] Hiroyuki Matsunaga. Free vibration and stability of functionally graded plates according to a 2-d higher-order deformation theory. *Composite Structures*, 82(4):499 – 512, 2008. ISSN 0263-8223. doi:10.1016/j.compstruct.2007.01.030. 80, 81

[93] X. Zhao, Y.Y. Lee, and K.M. Liew. Free vibration analysis of functionally graded plates using the element-free kp-ritz method. *Journal of Sound and Vibration*, 319 (3):918 – 939, 2009. ISSN 0022-460X. doi:10.1016/j.jsv.2008.06.025. 80, 81

[94] Chuh Mei and Kamolphan Decha-Umphai. A finite element method for nonlinear forced vibrations of rectangular plates. *AIAA Journal*, 23(7):1104–1110, 1985. doi:10.2514/3.9044. 113, 114

[95] Joe G. Eisley. Nonlinear vibration of beams and rectangular plates. *Zeitschrift f ü r angewandte Mathematik und Physik ZAMP*, 15(2):167–175, 1964. ISSN 1420-9039. doi:10.1007/BF01602658. 113, 114

[96] C.S. Hsu. On the application of elliptic functions in non-linear forced oscillations. *Quarterly of Applied Mathematics*, 17, 01 1960. doi:10.1090/qam/110250. 113, 114

[97] I.S. Raju, G.Venkateswara Rao, and K.Kanaka Raju. Effect of longitudinal or inplane deformation and inertia on the large amplitude flexural vibrations of slender beams and thin plates. *Journal of Sound and Vibration*, 49(3):415 – 422, 1976. ISSN 0022-460X. doi:10.1016/0022-460X(76)90431-4. 113, 114

[98] Xiao-Lin Huang and Hui-Shen Shen. Nonlinear vibration and dynamic response of functionally graded plates in thermal environments. *International Journal of Solids and Structures*, 41(9):2403 – 2427, 2004. ISSN 0020-7683. doi:10.1016/j.ijsolstr.2003.11.012. 114, 115